MARTIN MARIETTA ENERGY SYSTEMS LIBRARIES

3 4456 0319966 0

LACE TR-084
ORNL/M-991

ornl

OAK RIDGE
NATIONAL
LABORATORY

MARTIN MARIETTA

Comparison of (Posttest) Predictions of Aerosol Codes with Measurements in LWR Aerosol Containment Experiment (LACE) LA4

J. H. Wilson
P. C. Arwood

OAK RIDGE NATIONAL LABORATORY
CENTRAL RESEARCH LIBRARY
CIRCULATION SECTION
4500N ROOM 175
LIBRARY LOAN COPY
DO NOT TRANSFER TO ANOTHER PERSON
If you wish someone else to see this report, send in name with report and the library will arrange a loan.

OPERATED BY
MARTIN MARIETTA ENERGY SYSTEMS, INC.
FOR THE UNITED STATES
DEPARTMENT OF ENERGY

This report was prepared as an account of work sponsored by an agency of the United States Government. Neither the United States Government nor any agency thereof, nor any of their employees, makes any warranty, express or implied, or assumes any legal liability or responsibility for the accuracy, completeness, or usefulness of any information, apparatus, product, or process disclosed, or represents that its use would not infringe privately owned rights. Reference herein to any specific commercial product, process, or service by trade name, trademark, manufacturer, or otherwise, does not necessarily constitute or imply its endorsement, recommendation, or favoring by the United States Government or any agency thereof. The views and opinions of authors expressed herein do not necessarily state or reflect those of the United States Government or any agency thereof.

LACE TR-084
ORNL/M-991

Chemical Technology Division

COMPARISON OF (POSTTEST) PREDICTIONS OF AEROSOL CODES WITH MEASUREMENTS IN LWR AEROSOL CONTAINMENT EXPERIMENT (LACE) LA4

J. H. Wilson
P. C. Arwood

Prepared for
ELECTRIC POWER RESEARCH INSTITUTE
3412 Hillview Avenue
Palo Alto, California 94303

EPRI Project No. 2135-18

Date Published: February 1990

Prepared by the
OAK RIDGE NATIONAL LABORATORY
Oak Ridge, Tennessee 37831-6285
operated by
MARTIN MARIETA ENERGY SYSTEMS, INC.
for the
U. S. DEPARTMENT OF ENERGY
under contract DE-AC05-84OR21400

MARTIN MARIETTA ENERGY SYSTEMS LIBRARIES

3 4456 0319966 0

NOTICE

This report was prepared by the organization(s) named below as an account of work sponsored by the Electric Power Research Institute Inc. (EPRI). Neither EPRI, members of EPRI, the organization(s) named below, nor any person acting on behalf of any of them: (a) makes any warranty, express or implied, with respect to the use of any information, apparatus, method, or process disclosed in this report or that such use may not infringe privately owned rights; or (b) assumes any liabilities with respect to the use of, or for damages resulting from the use of, any information, apparatus, method, or process disclosed in this report.

Prepared by
OAK RIDGE NATIONAL LABORATORY
Oak Ridge, Tennessee 37831

[redacted]

CONTENTS

ABSTRACT.....vii

1. INTRODUCTION..... 1

2. SUMMARY OF SPECIFIED INPUTS AND REQUESTED CODE OUTPUTS FOR LA4 PRETEST CALCULATIONS..... 2

3. DESCRIPTIONS OF CODES PERFORMING LA4 CALCULATIONS..... 21

4. RESULTS OF LA4 POSTTEST CODE CALCULATIONS..... 23

5. LACE TEST LA4 EXPERIMENTAL DATA..... 91

6. CALCULATION AND ANALYSIS OF VARIANCE BETWEEN EXPERIMENTAL MEASUREMENTS AND CODE PREDICTIONS..... 94

7. COMPARISON OF EXPERIMENTAL RESULTS AND CODE PREDICTIONS.....101

8. CONCLUSIONS.....114

9. RECOMMENDATIONS.....115

10. REFERENCES.....117

APPENDIX A.....119

APPENDIX B.....121

APPENDIX C.....123

ABSTRACT

This report describes work performed as part of the LACE (LWR Aerosol Containment Experiment) Code Experiment Comparison Coordination Project, which is sponsored by the Electric Power Research Institute (EPRI Project No. 2135-18). The report presents and summarizes comparisons of test results and aerosol computer-code calculations for LACE test LA4. This and previous LACE tests were performed at the Westinghouse Hanford Engineering Development Laboratory (HEDL). LACE test LA4 was performed with a two-component aerosol under conditions which simulate a severe accident in an LWR with separate and overlapping aerosol species injection periods and a late containment failure.

COMPARISON OF (POSTTEST) PREDICTIONS OF AEROSOL CODES WITH MEASUREMENTS IN LWR AEROSOL CONTAINMENT EXPERIMENT (LACE) LA4

J. H. Wilson
P. C. Arwood

1. INTRODUCTION

The Light-Water Reactor Aerosol Containment Experiments (LACE) have been performed to investigate, at large scale, the inherent aerosol retention behavior in containment under simulated severe light-water reactor (LWR) accident conditions. An additional, and equally important, objective of these tests was to provide a data base for validating aerosol containment computer codes and related thermal-hydraulic computer codes. The LACE tests were internationally funded and were performed at the Westinghouse Hanford Engineering Development Laboratory (HEDL) under the leadership of an overall project board and the Electric Power Research Institute (EPRI).

The overall LACE project had two components: (1) the experiments performed at HEDL and (2) aerosol-transport and thermal-hydraulic code-comparison activities. The aerosol-transport code-comparison activities were coordinated by the Oak Ridge National Laboratory (ORNL), while the thermal-hydraulic code-comparison activities were coordinated by Intermountain Technologies, Inc. (ITI) in Idaho Falls, Idaho.

For each of the six planned LACE tests, pretest and blind posttest aerosol code calculations were performed. The ORNL code-comparison activities included (1) providing guidance to participating aerosol code analysts to help them in performing calculations, (2) compiling the results from calculations, and (3) critically evaluating the code results and comparisons to the test data.

This report summarizes the results from posttest aerosol calculations performed for LACE test LA4. These calculations were to have been "blind" in that the code analysts were not to have had access to the LA4 results when they performed their calculations. However, after the first LA4 aerosol posttest calculations were made, an error

was discovered in the steam feed rate values that were provided to the code analysts. By this time, some of the LA4 results had been made available. Even so, the decision was made to have the code analysts redo the calculations using the corrected steam feed rate values. The reason for this decision was that a comparison of experimental data with results of calculations which used incorrect steam rates would essentially be meaningless.

As defined in the LA4 test plan[1], this test was performed with a two-component aerosol under conditions which simulate a severe accident in an LWR with separate and overlapping aerosol species injection periods and a late containment failure. During the first injection period, CsOH, a hygroscopic aerosol, was injected into the containment vessel. Both CsOH and MnO were injected during the second period; and in the third period, MnO only was injected. Aerosol code calculations to model the behavior in the Containment Systems Test Facility (CSTF) vessel were performed.

Section 2 of this report presents an overall description of LACE test LA4 and then summarizes the defined code inputs and the requested code outputs for the LA4 posttest calculations. Section 3 describes the codes used in LA4 posttest calculations, and Sect. 4 presents their results. The LA4 experimental data are discussed in Sect. 5, and Sect. 6 describes the method used to calculate the variances between the experimental measurements and the code predictions. The experimental data and the code calculation results are compared in Sect. 7. The final section of the report presents the conclusions and recommendations.

2. SUMMARY OF SPECIFIED CODE INPUTS AND REQUESTED CODE OUTPUTS FOR LA4 POSTTEST CALCULATIONS

The experimental set-up for test LA4 is illustrated in Fig. 1; additional details are presented in the LA4 test plan.[1] MnO and CsOH aerosols were transported through a 0.2-m diam pipe and injected into the atmosphere of the 852-m^3 CSTF vessel. The three source periods for the MnO and CsOH aerosols were staggered. Initially only CsOH was

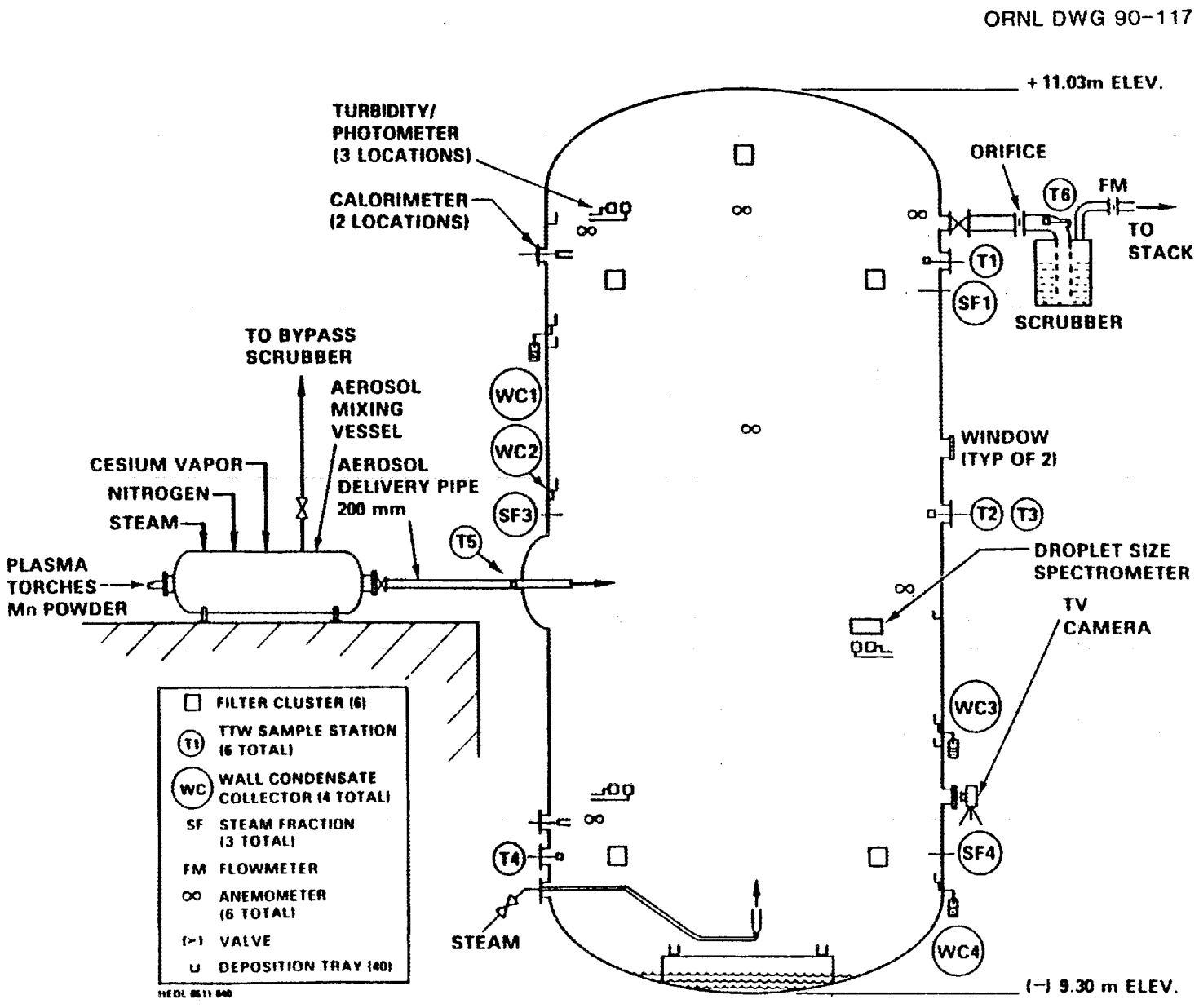

Fig. 1. Experimental setup for LACE test LA4.

injected, then both CsOH and MnO, and finally only MnO. The total aerosol injection period was 4812 s (1.34 h). At 16,800 s (4.67 h) after the start of the aerosol injection period, a valve was opened to start venting the CSTF vessel. The behavior of the aerosol during and following the injection period was studied. Experimental aerosol measurements were made over a total time of approximately 2 days.

Three letters describing aerosol code inputs and required code outputs for LA4 posttest calculations were sent to LACE program participants. The first letter[2] provided initial instructions for the LA4 aerosol calculations. The second[3] and third[4] letters gave additional experimental data and instructions. The general contents of these letters are summarized in this section.

The majority of the data required for performing the posttest calculations was contained on IBM floppy disks – in the form of text files – that were transmitted from HEDL to LACE program participants.[5] The text files containing aerosol input information were named LA4AB10.TXT, LA4AB10.DAT, LA4AB11.DAT, LA4AB20.DAT-LA4AB23.DAT, LA4AB30.DAT-LA4AB33.DAT, and LA4AB40.DAT-LA4AB43.DAT. These text files are referred to in this section. The LA4 aerosol experimental data also were summarized in report number LACE TR-025.[6] The data tables in this report are referred to in following sections.

The data used for performing the LA4 posttest aerosol calculations are summarized in Table 1. Aerosol source rate data are presented in Table 2. These were not included with the floppy disk data but were provided later.[3] Table 3 presents steam condensation rate data, and Table 4 presents CSTF atmosphere mol fraction data.[2] These steam condensation rates, which were supplied to the code analysts for their convenience, were calculated as equal to the inlet steam flow rate minus the rate of change of steam in the containment atmosphere minus the

Table 1. Summary of information needed for LA4 blind posttest vessel calculations

Code input data	Where information found[a]
1. CSTF vessel geometry, properties:	Tables 1,2,3,4: LA4AB10.TXT
2. Aerosol source rates:	Tables 12,13: LA4AB10.TXT
3. Aerosol source time:	CsOH: 0 to 1830 s CsOH+MnO: 1830 to 3030 s MnO: 3030 to 4812 s
4. Aerosol source particle size:	Table 14: LA4AB10.TXT
5. Aerosol agglomerate density and shape factor:	To be specified by code user. THEORETICAL SOLID DENSITY, CsOH = 3.68 g/cm^3 MnO = 5.44 g/cm^3 Dynamic shape factor estimated by HEDL to be 1.85
6. Test vessel temperatures:	Spacial-average values are in Tables A.1-A.2: LA4AB10.DAT Spacial variations are in Tables B1-B14: LA4AB11.DAT, LA4AB20.DAT-LA4AB23.DAT, LA4AB30.DAT-LA4AB32.DAT Thermocouple locations are in Section I.12: LA4AB10.TXT
7. Test vessel pressures:	Table A.1: LA4AB10.DAT
8. Vent flow rates from vessel:	Gas leak rates and pressures in Table C.2: LA4AB41.DAT Leak path temperature Table C.3: LA4AB42.DAT
9. Gas-wall temperature gradients:	To be specified by code user. An option involves: Use of temperature vs distance-from-wall data in Tables B.8-B.10: LA4AB22.DAT and LA4AB23.DAT
10. Steam conditions in vessel:	Table F: LA4AB43.DAT
11. Steam Condensation rates:	Table D.2: LA4AB43.DAT

[a]Refers to tables on IBM-format floppy disks - supplied by HEDL staff-containing input conditions for LA4 blind posttest aerosol code calculations.

Table 2. Aerosol source rates for LA4 blind posttest calclulations

Time (s)	Mno feed rate (g/s)	CsOH feed rate (g/s)
78	0.0000	1.0100
288	0.0000	0.6757
738	0.0000	1.0840
1218	0.0000	1.0673
1698	0.0000	0.9745
1902	0.9555	0.8739
2121	1.0909	0.9075
2532	0.7018	0.9883
2748	0.7178	1.0189
2952	0.5403	0.7556
3204	0.5811	0.0000
3438	1.1903	0.0000
3858	0.6895	0.0000
4338	0.5996	0.0000
4764	0.5052	0.0000

Table 3. Steam condensation rates

Time (min)	Steam condensation Rate[a] (g/s)	Steam condensation Cumulative (kg)	Time (min)	Steam condensation Rate[a] (g/s)	Steam condensation Cumulative (kg)
0.3	49.5	0.9	34.9	67.9	185.5
0.9	245.2	9.7	35.6	69.0	188.4
1.6	171.9	16.9	36.3	80.6	191.8
2.3	143.7	23.0	36.8	61.2	193.6
2.9	175.1	29.3	37.6	82.2	197.6
3.6	123.4	34.5	38.4	63.6	200.6
4.3	106.3	38.9	38.9	93.2	203.4
4.9	114.7	43.1	39.6	75.0	206.6
5.6	125.1	48.3	40.3	70.0	209.5
6.3	116.5	53.2	40.9	75.1	212.2
6.9	99.7	56.8	41.6	71.7	215.2
7.6	104.6	61.2	42.3	79.5	218.6
8.3	98.3	65.3	42.9	114.1	222.7
8.9	101.2	69.0	43.6	62.2	225.3
9.6	88.7	72.7	44.3	49.6	227.4
10.3	65.4	75.4	44.9	80.9	230.3
10.9	87.3	78.6	45.6	78.6	233.6
11.6	74.3	81.7	46.3	77.4	236.8
12.3	91.9	85.5	46.9	78.1	239.6
12.9	81.3	88.5	47.6	73.0	242.7
13.6	71.5	91.5	48.4	95.1	247.3
14.3	75.3	94.6	49.0	68.2	249.7
14.9	75.3	97.3	49.6	64.0	252.0
15.6	78.1	100.6	50.3	75.9	255.2
16.3	88.2	104.3	50.9	89.6	258.4
16.9	64.3	106.6	51.6	74.8	261.6
17.6	81.1	110.1			
18.3	85.4	113.6			
18.9	82.1	116.6			
19.6	75.8	119.8			
20.3	77.7	123.0			
20.9	86.0	126.1			
21.6	63.3	128.8			
22.3	88.0	132.5			
22.9	74.7	135.2			
23.6	79.5	138.5			
24.3	82.7	142.0			
24.9	87.4	145.1			
25.6	72.3	148.2			

Table 3. Steam condensation rates (continued)

Time (min)	Steam condensation Rate[a] (g/s)	Steam condensation Cumulative (kg)	Time (min)	Steam condensation Rate[a] (g/s)	Steam condensation Cumulative (kg)
52.3	81.3	265	78.3	61.8	384.6
52.9	101.4	268.7	78.9	65.1	387
53.6	79.9	272	79.6	138.9	392.8
54.3	70.1	275	80.3	12.3	393.3
54.9	101.1	278.6	80.9	67.1	395.7
55.6	88	282.3	81.6	94.6	399.7
56.3	56.1	284.6	82.3	83.8	403.2
56.9	108.4	288.5	82.9	73.1	405.9
57.6	79.1	291.9	83.6	62.1	408.5
58.3	69.7	294.8	84.3	62	411.1
58.9	77.4	297.6	84.9	73.4	413.7
59.6	74	300.7	85.6	59.9	416.2
60.3	72.2	303.7	86.3	48.4	418.3
60.9	66.4	306.1	86.9	49.8	420
61.6	82.6	309.6	87.6	55.7	422.4
62.3	77.5	312.8	88.3	31	423.7
62.9	65.7	315.2	88.9	51.7	425.6
63.6	74.7	318.3	89.6	55.8	427.9
64.3	79.4	321.7	90.3	40.3	429.6
64.9	76	324.4	90.9	45	431.2
65.6	78.2	327.7	91.6	36.8	432.8
66.3	78.1	331	92.3	46	434.7
66.9	62.8	333.2	92.9	37.1	436
67.6	81.5	336.7	93.6	33.3	437.4
68.3	71	339.6	94.3	57.6	439.8
68.9	98.8	343.2	94.9	55.3	441.8
69.6	51.2	345.3	95.6	40.8	443.5
70.3	73	348.4	96.3	30.6	444.8
70.9	81.7	351.4	96.9	27	445.8
71.6	75.5	354.5	97.6	37.9	447.4
72.3	81.5	357.9	98.3	40.7	449.1
72.9	82.9	360.9	98.9	29.1	450.1
73.6	74.1	364	99.6	38.3	451.8
74.3	56.8	366.4	100.9	43.4	455.1
74.9	66.9	368.8	102.3	20.4	456.9
75.6	91.9	372.7	103.6	39.4	459.9
76.3	75.7	375.9	104.9	36.6	462.8
76.9	58.4	378	106.3	36.9	465.9
77.6	96.1	382	107.6	32.4	468.4

Table 3. Steam condensation rates (continued)

Time (min)	Steam condensation Rate[a] (g/s)	Steam condensation Cumulative (kg)	Time (min)	Steam condensation Rate[a] (g/s)	Steam condensation Cumulative (kg)
108.9	36	471.2	186	27.7	619
110.3	35.5	474.2	188	33.6	623.1
111.6	30.3	476.6	190	31.9	626.9
114.0	34.2	481.5	192	33.1	630.9
116.0	31.2	485.2	194	28.7	634.3
118.0	36.2	489.6	196	32.4	638.2
120.0	33.9	493.6	198	32.8	642.2
122.0	31.1	497.4	200	30.8	645.8
124.0	35.2	501.6	202	29.4	649.4
126.0	31.7	505.4	204	29.0	652.9
128.0	32.1	509.3	206	35.6	657.1
130.0	28.2	512.7	208	29.1	660.6
132.0	31.3	516.4	210	28.6	664.1
134.0	38.9	521.1	212	30.7	667.7
136.0	26.4	524.2	214	30.8	671.4
138.0	40.2	529.1	216	31.0	675.2
140.0	26.7	532.3	218	30.5	678.8
142.0	33.3	536.3	220	29.0	682.3
144.0	28.1	539.6	222	30.0	685.9
146.0	30.1	543.3	224	29.3	689.4
148.0	30.7	546.9	226	31.1	693.1
150.0	29.7	550.5	228	28.0	696.5
152.0	32.1	554.4	230	29.7	700.0
154.0	34.0	558.4	232	31.6	703.8
156.0	34.9	562.6	234	26.4	707.0
158.0	25.6	565.7	236	31.8	710.8
160.0	33.6	569.7	238	27.1	714.1
162.0	31.7	573.5	240	24.0	717.0
164.0	35.8	577.8	242	38.9	721.6
166.0	31.3	581.6	244	27.4	724.9
168.0	28.0	584.9	246	32.2	728.8
170.0	33.7	589.0	248	27.5	732.1
172.0	31.7	592.8	250	37.0	736.5
174.0	32.6	596.7	252	22.4	739.2
176.0	31.3	600.5	254	39.5	743.9
178.0	31.2	604.2	256	23.1	746.7
180.0	29.6	607.8	258	27.2	750.0
182.0	30.8	611.4	260	30.8	753.7
184.0	35.5	615.7	262	32.2	757.5

Table 3. Steam condensation rates (continued)

Time (min)	Steam condensation Rate[a] (g/s)	Steam condensation Cumulative (kg)	Time (min)	Steam condensation Rate[a] (g/s)	Steam condensation Cumulative (kg)
264	30.1	761.1	342	-1.9	755.3
266	30.3	764.8	344	-0.5	755.3
268	26.1	767.9	346	-1.1	755.1
270	29.9	771.5	348	-4.4	754.6
272	28.8	775.0	350	1.3	754.8
274	39.7	779.7	352	-4.3	754.2
276	18.9	782.0	354	1.5	754.4
278	31.3	785.7	356	-1.9	754.2
280	35.1	790.0	358	1.0	754.3
282	25.5	793.0	360	-0.9	754.2
284	6.1	793.7	362	1.7	754.4
286	9.5	794.9	364	3.4	754.8
288	-7.7	793.9	366	6.4	755.6
290	-5.6	793.3	368	2.7	755.9
292	-22.4	790.6	370	1.9	756.1
294	-26.9	787.4	372	0.9	756.2
296	-24.7	784.4	374	1.1	756.4
298	-23.7	781.5	376	4.4	756.9
300	-23.4	778.7	378	3.1	757.3
302	-17.1	776.7	380	0.6	757.3
304	-19.6	774.3	382	8.7	758.4
306	-6.3	773.6	384	2.9	758.7
308	-15.3	771.7	386	8.3	759.7
310	-20.0	769.3	388	5.9	760.4
312	-16.4	767.4	390	10.4	761.7
314	-13.2	765.8	392	7.4	762.6
316	-18.6	763.5	394	12.4	764.1
318	-10.0	762.3	396	8,0	765.0
320	4.0	762.8	398	10.2	766.2
322	-18.6	760.6	400	10.0	767.4
324	-8.6	759.6	402	15.3	769.3
326	-7.5	758.7	404	14.1	771
328	-10.5	757.4	406	15.5	772.8
330	-4.8	756.8	408	14.8	774.6
332	-2.6	756.5	410	12.2	776.1
334	-4.6	756.0	412	18.1	778.2
336	-0.1	756.0	414	19.1	780.5
338	-2.5	755.7	416	15.8	782.4
340	-1.0	755.5	418	19.1	784.7

Table 3. Steam condensation rates (continued)

Time (min)	Steam condensation Rate[a] (g/s)	Steam condensation Cumulative (kg)	Time (min)	Steam condensation Rate[a] (g/s)	Steam condensation Cumulative (kg)
420	21.9	787.3	730	6.8	1127.7
422	20.8	789.8	740	6.6	1131.7
424	24.7	792.8	750	6.3	1135.4
426	19.4	795.1	760	6.3	1139.2
428	26.0	798.3	770	6.2	1142.9
430	17.3	800.3	780	5.6	1146.3
432	26.5	803.5	790	5.4	1149.5
434	26.2	806.6	800	5.4	1152.8
436	29.3	810.2	820	5.	1159.0
438	28.5	813.6	840	4.9	1164.9
440	27.0	816.8	860	4.7	1170.5
450	23.3	830.8	880	4.2	1175.5
460	25.4	846.1	900	5.2	1181.7
470	24.6	860.8	920	3.8	1186.2
480	25.7	876.2	940	4.0	1191.1
490	25.7	891.6	960	4.0	1195.9
500	26.3	907.4	980	4.1	1200.8
510	26.4	923.3	1000	3.5	1205.0
520	26.8	939.4	1020	3.4	1209.1
530	26.0	955.0	1040	3.3	1213.1
540	26.8	971.0	1060	3.3	1217.1
550	26.7	987.1	1080	2.9	1220.6
560	25.4	1002.3	1100	2.7	1223.8
570	26.1	1018.0	1120	2.9	1227.2
580	28.7	1035.2	1140	2.8	1230.6
590	24.7	1050.0	1160	2.6	1233.8
600	26.9	1066.1	1180	2.6	1236.9
610	13.6	1074.3	1200	3.1	1240.7
620	9.0	1079.6	1220	2.5	1243.7
630	9.2	1085.1	1240	2.5	1246.6
640	8.0	1089.9	1260	2.2	1249.3
650	7.4	1094.4	1280	2.4	1252.2
660	7.6	1099.0	1300	2.1	1254.7
670	7.2	1103.3	1360	2.0	1261.7
680	7.3	1107.7	1420	1.8	1268.0
690	6.9	1111.8	1480	1.4	1272.9
700	6.6	1115.8	1540	1.3	1277.5
710	6.9	1119.9	1600	1.1	1281.6
720	6.2	1123.6	1660	1.1	1285.6

Table 3. Steam condensation rates (continued)

Time (min)	Steam condensation Rate[a] (g/s)	Steam condensation Cumulative (kg)	Time (min)	Steam condensation Rate[a] (g/s)	Steam condensation Cumulative (kg)
1720.0	1.1	1289.4	6462.3	0	1368.6
1846.5	1.0	1297	6582.3	0	1368.8
1966.5	0.9	1303.3	6702.3	0	1369.0
2086.5	0.8	1309.0	6822.3	0	1369.2
2206.5	0.7	1314.1	6942.3	0	1369.5
2326.5	0.6	1318.8	7062.3	0	1369.4
2446.5	0.6	1323.0	7182.3	-0.1	1368.7
2566.5	0.5	1326.7			
2686.	0.5	1330.1			
2806.5	0.4	1333.1			
2926.5	0.4	1336.0			
3046.5	0.5	1339.3			
3166.5	0.4	1342.2			
3286.5	0.3	1344.5			
3406.5	0.3	1346.6			
3526.5	0.3	1348.5			
3646.5	0.2	1350.3			
3766.5	0.2	1351.8			
3886.5	0.2	1353.2			
4006.5	0.2	1354.4			
4126.5	0.2	1355.7			
4246.5	0.2	1356.8			
4366.5	0.1	1357.8			
4486.5	0.1	1358.6			
4606.5	0.1	1359.4			
4726.5	0.1	1360.1			
4846.5	0.1	1360.6			
4966.5	0.1	1361.1			
5086.5	0.1	1361.7			
5206.5	0.1	1362.3			
5326.5	0.1	1362.7			
5446.5	0.1	1363.2			
5566.5	0.1	1363.7			
5692.3	0.1	1364.8			
5812.3	0.4	1368.0			
5932.3	0.0	1367.7			
6102.3	0.0	1368.0			
6222.3	0.0	1368.2			
6342.3	0.0	1368.4			

[a]Condensation rate is an average value for the time period from previous time to time for which condensation rate is given.

Table 4. Steam mol fractions in CSTF atmosphere.

Time (min)	Saturated steam mol fraction Upper cell	Saturated steam mol fraction Lower cell	Time (min)	Saturated steam mol fraction Upper cell	Saturated steam mol fraction Lower cell
0.3	0.4721	0.2996	34.9	0.4410	0.2202
0.9	0.4690	0.2922	35.6	0.4408	0.2213
1.6	0.4672	0.2858	36.3	0.4403	0.2196
2.3	0.4658	0.2838	36.8	0.4401	0.2191
2.9	0.4632	0.2809	37.6	0.4395	0.2198
3.6	0.4623	0.2752	38.4	0.4396	0.2187
4.3	0.4622	0.2689	38.9	0.4389	0.2173
4.9	0.4613	0.2675	39.6	0.4383	0.2195
5.6	0.4599	0.2636	40.3	0.4383	0.2171
6.3	0.4589	0.2597	40.9	0.4377	0.2179
6.9	0.4582	0.2578	41.6	0.4376	0.2168
7.6	0.4574	0.2539	42.3	0.4369	0.2178
8.3	0.4567	0.2527	42.9	0.4350	0.2184
8.9	0.4557	0.2504	43.6	0.4350	0.2182
9.6	0.4551	0.2478	44.3	0.4356	0.2187
10.3	0.4552	0.2476	44.9	0.4350	0.2183
10.9	0.4543	0.2462	45.6	0.4344	0.2177
11.6	0.4538	0.2456	46.3	0.4340	0.2181
12.3	0.4527	0.2456	46.9	0.4334	0.2173
12.9	0.4520	0.2458	47.6	0.4332	0.2183
13.6	0.4517	0.2448	48.4	0.4316	0.2179
14.3	0.4513	0.2434	49.0	0.4316	0.2179
14.9	0.4507	0.2413	49.6	0.4316	0.2183
15.6	0.4500	0.2401	50.3	0.4313	0.2181
16.3	0.4488	0.2400	50.9	0.4304	0.2185
16.9	0.4489	0.2376	51.6	0.4300	0.2173
17.6	0.4480	0.2381	52.3	0.4292	0.2168
18.3	0.4471	0.2358	52.9	0.4279	0.2177
18.9	0.4463	0.2359	53.6	0.4274	0.2165
19.6	0.4457	0.2355	54.3	0.4272	0.2171
20.3	0.4450	0.2350	54.9	0.4259	0.2160
20.9	0.4441	0.2344	55.6	0.4250	0.2146
21.6	0.4443	0.2332	56.3	0.4255	0.2169
22.3	0.4436	0.2315	56.9	0.4238	0.2161
22.9	0.4432	0.2300			
23.6	0.4428	0.2285			
24.3	0.4420	0.2303			
24.9	0.4411	0.2287			
25.6	0.4409	0.2269			
26.3	0.4404	0.2265			
26.9	0.4402	0.2271			
27.6	0.4404	0.2266			
28.3	0.4397	0.2240			

Table 4. Steam mol fractions in CSTF atmosphere (continued).

Time (min)	Saturated steam mol fraction Upper cell	Lower cell	Time (min)	Saturated steam mole fraction Upper cell	Lower cell
57.6	0.4233	0.215	86.3	0.4004	0.2102
58.3	0.4232	0.2149	86.9	0.3997	0.211
58.9	0.4225	0.2167	87.6	0.3989	0.2109
59.6	0.4221	0.2168	88.3	0.3987	0.2122
60.3	0.422	0.2156	88.9	0.398	0.2118
60.9	0.4217	0.2165	89.6	0.3971	0.2115
61.6	0.4213	0.2145	90.3	0.3968	0.2115
62.3	0.4208	0.2164	90.9	0.3965	0.2099
62.9	0.4207	0.2154	91.6	0.3961	0.2124
63.6	0.4203	0.2154	92.3	0.3955	0.211
64.3	0.4198	0.2145	92.9	0.3952	0.2114
64.9	0.4194	0.2151	93.6	0.3951	0.2111
65.6	0.4189	0.2152	94.3	0.3941	0.212
66.3	0.4183	0.2156	94.9	0.3932	0.2118
66.9	0.4185	0.2138	95.6	0.3929	0.2115
67.6	0.4179	0.2146	96.3	0.393	0.2105
68.3	0.4176	0.2151	96.9	0.3929	0.2143
68.9	0.4165	0.2136	97.6	0.3927	0.2134
69.6	0.417	0.2148	98.3	0.3922	0.213
70.3	0.417	0.2138	98.9	0.3923	0.2131
70.9	0.4162	0.2146	99.6	0.392	0.2118
71.6	0.4161	0.2125	100.9	0.3909	0.2166
72.3	0.4154	0.2136	102.3	0.3917	0.2159
72.9	0.4148	0.2131	103.6	0.391	0.2155
73.6	0.4144	0.2138	104.9	0.3905	0.2161
74.3	0.4149	0.2133	106.3	0.3899	0.2155
74.9	0.4147	0.2144	107.6	0.3897	0.2165
75.6	0.4138	0.2134	108.9	0.3892	0.2178
76.3	0.4134	0.213	110.3	0.3889	0.2167
76.9	0.4138	0.2113	111.6	0.3887	0.2176
77.6	0.4125	0.2127	114	0.3881	0.2183
78.3	0.4128	0.2115	116	0.388	0.2192
78.9	0.4127	0.2116	118	0.3873	0.2179
79.6	0.4122	0.2132	120	0.3867	0.2185
80.3	0.4119	0.2104	122	0.3867	0.2198
80.9	0.4111	0.2121	124	0.3861	0.2204
81.6	0.4087	0.2119	126	0.3858	0.2202
82.3	0.4069	0.2113	128	0.3854	0.2218
82.9	0.4055	0.2117	130	0.3855	0.2237
83.6	0.4046	0.2101	132	0.3852	0.2243
84.3	0.4033	0.2136	134	0.3841	0.225
84.9	0.4021	0.2109	136	0.3845	0.2255
85.6	0.4012	0.2106	138	0.3832	0.2264

Table 4. Steam mol fractions in CSTF atmosphere (continued).

Time (min)	Saturated steam mol fraction Upper cell	Saturated steam mol fraction Lower cell	Time (min)	Saturated steam mol fraction Upper cell	Saturated steam mol fraction Lower cell
140	0.3836	0.2262	226	0.3757	0.2483
142	0.3832	0.2279	228	0.3759	0.2481
144	0.3833	0.2273	230	0.3757	0.2494
146	0.3831	0.2305	232	0.3753	0.2519
148	0.3831	0.2298	234	0.3756	0.2523
150	0.383	0.2312	236	0.3753	0.2519
152	0.3826	0.2328	238	0.3754	0.2533
154	0.3822	0.2332	240	0.3759	0.2536
156	0.3817	0.2317	242	0.3749	0.2541
158	0.382	0.2336	244	0.375	0.2551
160	0.3816	0.2322	246	0.3748	0.2539
162	0.3813	0.2347	248	0.3748	0.2571
164	0.3809	0.2315	250	0.374	0.2562
166	0.3807	0.2323	252	0.3747	0.2573
168	0.3807	0.2345	254	0.3738	0.2564
170	0.3804	0.233	256	0.3744	0.2584
172	0.3801	0.2354	258	0.3745	0.2598
174	0.3798	0.2335	260	0.3745	0.259
176	0.3796	0.2341	262	0.3741	0.2602
178	0.3795	0.2349	264	0.3741	0.2607
180	0.3795	0.234	266	0.374	0.2607
182	0.3794	0.2359	268	0.3743	0.2618
184	0.379	0.2338	270	0.3742	0.2628
186	0.3791	0.2372	272	0.3743	0.2634
188	0.3787	0.2358	274	0.3733	0.2647
190	0.3785	0.2352	276	0.3744	0.2653
192	0.3781	0.2345	278	0.3741	0.2658
194	0.3782	0.2353	280	0.3744	0.2644
196	0.3778	0.2361	282	0.3743	0.2635
198	0.3774	0.2361	284	0.3758	0.2647
200	0.3773	0.2353	286	0.3771	0.265
202	0.3774	0.2374	288	0.3801	0.2654
204	0.3775	0.2376	290	0.3824	0.2676
206	0.3769	0.2371	292	0.3849	0.2689
208	0.377	0.2374	294	0.3881	0.2716
210	0.377	0.2384	296	0.3911	0.2759
212	0.3769	0.2402	298	0.3944	0.2763
214	0.3767	0.2398	300	0.3976	0.2798
216	0.3763	0.2417	302	0.4001	0.2825
218	0.3762	0.2442	304	0.4033	0.2848
220	0.3761	0.2443	306	0.4046	0.2867
222	0.376	0.2451	308	0.4075	0.2908
224	0.376	0.2473	310	0.4112	0.2949

Table 4. Steam mol fractions in CSTF atmosphere (continued)

Time (min)	Saturated steam mol fraction Upper cell	Saturated steam mol fraction Lower cell	Time (min)	Saturated steam mol fraction Upper cell	Saturated steam mol fraction Lower cell
312	0.4144	0.2959	398	0.5442	0.424
314	0.4176	0.2982	400	0.5469	0.4265
316	0.4214	0.3023	402	0.5483	0.4287
318	0.4242	0.3034	404	0.5501	0.4326
320	0.4251	0.3066	406	0.5516	0.4327
322	0.4294	0.3091	408	0.5533	0.4356
324	0.4326	0.3125	410	0.5556	0.4378
326	0.4355	0.3166	412	0.5568	0.4407
328	0.4393	0.319	414	0.558	0.4406
330	0.4421	0.3229	416	0.5603	0.4423
332	0.4449	0.324	418	0.5616	0.4455
334	0.4479	0.3297	420	0.5627	0.4459
336	0.4503	0.3307	422	0.5638	0.4502
338	0.4533	0.3345	424	0.5642	0.4521
340	0.456	0.3374	426	0.5657	0.4546
342	0.4587	0.3409	428	0.5662	0.4556
344	0.4615	0.3438	430	0.5691	0.4585
346	0.4645	0.3464	432	0.5693	0.4571
348	0.4683	0.3483	434	0.5706	0.4601
350	0.4712	0.3507	436	0.5714	0.4596
352	0.4749	0.3539	438	0.5721	0.463
354	0.4777	0.3573	440	0.573	0.4648
356	0.4812	0.3609	450	0.5765	0.4711
358	0.4845	0.3642	460	0.5769	0.4763
360	0.4879	0.3685	470	0.5781	0.4778
362	0.4912	0.3706	480	0.5784	0.4803
364	0.4942	0.3739	490	0.5788	0.4844
366	0.4965	0.3766	500	0.579	0.4871
368	0.4998	0.3805	510	0.5787	0.4883
370	0.503	0.3846	520	0.5785	0.4884
372	0.5066	0.3864	530	0.5785	0.4932
374	0.5103	0.3911	540	0.5786	0.4939
376	0.5133	0.3934	550	0.5788	0.4957
378	0.5164	0.3982	560	0.5801	0.4967
380	0.5208	0.4033	570	0.58	0.4987
382	0.5228	0.4037	580	0.5775	0.4979
384	0.527	0.4069	590	0.5801	0.5001
386	0.5292	0.4092	600	0.5808	0.5011
388	0.5325	0.4123	610	0.5747	0.4926
390	0.5348	0.4152	620	0.5703	0.4847
392	0.5376	0.4186	630	0.5655	0.4779
394	0.5387	0.4219	640	0.5617	0.4709
396	0.5416	0.4219	650	0.5569	0.4648

Table 4. Steam mol fractions in CSTF atmosphere (continued)

Time (min)	Saturated steam mol fraction Upper cell	Saturated steam mol fraction Lower cell	Time (min)	Saturated steam mol fraction Upper cell	Saturated steam mol fraction Lower cell
660	0.5524	0.4577	1540	0.225	0.2275
670	0.5481	0.4527	1600	0.2168	0.2202
680	0.5436	0.4483	1660	0.2089	0.212
690	0.5389	0.4438	1720	0.2014	0.206
700	0.5348	0.4393	1846.5	0.1863	0.1896
710	0.53	0.435	1966.5	0.1737	0.1769
720	0.5254	0.4314	2086.5	0.1625	0.1661
730	0.5208	0.4281	2206.5	0.1523	0.1555
740	0.5161	0.4249	2326.5	0.1432	0.1457
750	0.5117	0.4233	2446.5	0.1348	0.137
760	0.5076	0.4204	2566.5	0.1276	0.1299
770	0.5024	0.4193	2686.5	0.1209	0.1227
780	0.4983	0.4184	2806.5	0.1152	0.1177
790	0.4948	0.4161	2926.5	0.1097	0.1121
800	0.4901	0.4151	3046.5	0.1033	0.1041
820	0.4767	0.4087	3166.5	0.098	0.0989
840	0.4631	0.4015	3286.5	0.0936	0.0947
860	0.451	0.3945	3406.5	0.0894	0.0912
880	0.4401	0.3881	3526.5	0.0856	0.0873
900	0.4265	0.3814	3646.5	0.0823	0.0837
920	0.4167	0.3758	3766.5	0.0793	0.081
940	0.4062	0.37	3886.5	0.0766	0.0775
960	0.3958	0.3635	4006.5	0.0742	0.0754
980	0.385	0.3572	4126.5	0.0718	0.0727
1000	0.376	0.3501	4246.5	0.0697	0.0704
1020	0.3672	0.3449	4366.5	0.0679	0.0685
1040	0.3587	0.3383	4486.5	0.0663	0.0671
1060	0.3504	0.332	4606.5	0.065	0.0656
1080	0.3431	0.3249	4726.5	0.0638	0.0644
1100	0.336	0.3191	4846.5	0.0627	0.0629
1120	0.3291	0.3128	4966.5	0.0617	0.0618
1140	0.3221	0.3069	5086.5	0.0605	0.0607
1160	0.3152	0.3016	5206.5	0.0595	0.0596
1180	0.3087	0.2959	5326.5	0.0586	0.0587
1200	0.3011	0.2902	5446.5	0.0576	0.0577
1220	0.2948	0.2852	5566.5	0.0567	0.0566
1240	0.2881	0.281	5692.3	0.0547	0.0541
1260	0.2825	0.276	5812.3	0.0482	0.0488
1280	0.277	0.272	5932.3	0.0495	0.0498
1300	0.2721	0.2673	6102.3	0.049	0.0483
1360	0.2574	0.2552	6222.3	0.0487	0.048
1420	0.2438	0.243	6342.3	0.0484	0.0474
1480	0.2338	0.235	6462.3	0.0479	0.0468

Table 4. Steam mol fractions in CSTF atmosphere (continued)

Time (min)	Saturated steam mol fraction Upper cell	Lower cell
6582.3	0.0476	0.0463
6702.3	0.0471	0.0458
6822.3	0.0467	0.0453
6942.3	0.0462	0.0448
7062.3	0.0464	0.044
7182.3	0.0476	0.0443

outlet steam flow rate. The rate of change of steam in the containment was calculated as the change with respect to time of

$$(SF)PVM_w/RT \qquad (1)$$

where SF is the mol fraction of steam in the containment atmosphere (Table 4), P is pressure, V is volume, M_w is the molecular weight of water, R is the gas constant, and T is temperature. The condensation rates calculated in this manner are actually the sum of the steam condensation rate onto the wall and the steam condensation rate onto the aerosol. These condensation rates were provided to the code analysts for their use only if so desired. The analysts were free to use the method of their choice for determining condensation rates, and no recommendation was given as to any preferred method. The code analysts were also to provide estimates of other parameters such as aerosol shape factors, aerosol densities, and gas-wall temperature gradients.

Table 5 summarizes the requested code outputs for the LA4 posttest aerosol calculations. Code outputs were requested for 24 different times - 8 times for the aerosol source period and 16 times after the end of the source. These times corresponded to the times at which the experimental measurements were made.

In the LA4 posttest instruction letter,[2] guidelines were given for the calculation of the aerodynamic mass median diameter (AMMD) and the geometric standard deviation (GSD). The objective was to ensure that these parameters were calculated in a manner consistent with the experimental measurement of these same parameters by the cascade impactors. Appendixes A and B discuss the recommended methods for determining AMMD and GSD, respectively.

The LA4 participants were also requested to submit a summary of any major input parameter assumptions (other than those specified in the instruction letters) used in their code calculations. This would include parameters such as the assumed value for the thermal boundary-layer thickness. Futhermore, the code users were requested to provide copies of the actual computer input and the output for their codes.

Table 5. Summary of requested code output parameters for LA4 blind posttest vessel calculations

OUTPUT PARAMETERS AND UNITS FOR OUTPUT TIMES OF: 130; 760; 1,530; 1,830; 2,980; 4,780; 6,060; 10,440; 15,150; 16,320; 16,920; 18,600; 21,720; 25,380; 36,600; 57,120;.81,000; 98,400; and 168,000 SECONDS.

1. Suspended aerosol mass concentration (excluding water) - for MIXED aerosol and for EACH species (if possible) - in g/m^3.

2. Concentration of water condensed on airborne CsOH and ##0 aerosols - in g/m^3.

3. Cumulative aerosol (excluding water) settled in vessel - for MIXED aerosol and for EACH species (if possible) - in grams.

4. Cumulative aerosol (excluding water) plated on vessel walls and ceilings - for MIXED aerosol and for EACH species (if possible) - in grams. Also, tabulate the plated aerosol according to mechanism, if possible. Such mechanisms may include diffusiophoresis, thermophoresis, Brownian diffusion, etc.

5. Cumulative aerosol (excluding water) leaked from vessel through each leak path - for MIXED aerosol and for EACH species (if possible) - in grams.

6. The settling flux or the settling rate of aerosol (excluding water) - for MIXED aerosol and for EACH species (if possible) - in $g/(m^2s)$ or in g/s.

OUTPUT PARAMETERS AND UNITS FOR OUTPUT TIMES OF: 1,530; 2,640; 4,400; 6,060; 11,100; 15,150; 20,700; and 26,600 SECONDS:

1. The aerodynamic mass-median diametera (AMMD) - in microns - and the geometric standard deviation (GSD) - dimensionless - for MIXED aerosol and for EACH species (if possible).

2. "DISCRETE" code users should provide tables of aerosol (excluding water) mass - in grams - or mass concentration - in g/m_3 - in each size group - for MIXED aerosol and for EACH species (if possible). The mass or mass concentration of water condensed on the aerosol in each size group should be provided separately.

[a]AMMD should be determined (by "DISCRETE" code users) by plotting cumulative mass fraction vs <u>upper</u>, not average, bin size.

Finally, it was requested that the plated aerosol mass be tabulated according to deposition mechanism.

3. DESCRIPTION OF CODES USED IN PERFORMING LA4 CALCULATIONS

Blind posttest calculations for LACE test LA4 were performed by twelve investigators. Table 6 lists the codes used and the names of the code analysts. The results from the NAUA-5(ENEL) code included three cases. One case, designated as NAUA-5(NC,ENEL) (NC denoting no condensation), assumed no condensation of steam on the aerosol. The other two cases included condensation of steam on the aerosol. In one of these cases, designated as NAUA-5(C,ENEL C.R.) (C denoting condensation and C.R. denoting critical radius), the Kelvin effect was contained in the condensation model. In the remaining case, designated as NAUA-5(C,ENEL N.C.R.) (N.C.R. denoting no critical radius), the condensation model did not contain the Kelvin effect; and therefore, there was no critical particle radius below which condensation did not occur. In the text, the codes that calculated steam condensation on the aerosol are referred to as "wet" codes and the others as "dry" codes.

The MAAP-3 code assumes that the aerosol approaches an asymptotic size distribution. All other codes listed in Table 6 utilize a discrete particle size distribution (PSD) model. The "multicomponent" codes calculated particle compositions that varied with particle size. Such codes were AEROSIM-M(UK), CONTAIN(ORNL), CONTAIN(SANDIA), CONTAIN(UK), REMOVAL/2G(JN), and SWNAUA(US). All others were "single component" codes, which assumed the particle composition to be independent of particle size. The CONTAIN codes assume the density of the dry aerosol to be independent of particle composition (and, therefore, independent of particle size) and, under conditions of steam condensation on the aerosol, assume the density of water to be the same as the average density of the dry aerosol. The NAUA-type codes – NAUA(EPRI), NAUA-HYGROS(FN), NAUA(ENEL), NAUA(UNIV. ROME) and SWNAUA(US) – calculate the density of water at the existing conditions and, when steam condenses on the aerosol, account for the variation of density with particle size

Table 6. Summary of codes used for LA4 posttest vessel calculations

Code[a]	Code analysts	Affiliation
AEROSIM-M(UK)	S. A. Ramsdale I. H. Dunbar	United Kingdom, Safety and Reliability Directorate
CONTAIN(ORNL)	M. L. Tobias	United States, Oak Ridge National Laboratory
CONTAIN(SANDIA)	K. D. Bergeron	United States, Sandia National Laboratory
CONTAIN(UK)	P. N. Smith G. J. Roberts	United Kingdom, Atomic Energy Authority
MAAP-3(SW)	H. Haggblom	Sweden, Studsvik Energiteknik AB
MCT-2(US)	P. Bieniarz	United States, Risk Management Associates
NAUA-HYGROS(FN)	J. Jokiniemi	Finland, Technical Research Centre
NAUA(EPRI)	R. Sher	United States, Electric Power Research Institute
NAUA-5(ENEL,IT)	M. Valisi	Italy, ENEL-CRTN
NAUA-5(UNIV. ROME,IT)	L. Ferroni L. Sorabella F. Pagno	Italy, Energetics Department, University of Rome
REMOVAL/2G(JN)	K. Muramatsu	Japan, Atomic Energy Research Institute
SWNAUA(US)	A. Drozd J. Baron	United States, Stone and Webster

[a]Initials in parenthesis indicate country or organization.

which results from the variation of water content with particle size. The REMOVAL/2G(JN) code calculates the density of each particle size bin as a function of the aerosol composition of that bin. The density of each bin is then used to determine the settling rate for particles in that size bin.

The NAUA(EPRI), NAUA-HYGROS(FN), and SWNAUA(US) codes accounted for the hygroscopicity of the CsOH aerosol. AEROSIM-M(UK) takes as input the total condensation rate onto the airborne aerosols.

Information is presented in Table 7 that may be useful in interpreting the results that follow. The table lists the plating mechanisms invoked by the codes and other information for each code.

4. RESULTS OF LA4 POSTTEST CODE CALCULATIONS

The calculated and experimental aerosol concentrations in the CSTF vessel are plotted as a function of time in Figs. 2 through 7. Plots of total aerosol concentration and the concentration of each aerosol species, MnO and CsOH, are included. In all cases, the concentrations are those of the dry aerosol; i.e., any steam that has condensed on the aerosol is not included. The codes have been divided into two groups for the purpose of clarity, the NAUA-type codes comprising one of the groups. The MnO/CsOH mass ratio of the airborne aerosol is shown in Fig. 8.

Figures 9 and 10 shows the concentration of water that has condensed on the aerosol plotted vs time. Airborne liquid water measurements were performed by HEDL[6] using two droplet calorimeters. Because of the relatively slow response of these instruments to changes, no measurements were made during heatup and aerosol production. Also, the performance during the venting period was uncertain.

The cumulative dry aerosol mass leaked from the CSTF vessel as a function of time is presented in Figs. 11 and 12. The experimental

Table 7. Features of computer codes used for LA4 postest calculations

	Feature of code					
›de	Diffusio-phoresis[a]	Thermo-phoresis[a]	Diffusion[a,c]	Steam condensation on aerosol	Multi-component	Comments
:M-M(UK)	Yes	Yes	Yes	Yes	Yes	
:N(ORNL)	Yes	Yes	Yes	Yes	Yes	Calculated thermal-hydraulics
:N(SANDIA)	Yes	Yes	Yes	Yes	Yes	Calculated thermal-hydraulics
:N(UK)	Yes	Yes	Yes	Yes	Yes	Calculated thermal-hydraulics
›(SW)	No	Correlation	Inspection	No	No	Settled and plated aerosol mass were combined
US)	Yes	Yes	Yes	No	No	Settled and plated aerosol mass were combined
ſYGROS(FN)	Yes	No	Yes	Yes	No	
:PRI)	Yes	No	Yes	Yes	No	
›(IT)	Yes	No	Yes	b	No	
.L/2G(JN)	Yes	Yes	Yes	No	Yes	
›(US)	Yes	No	Yes	Yes	Yes	

lating mechanism
:ovided three cases, two with and one without code feature.
:ownian diffusion.

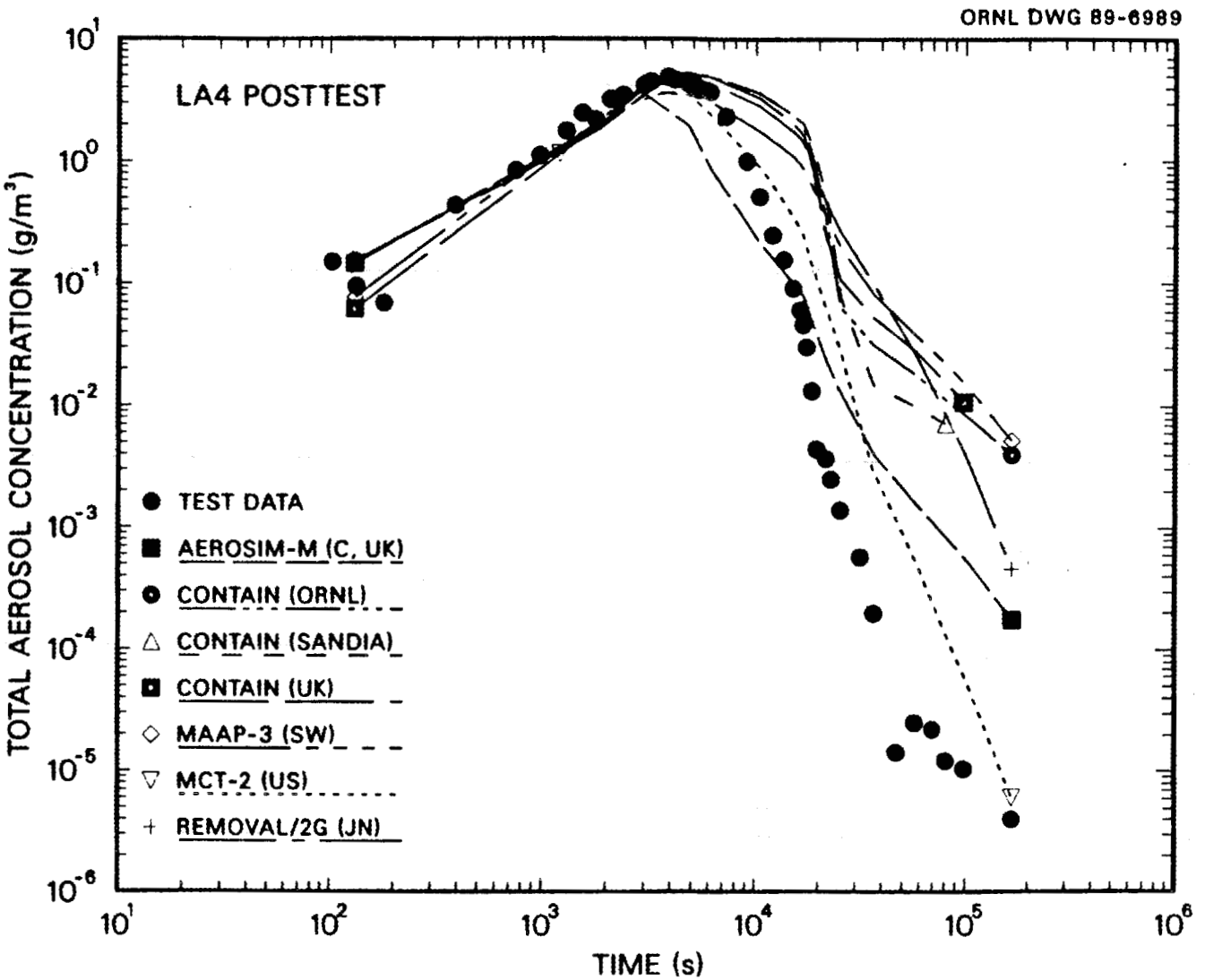

Fig. 2. LA4 posttest calculations - airborne MnO + CsOH aerosol concentration vs time - for group 1 codes.

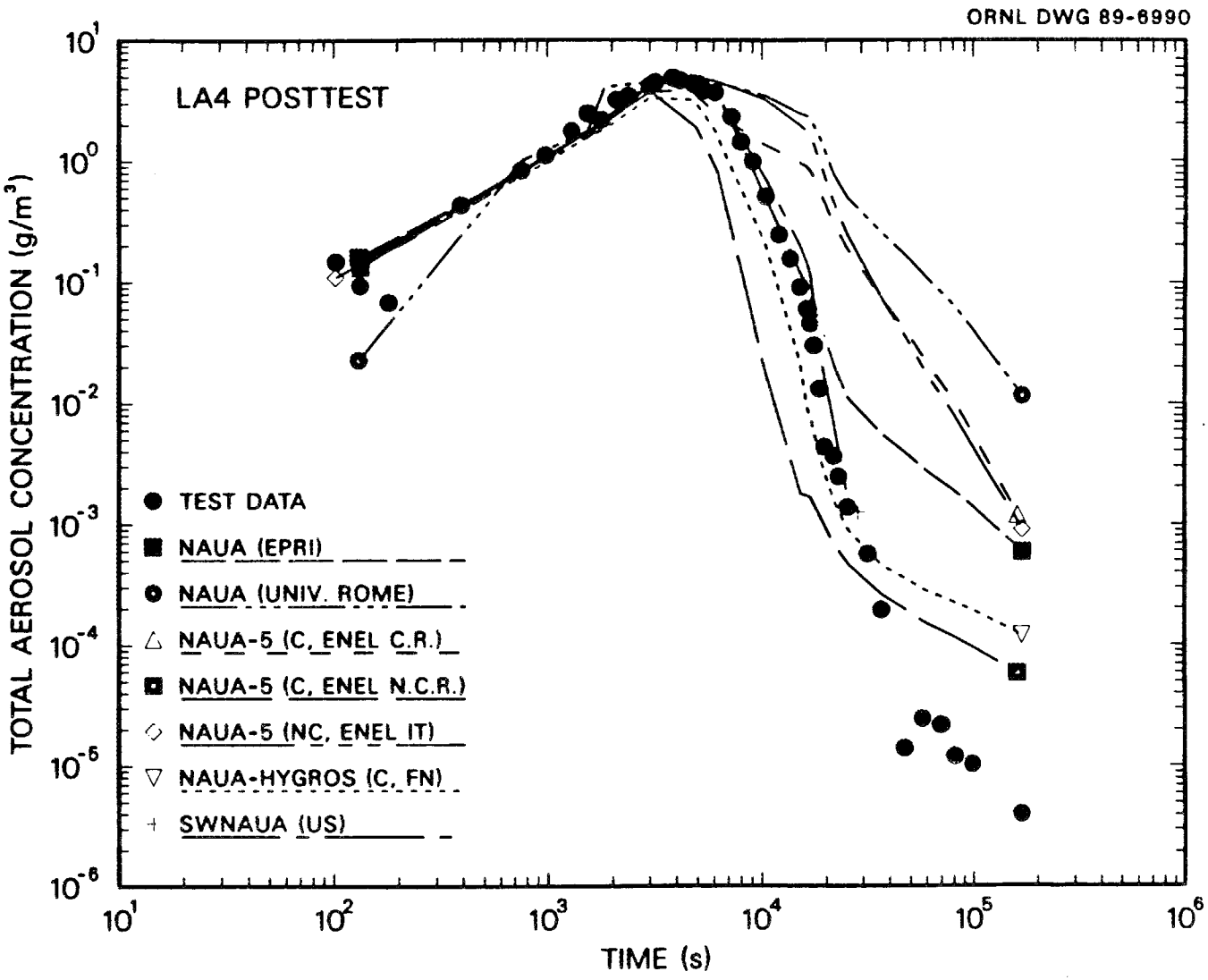

Fig. 3. LA4 posttest calculations - airborne MnO + CsOH aerosol concentration vs time - for group 2 codes.

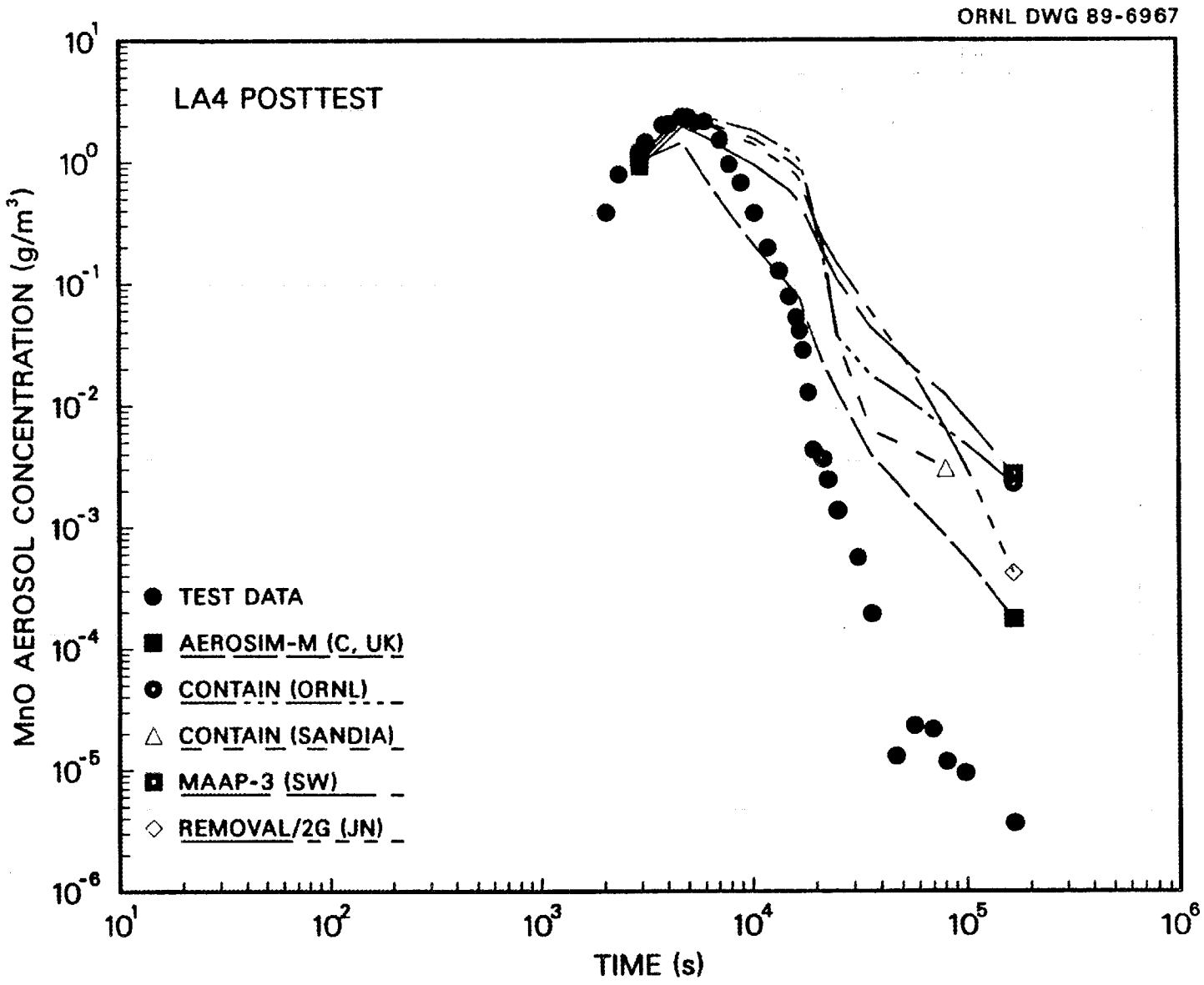

Fig. 4. LA4 posttest calculations - airborne MnO concentration vs time - for group 1 codes.

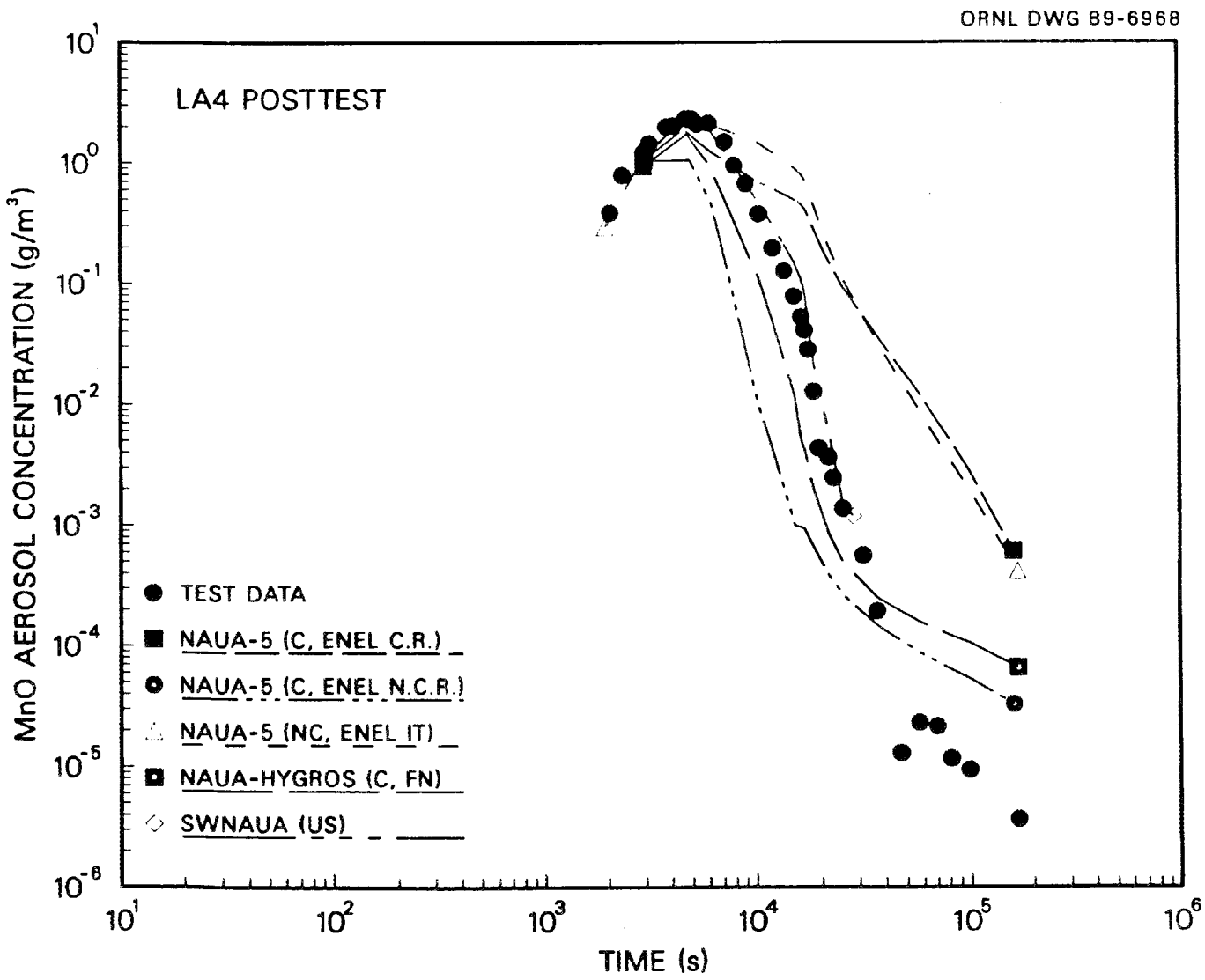

Fig. 5. LA4 posttest calculations - airborne MnO concentration vs time - for group 2 codes.

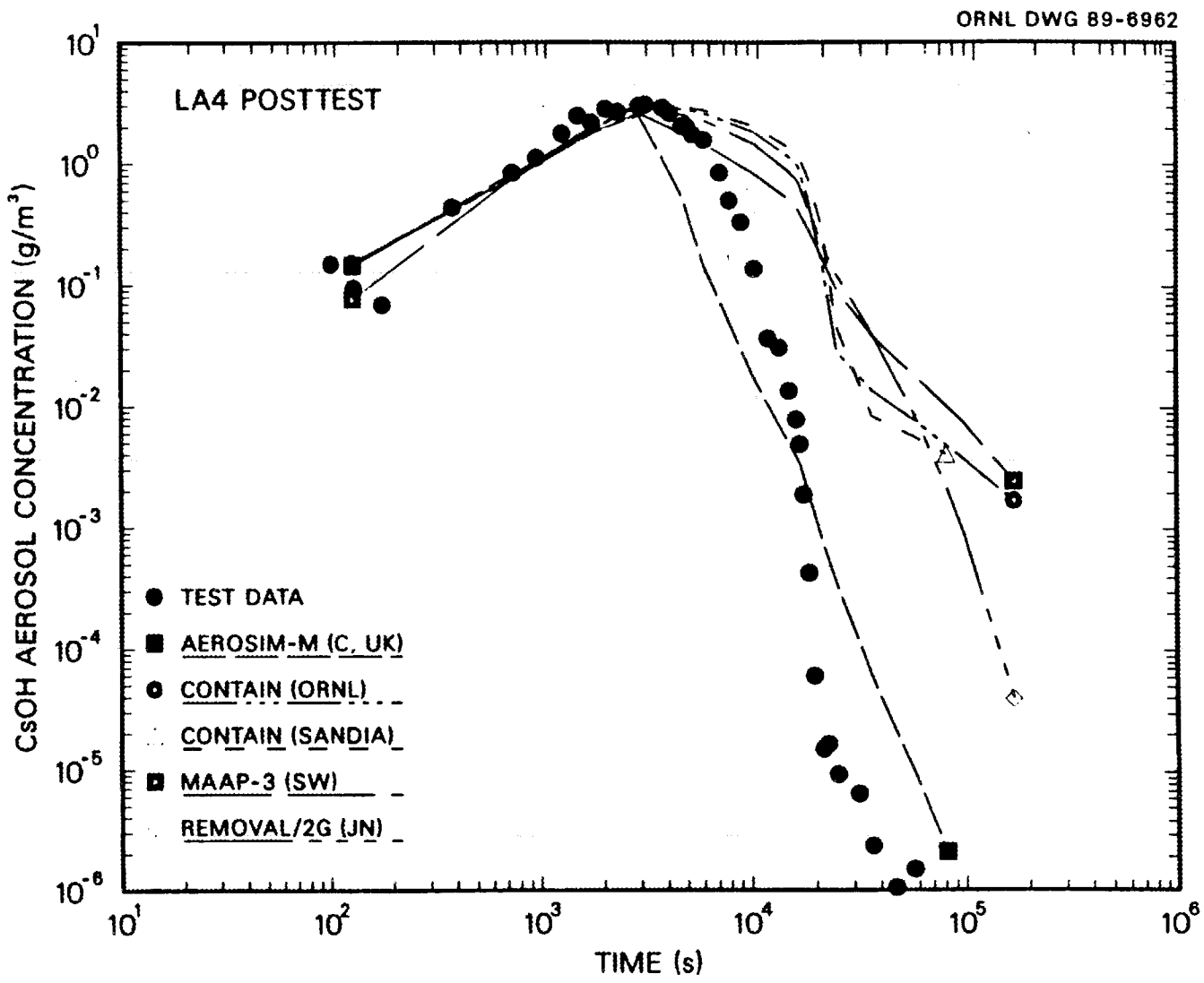

Fig. 6. LA4 posttest calculations - airborne CsOH concentration vs time - for group 1 codes.

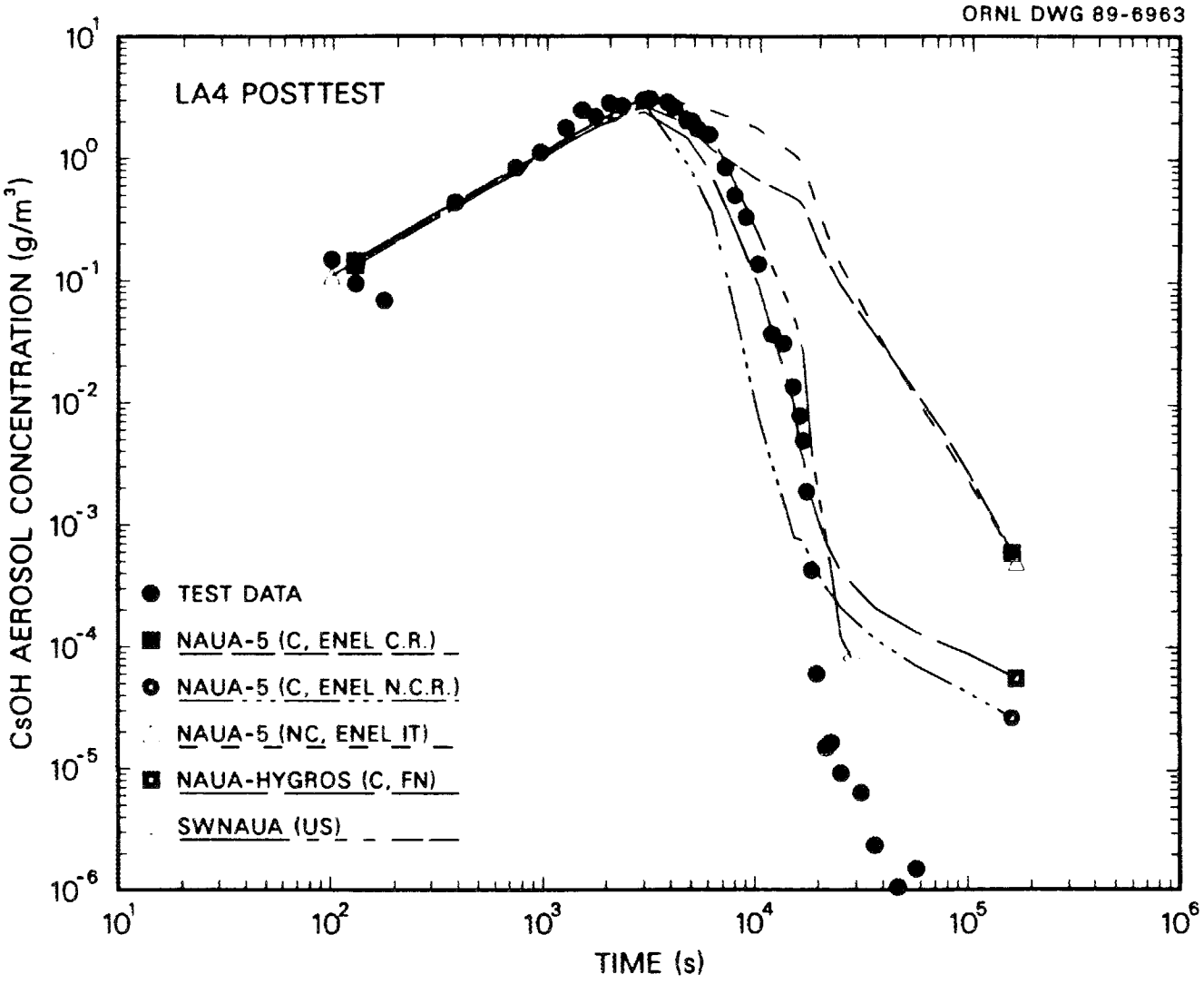

Fig. 7. LA4 posttest calculations - airborne CsOH concentration vs time - for group 2 codes.

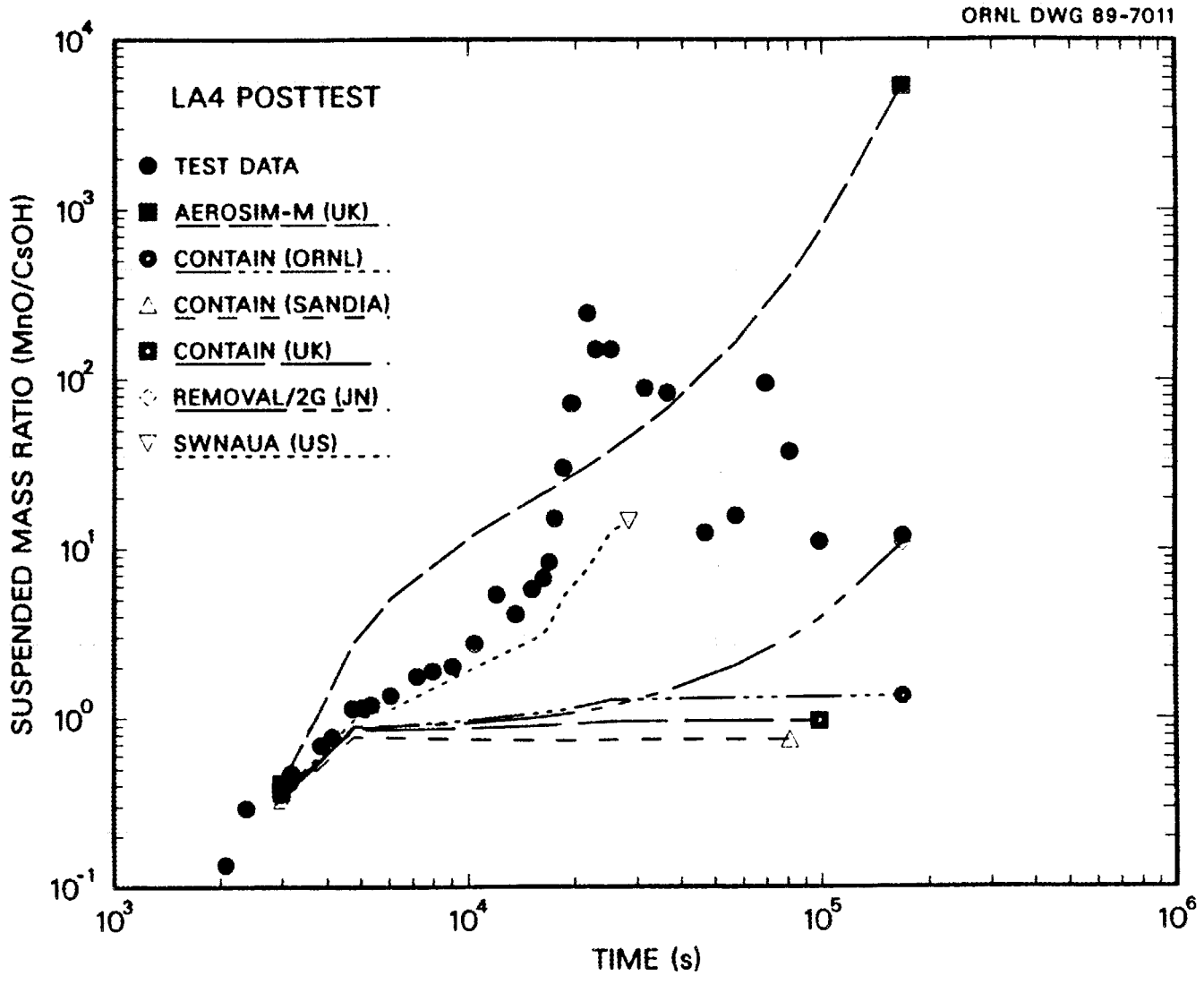

Fig. 8. LA4 posttest calculations - MnO/CsOH mass ratio of airborne aerosol vs time.

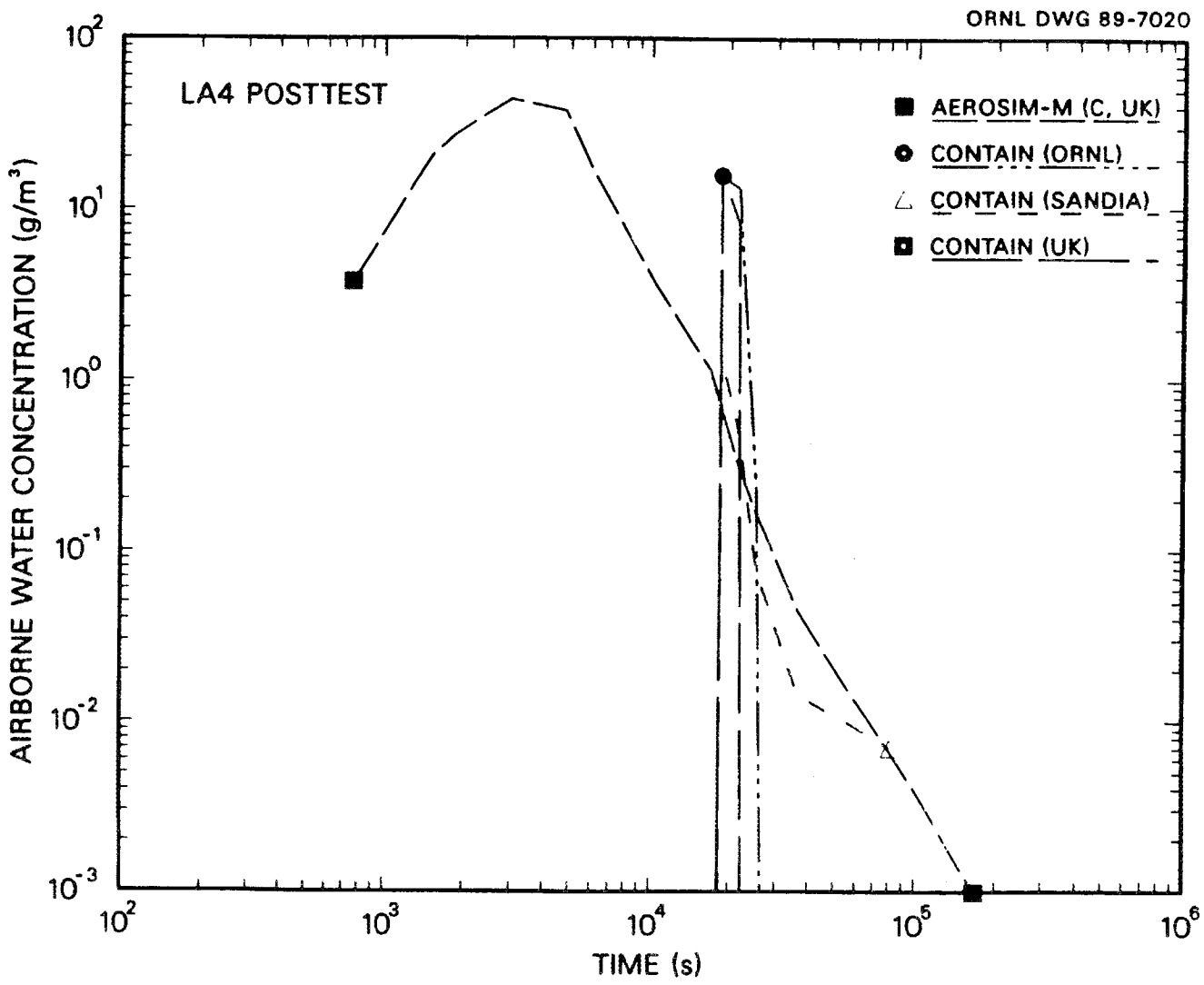

Fig. 9. LA4 posttest calculations - airborne water concentration vs time - for group 1 codes.

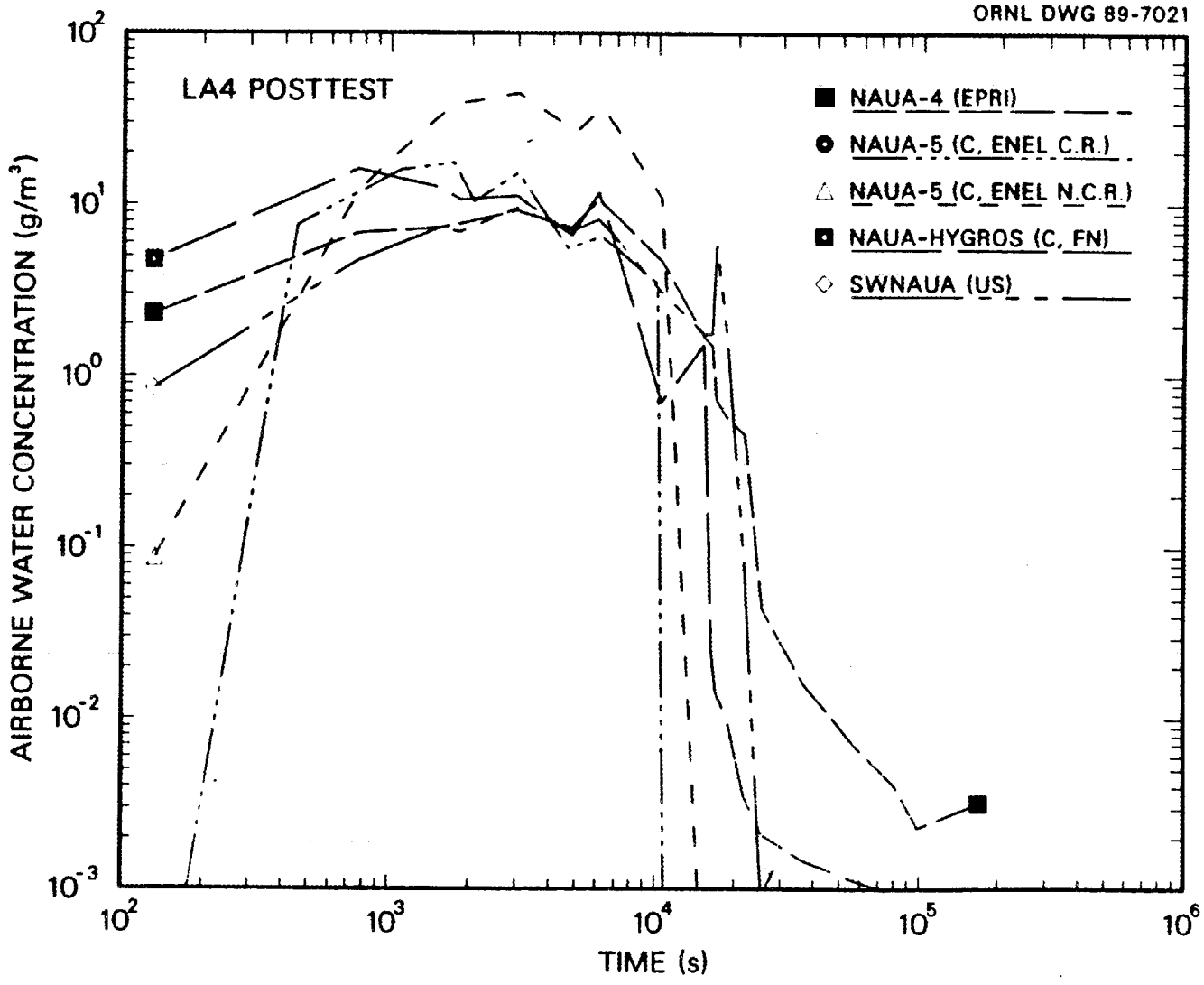

Fig. 10. LA4 posttest calculations - airborne water concentration vs time - for group 2 codes.

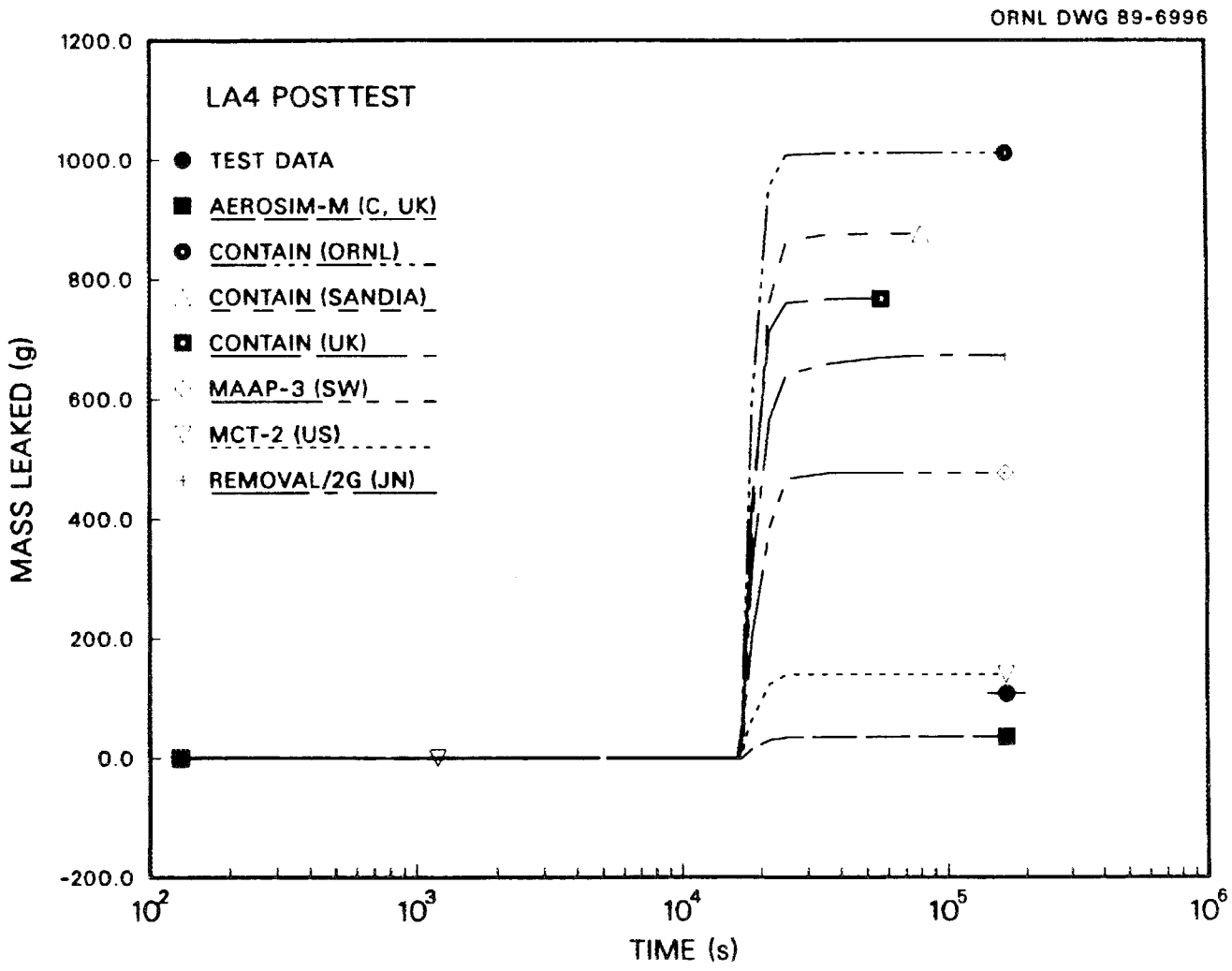

Fig. 11. LA4 posttest calculations - cumulative mass of aerosol leaked from CSTF vessel vs time - for group 1 codes.

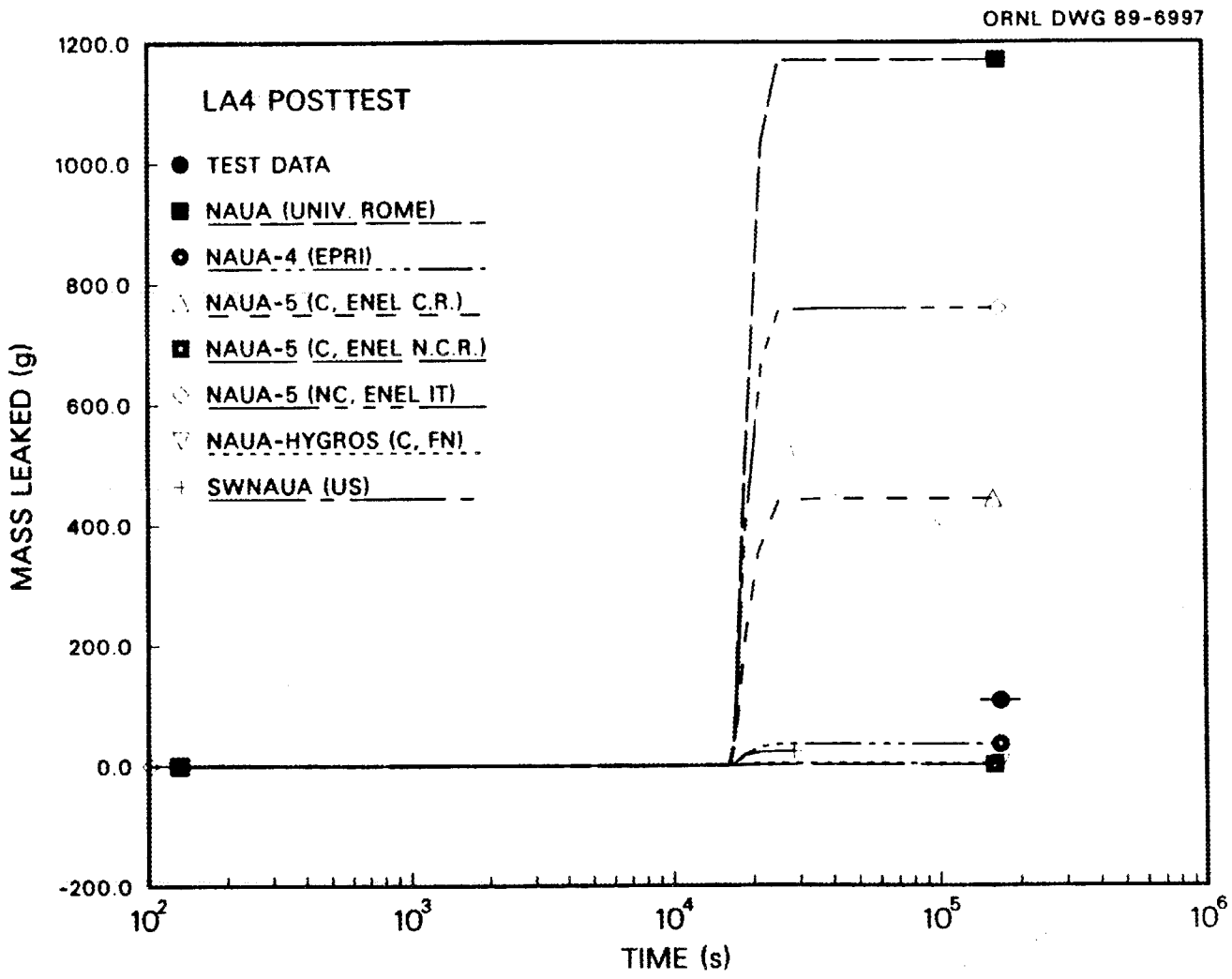

Fig. 12. LA4 posttest calculations - cumulative mass of aerosol leaked from CSTF vessel vs time - for group 2 codes.

value in Figs. 11 and 12 was determined by HEDL[6] by integrating over time the product of the CSTF vessel volumetric leak rate (as given in Table C.2 of File LA4AB41.DAT[5]) and the experimental aerosol concentration (as given in Table 6.21 of LACE TR-025[6]). The cumulative dry aerosol mass retained in the CSTF vessel as a function of time is shown in Figs. 13 and 14. The cumulative aerosol retained is equal to the sum of the cumulative settled and plated masses.

The settling velocity of the airborne aerosol is equal to the settling flux divided by the concentration of the aerosol. Figures 15 through 18 present the aerosol settling velocities as calculated from the settling flux and the airborne aerosol concentration values that were reported by the codes and that were measured experimentally. The ratio of the settling velocity of MnO to that of CsOH is shown in Fig. 19.

The cumulative dry mass of aerosol removed from the CSTF vessel atmosphere by settling is shown in Figs. 20 and 21. The MnO/CsOH mass ratio of the cumulative settled aerosol is shown in Figs. 22 and 23. Figures 24 and 25 show the cumulative dry mass of aerosol removed by plating and Figs. 26 and 27 present the MnO/CsOH mass ratio of the cumulative plated aerosol. Plating by thermophoresis and Brownian diffusion is presented in Fig. 28. All other plating occurred by diffusiophoresis.

The calculated and experimental values of the dry aerosol settling flux in the CSTF vessel are plotted as a function of time in Figs. 29 through 34. Plots of total dry aerosol settling flux and the settling flux of each aerosol species, MnO and CsOH, are included. The MnO/CsOH settling flux mass ratio is shown in Figs. 35 and 36.

The aerodynamic mass-median diameter (AMMD) of the mixed (MnO + CsOH) aerosol is plotted vs time in Figs. 37 and 38. Figures 39 and 40 show the AMMD values for the individual species. As discussed previously, the code users were requested to use the method described in Appendix A to calculate AMMD. We also calculated the AMMD according to Appendix A using the particle size distribution (PSD) data reported by the code analysts as requested in Table 5. The geometric standard

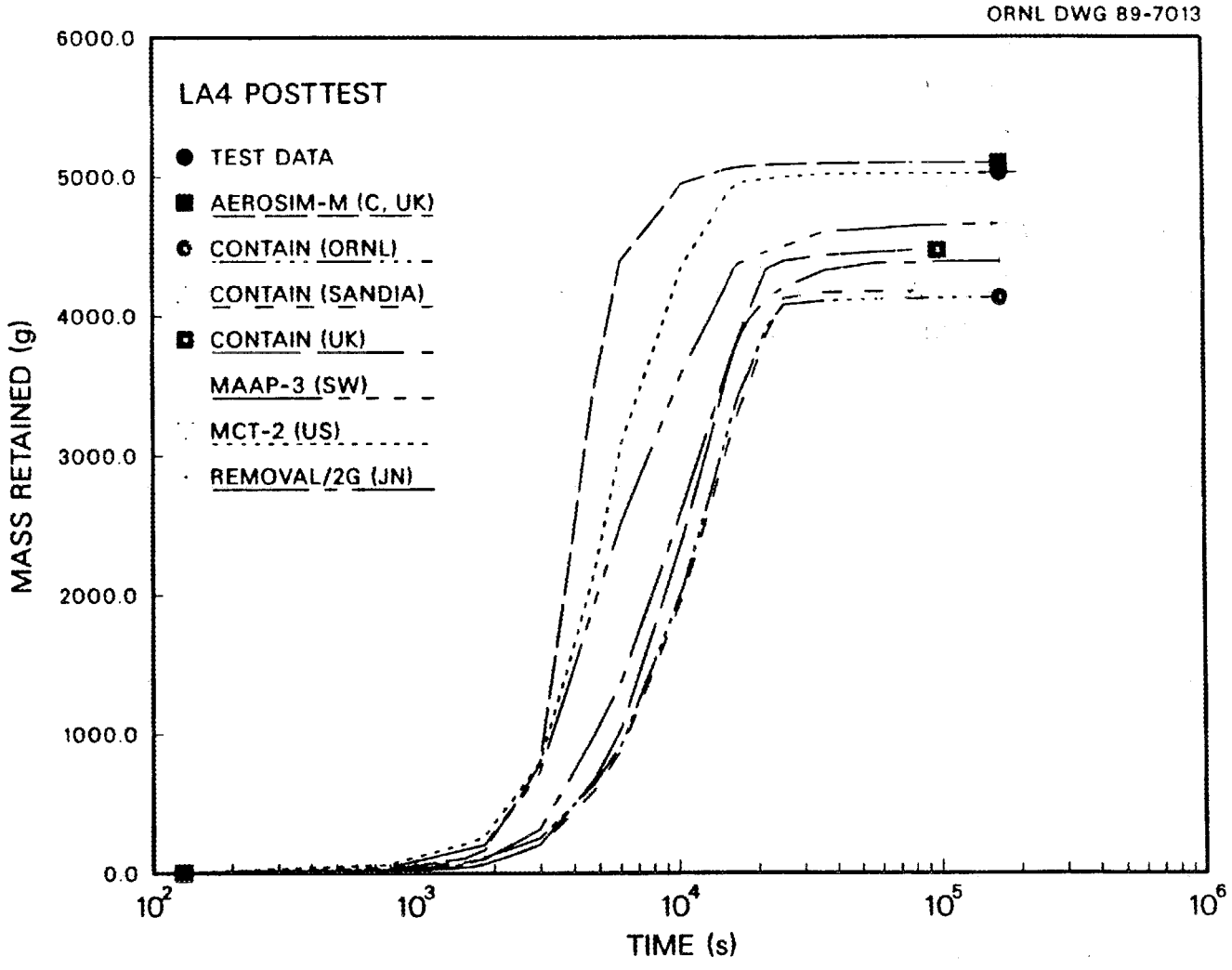

Fig. 13. LA4 posttest calculations - cumulative mass of aerosol retained in CSTF vessel vs time - for group 1 codes.

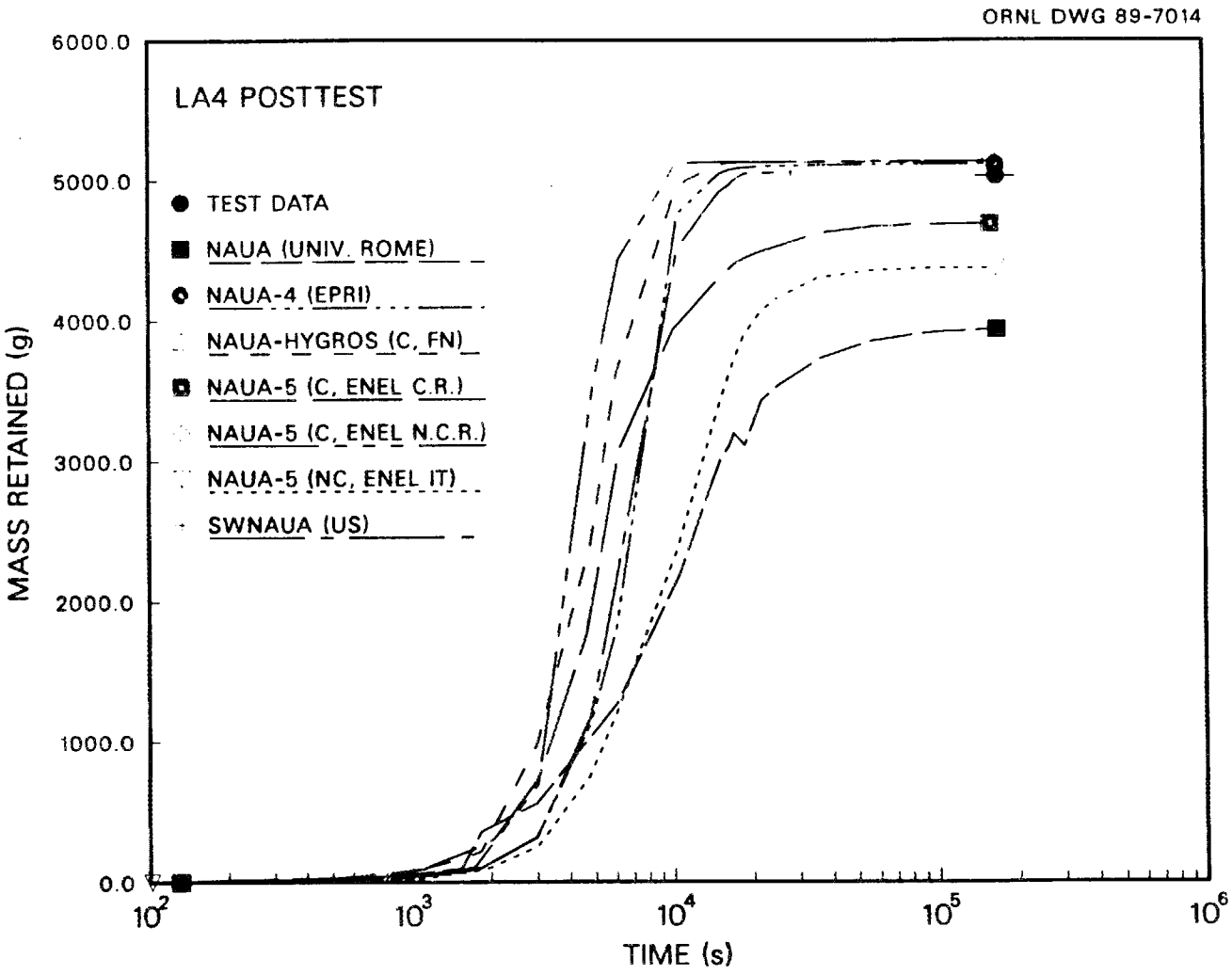

Fig. 14. LA4 posttest calculations - cumulative mass of aerosol retained in CSTF vessel vs time - for group 2 codes.

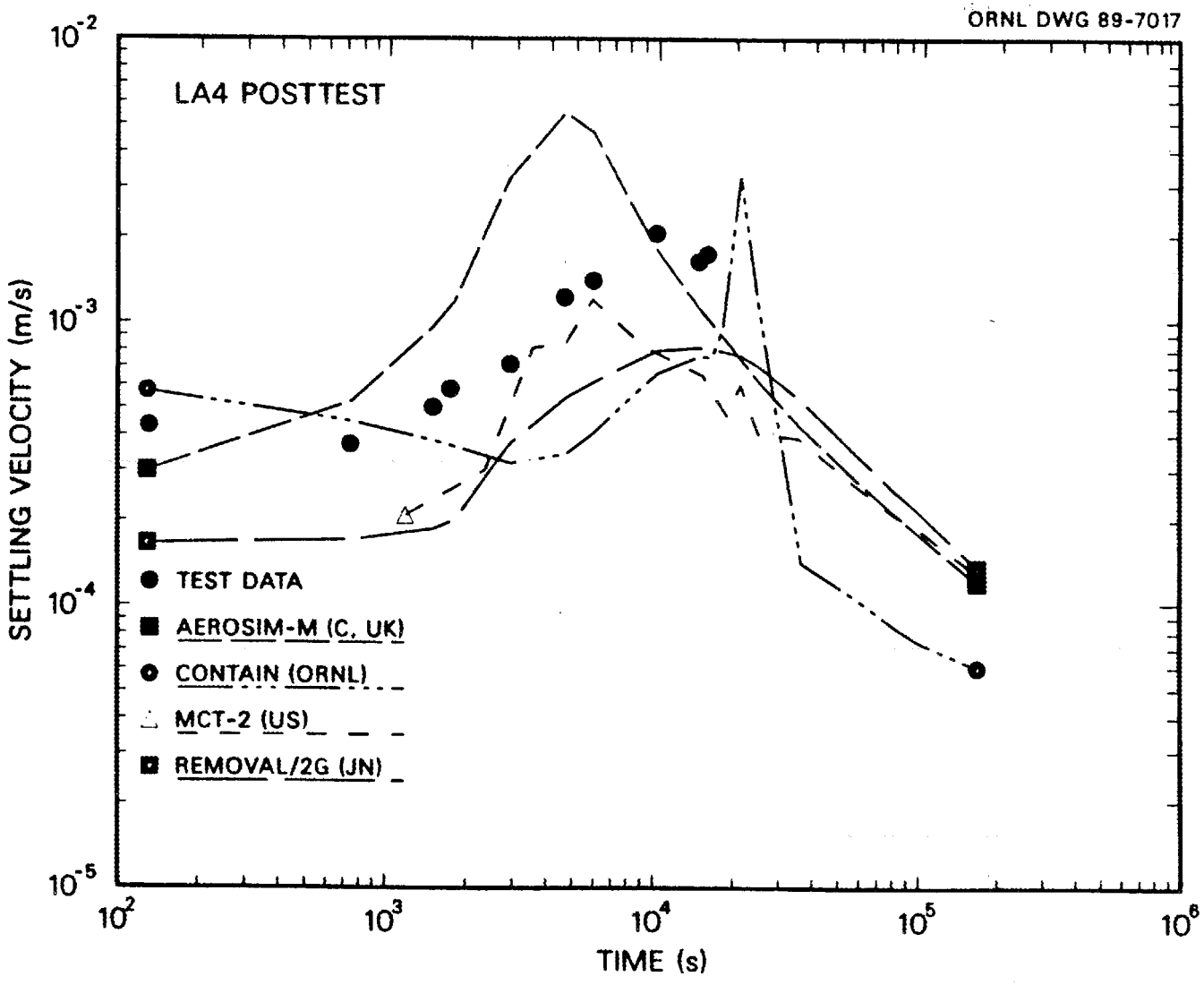

Fig. 15. LA4 posttest calculations - Total aerosol settling velocity - for group 1 codes.

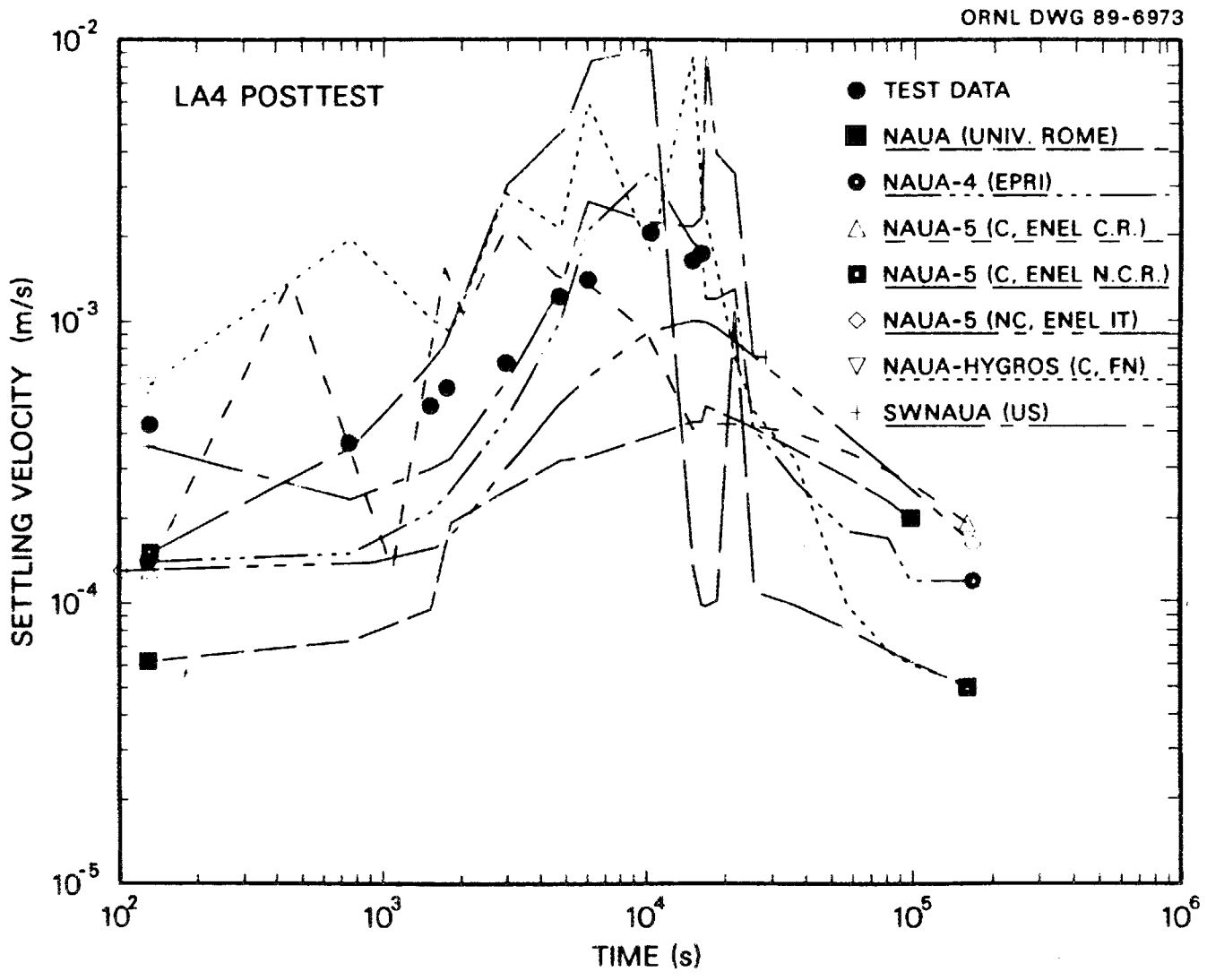

Fig. 16. LA4 posttest calculations - Total aerosol settling velocity - for group 2 codes.

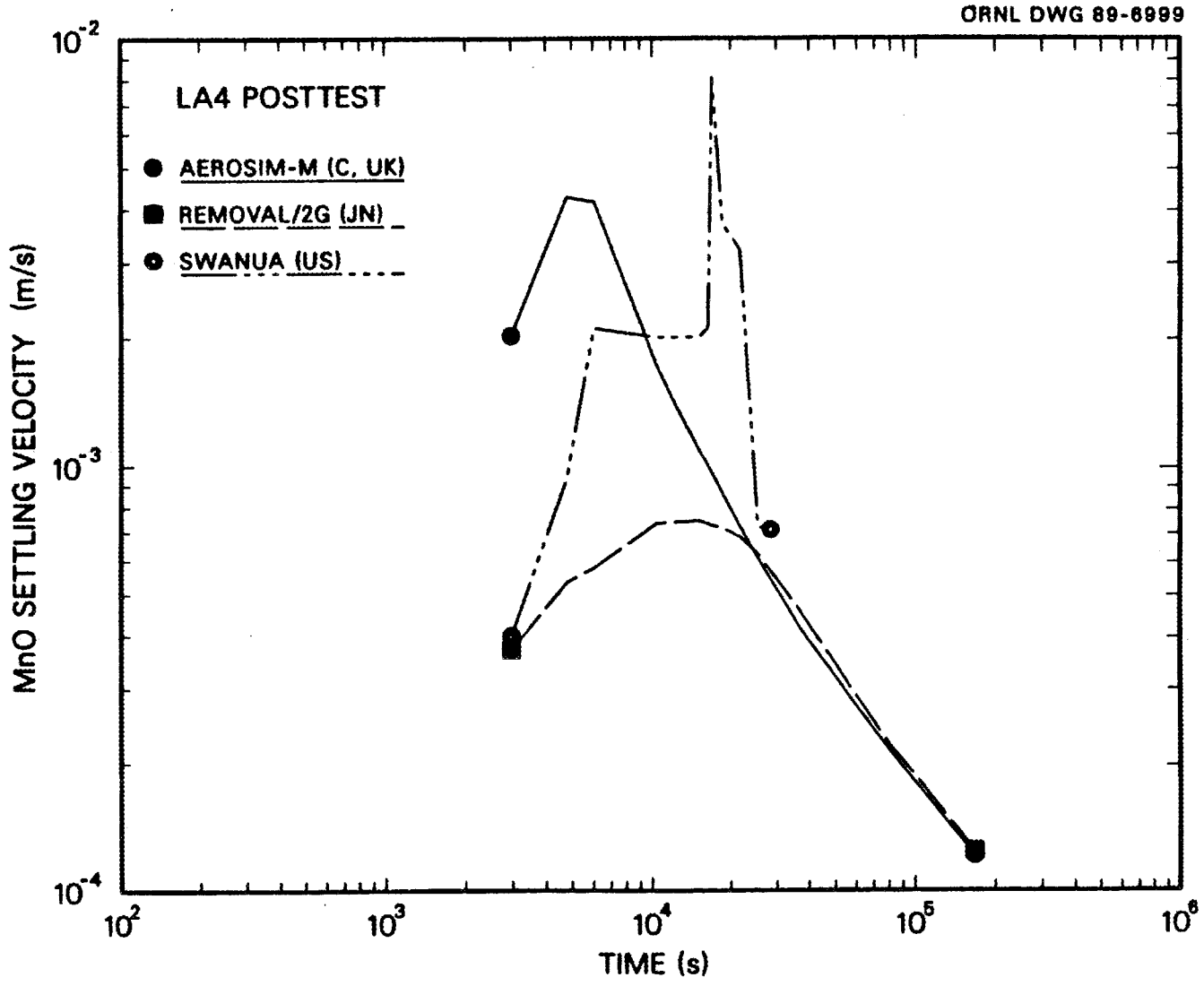

Fig. 17. LA4 posttest calculations - MnO aerosol settling velocity.

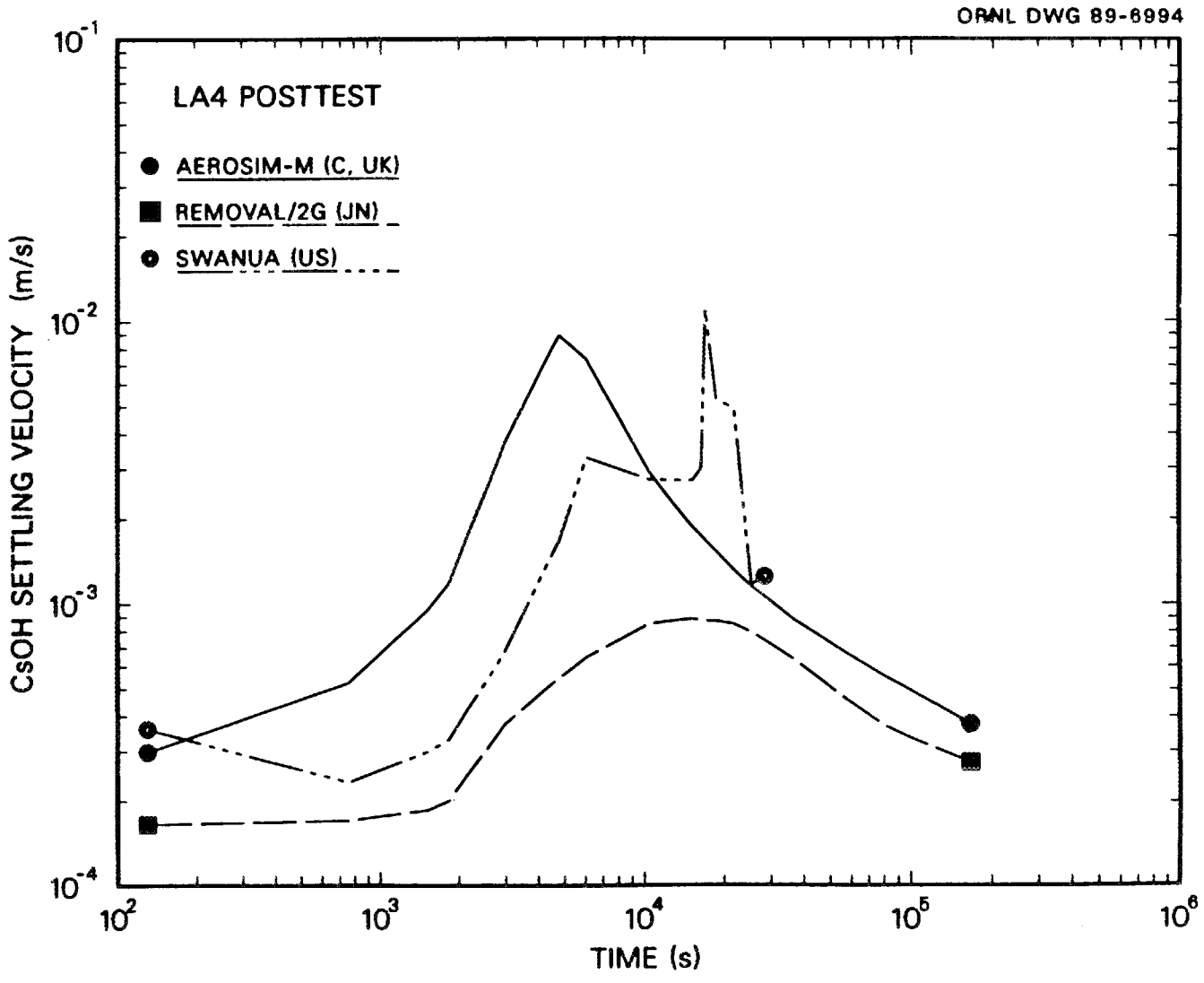

Fig. 18. LA4 posttest calculations - CsOH aerosol settling velocity.

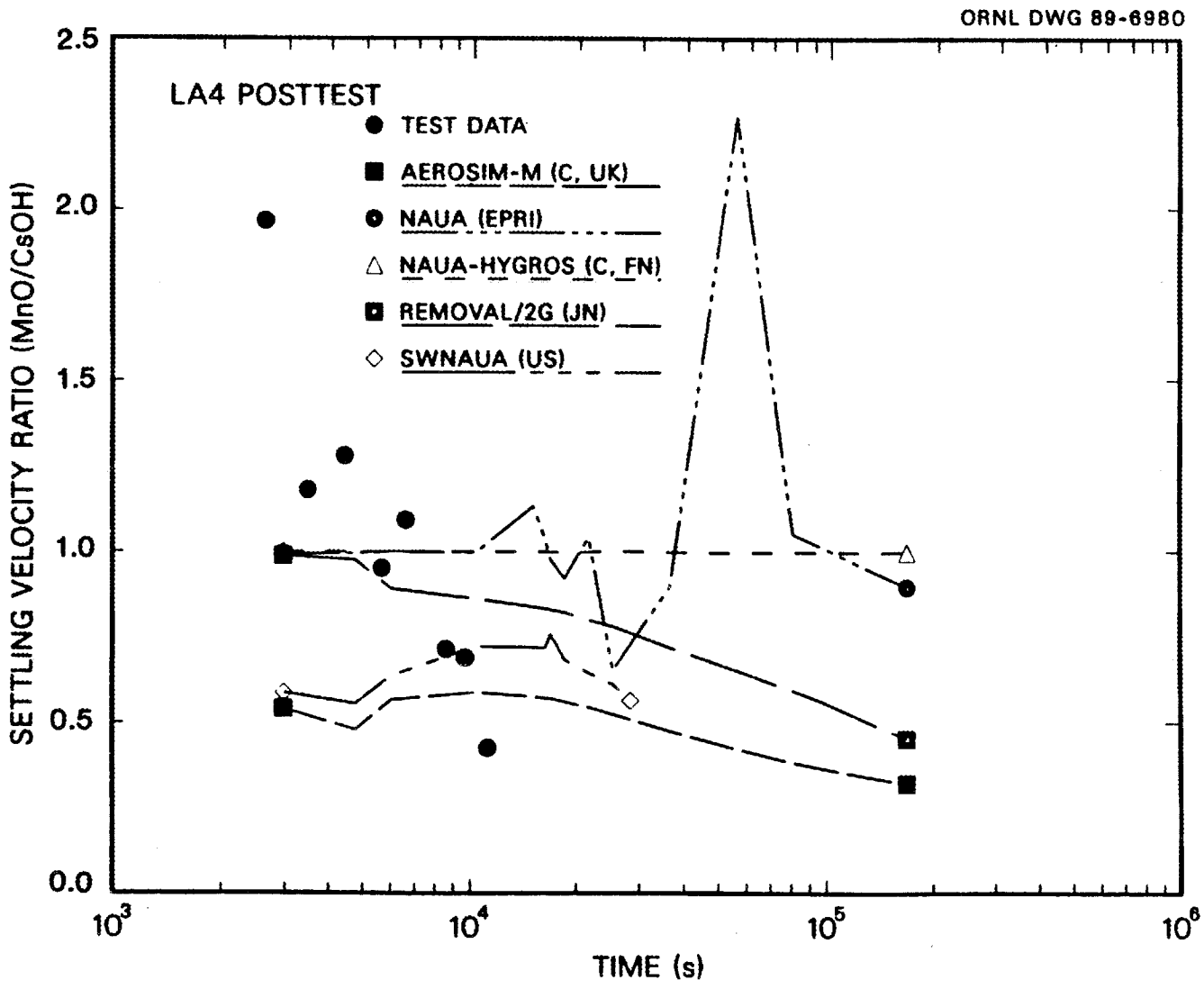

Fig. 19. LA4 posttest calculations - MnO/CsOH aerosol settling velocity ratio.

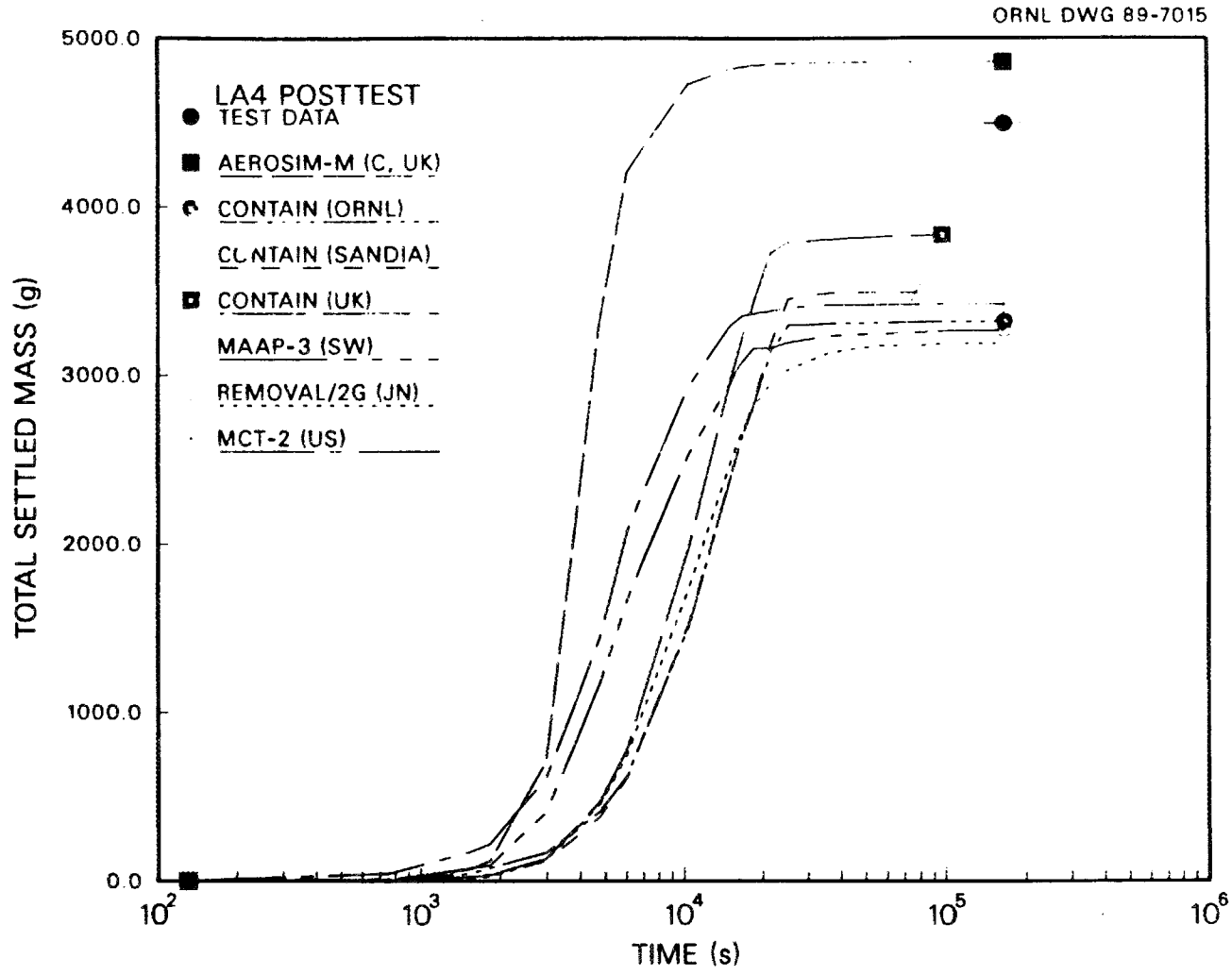

Fig. 20. LA4 posttest calculations - cumulative mass of aerosol settled in CSTF vessel vs time - for group 1 codes.

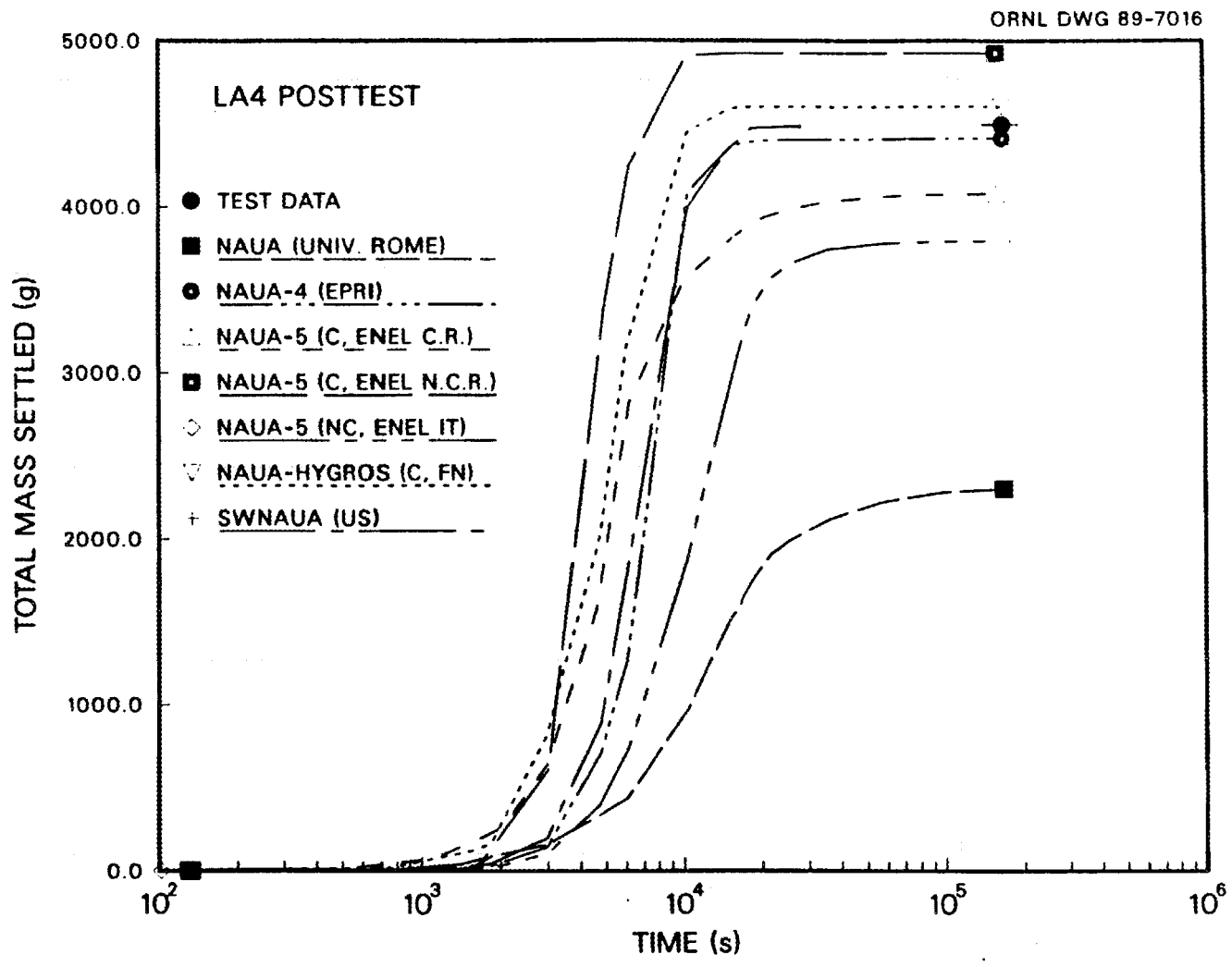

Fig. 21. LA4 posttest calculations - cumulative mass of aerosol settled in CSTF vessel vs time - for group 2 codes.

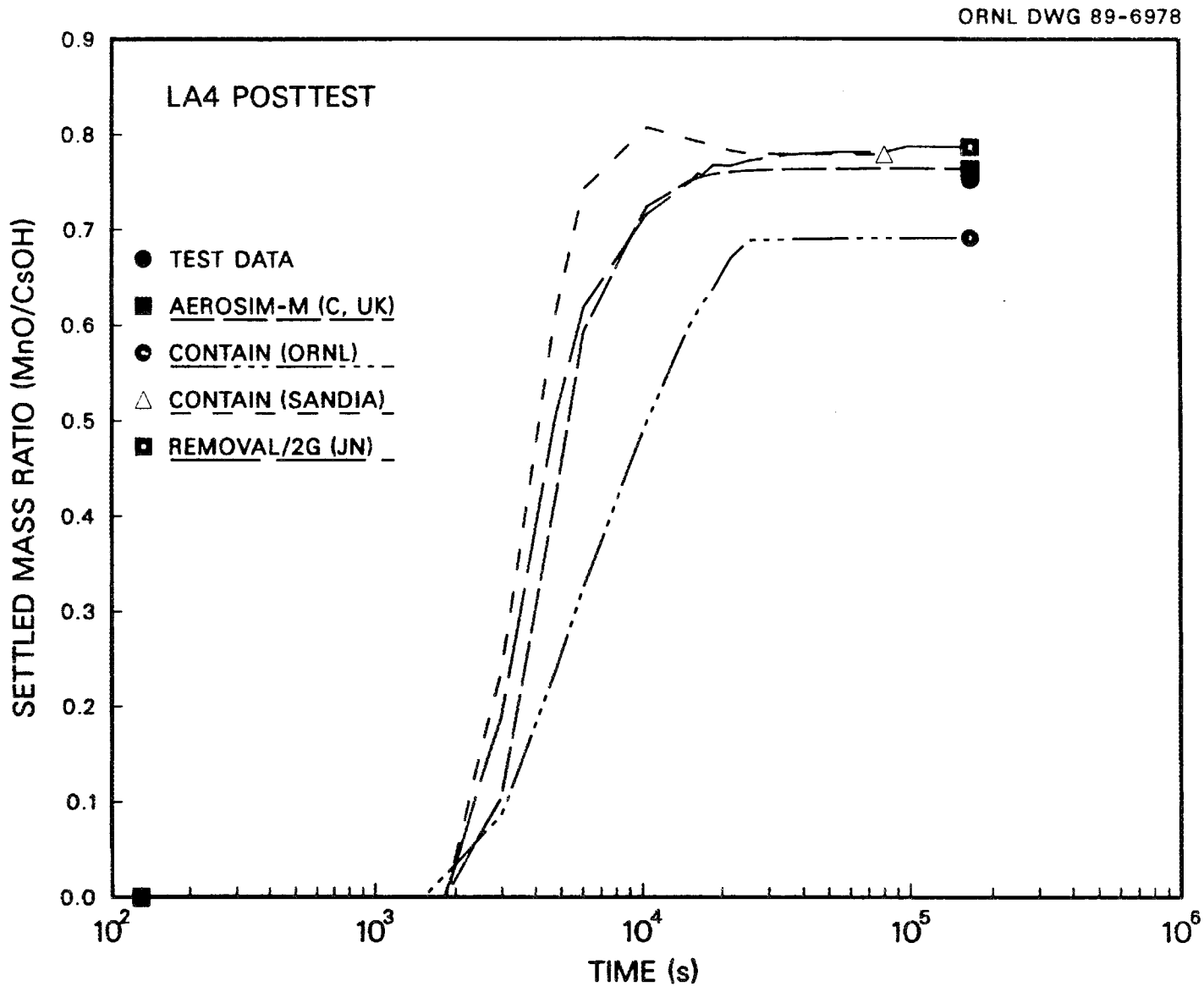

Fig. 22. LA4 posttest calculations - MnO/CsOH mass ratio of aerosol settled in CSTF vessel vs time - for group 1 codes.

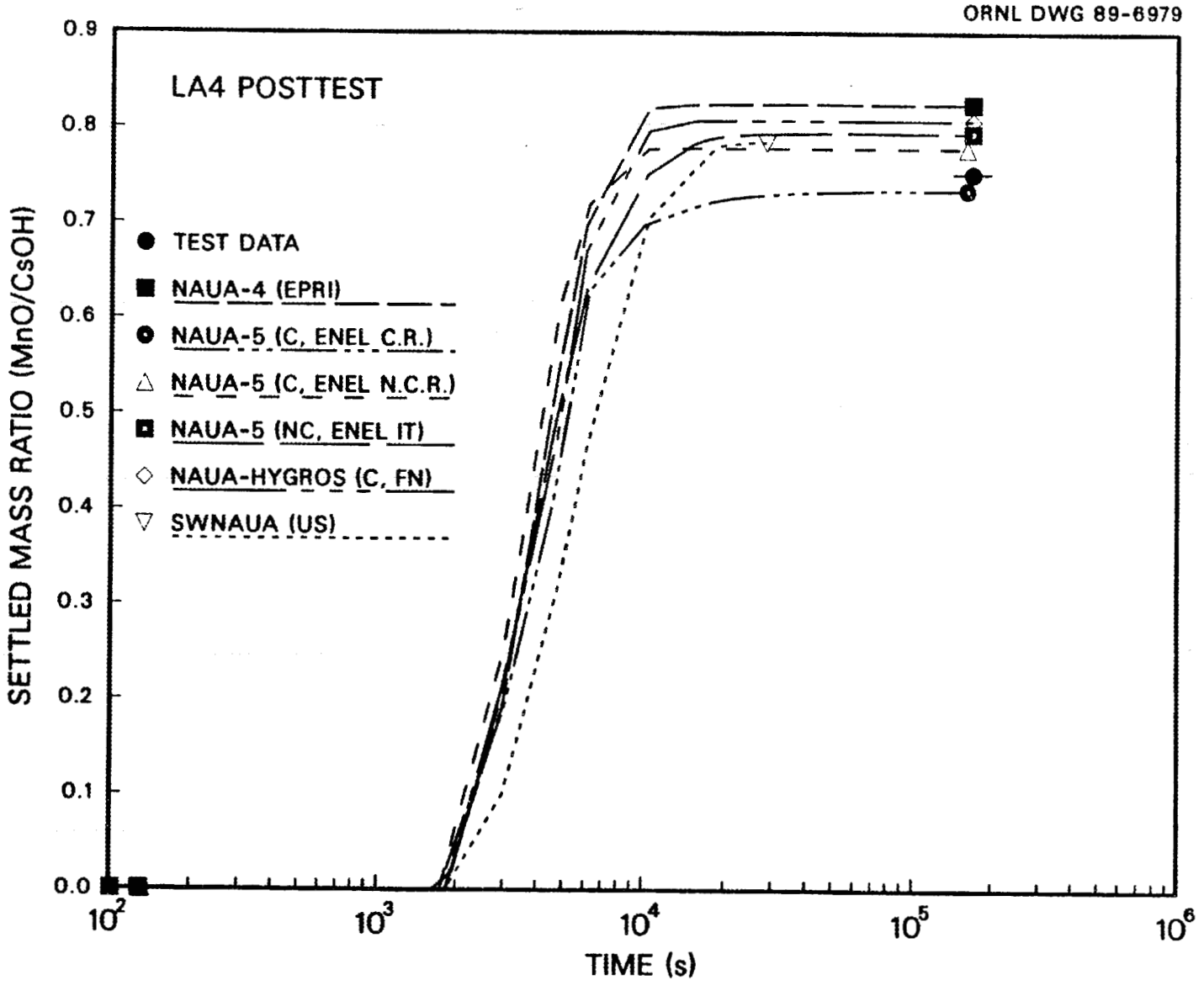

Fig. 23. LA4 posttest calculations - MnO/CsOH mass ratio of aerosol settled in CSTF vessel vs time - for group 2 codes.

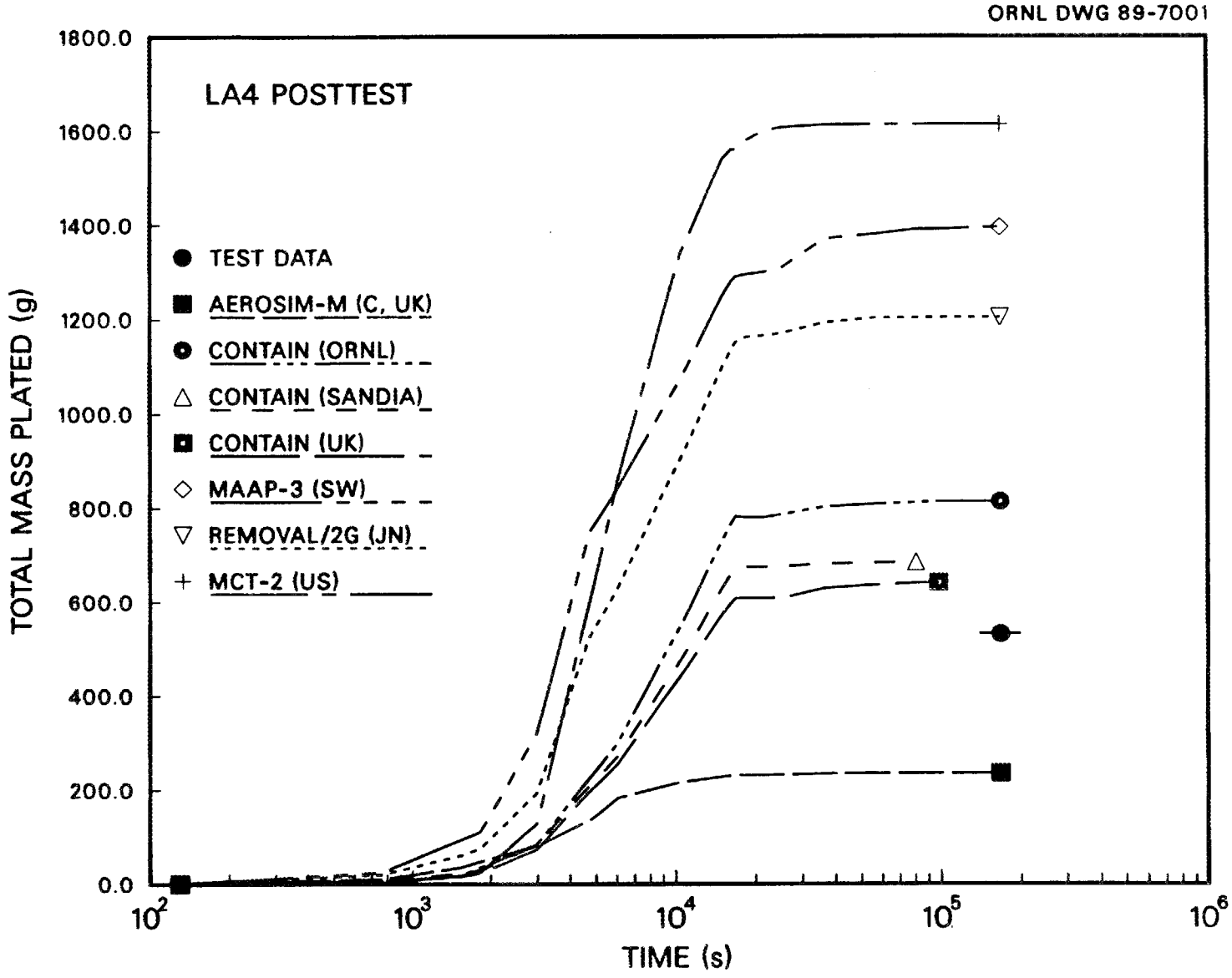

Fig. 24. LA4 posttest calculations - cumulative mass of aerosol plated in CSTF vessel vs time - for group 1 codes.

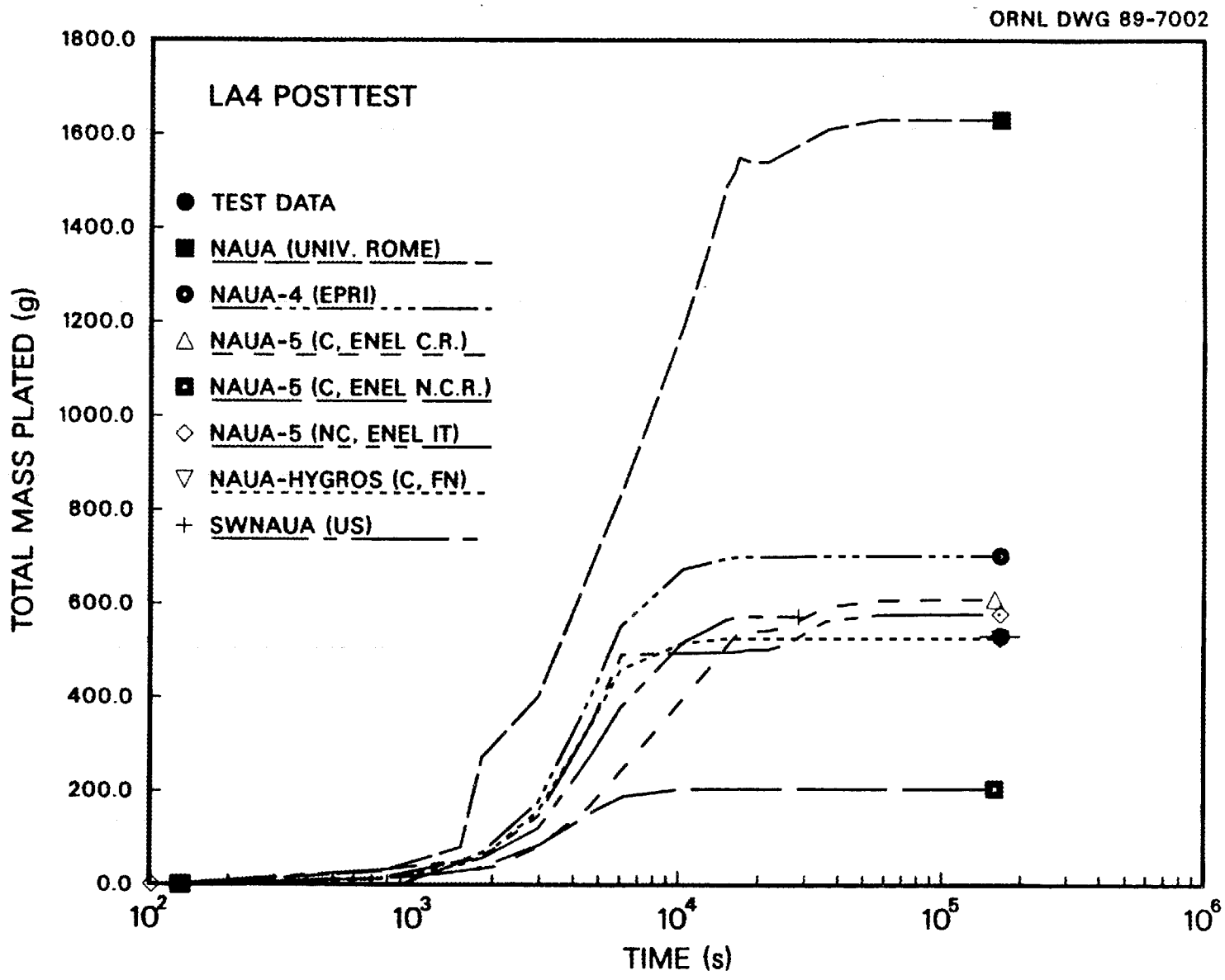

Fig. 25. LA4 posttest calculations - cumulative mass of aerosol plated in CSTF vessel vs time - for group 2 codes.

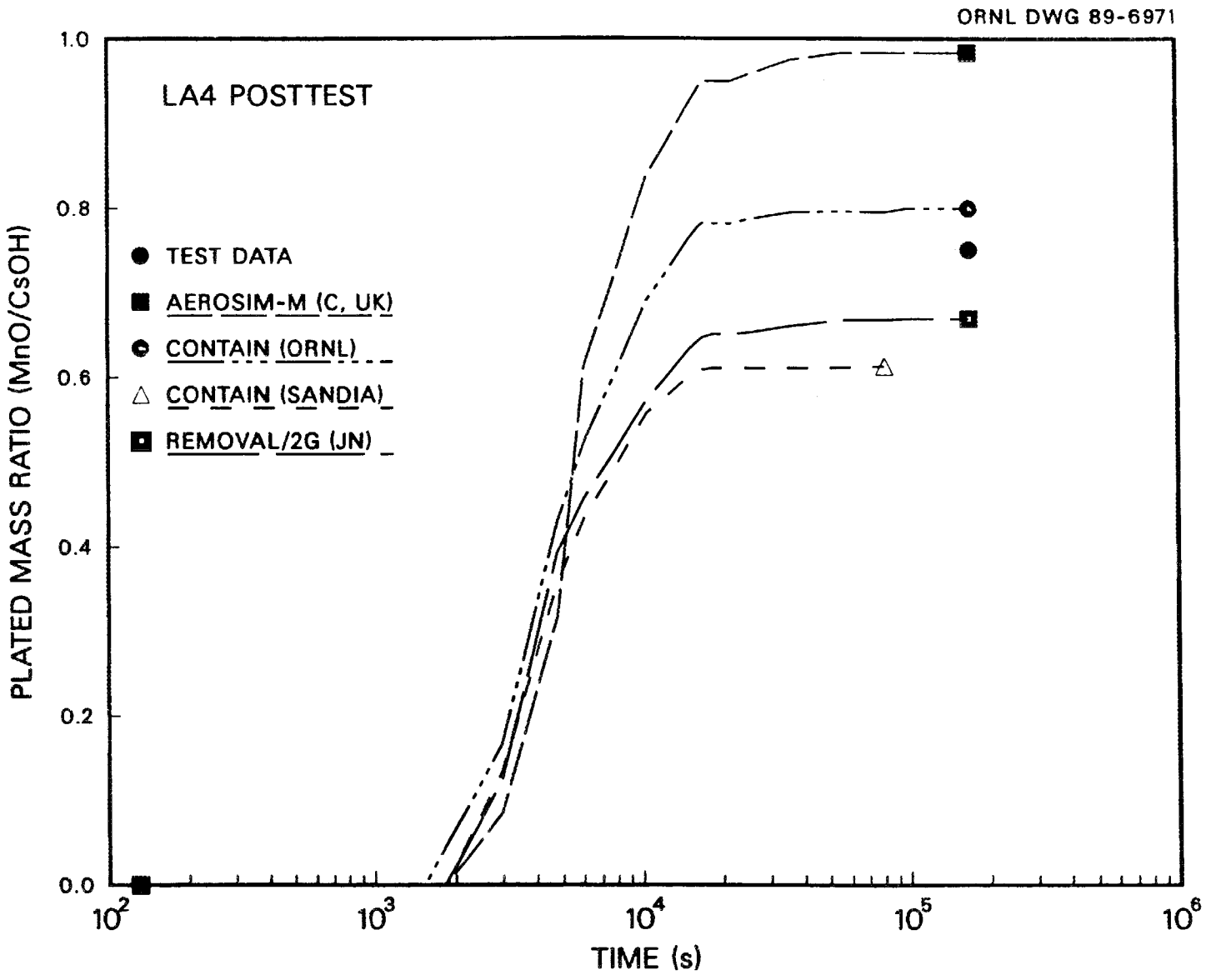

Fig. 26. LA4 posttest calculations - MnO/CsOH mass ratio of aerosol plated in CSTF vessel vs time - for group 1 codes.

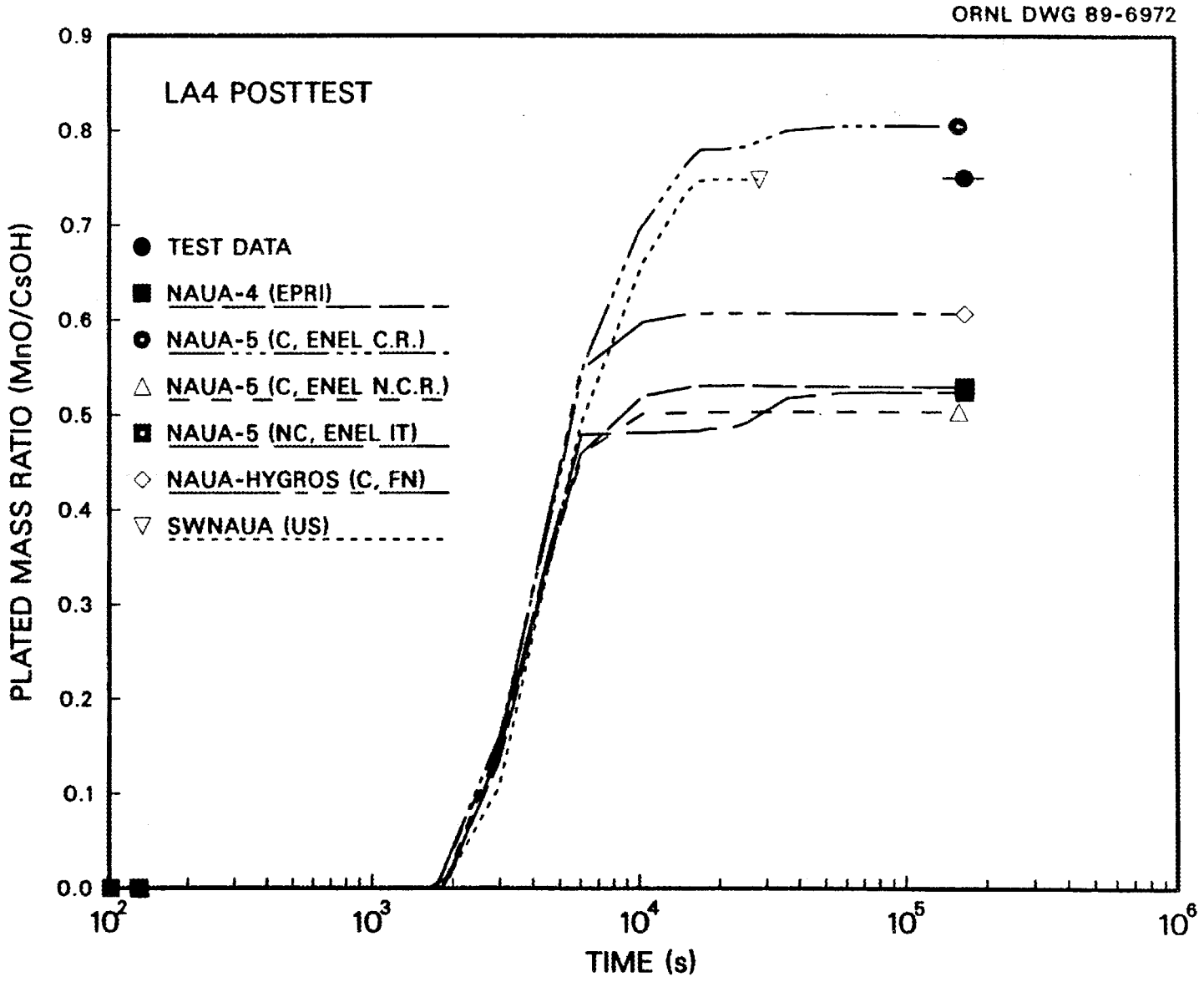

Fig. 27. LA4 posttest calculations - MnO/CsOH mass ratio of aerosol plated in CSTF vessel vs time - for group 2 codes.

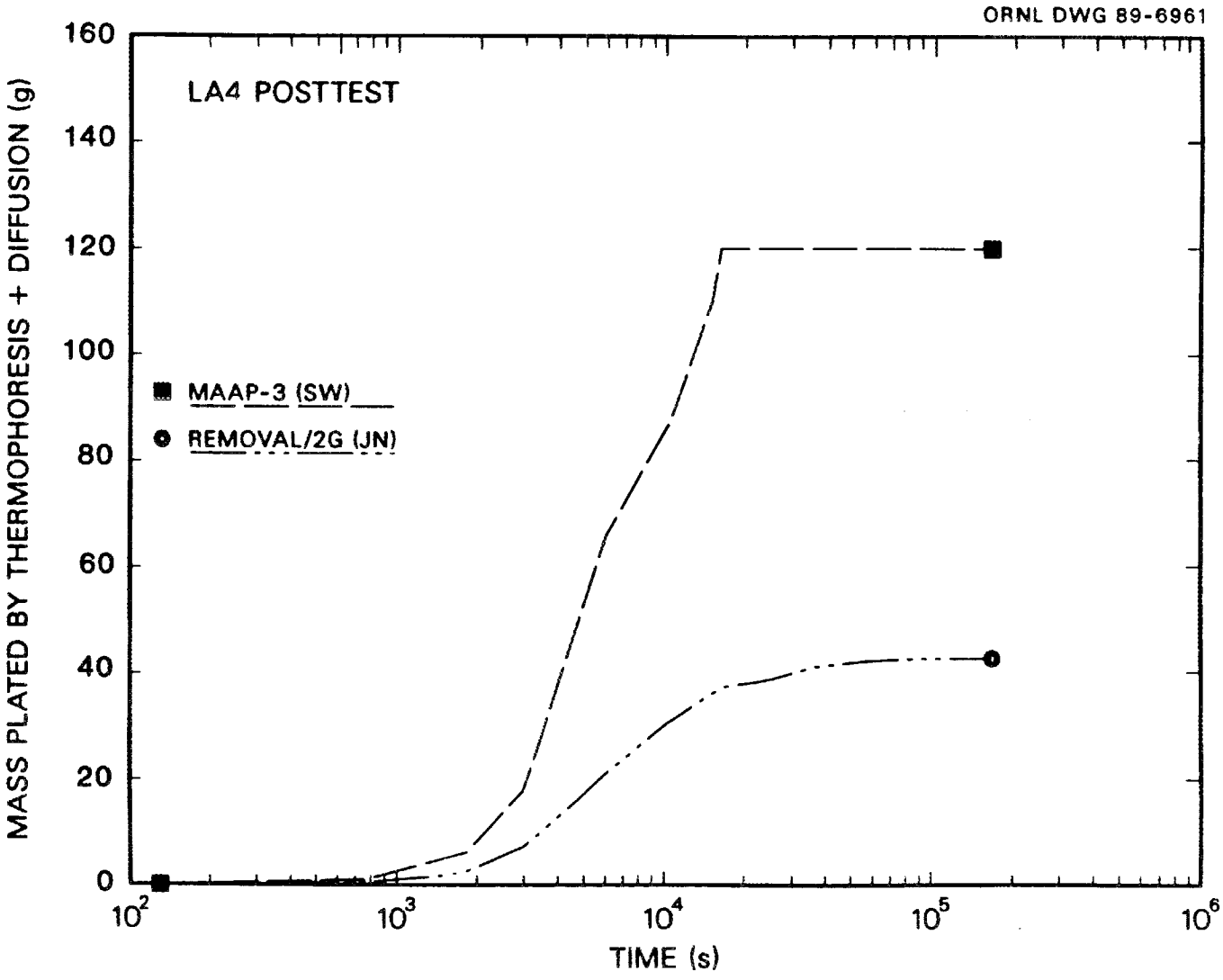

Fig. 28. LA4 posttest calculations - cumulative mass of aerosol plated in CSTF vessel by thermophoresis + Brownian diffusion vs time.

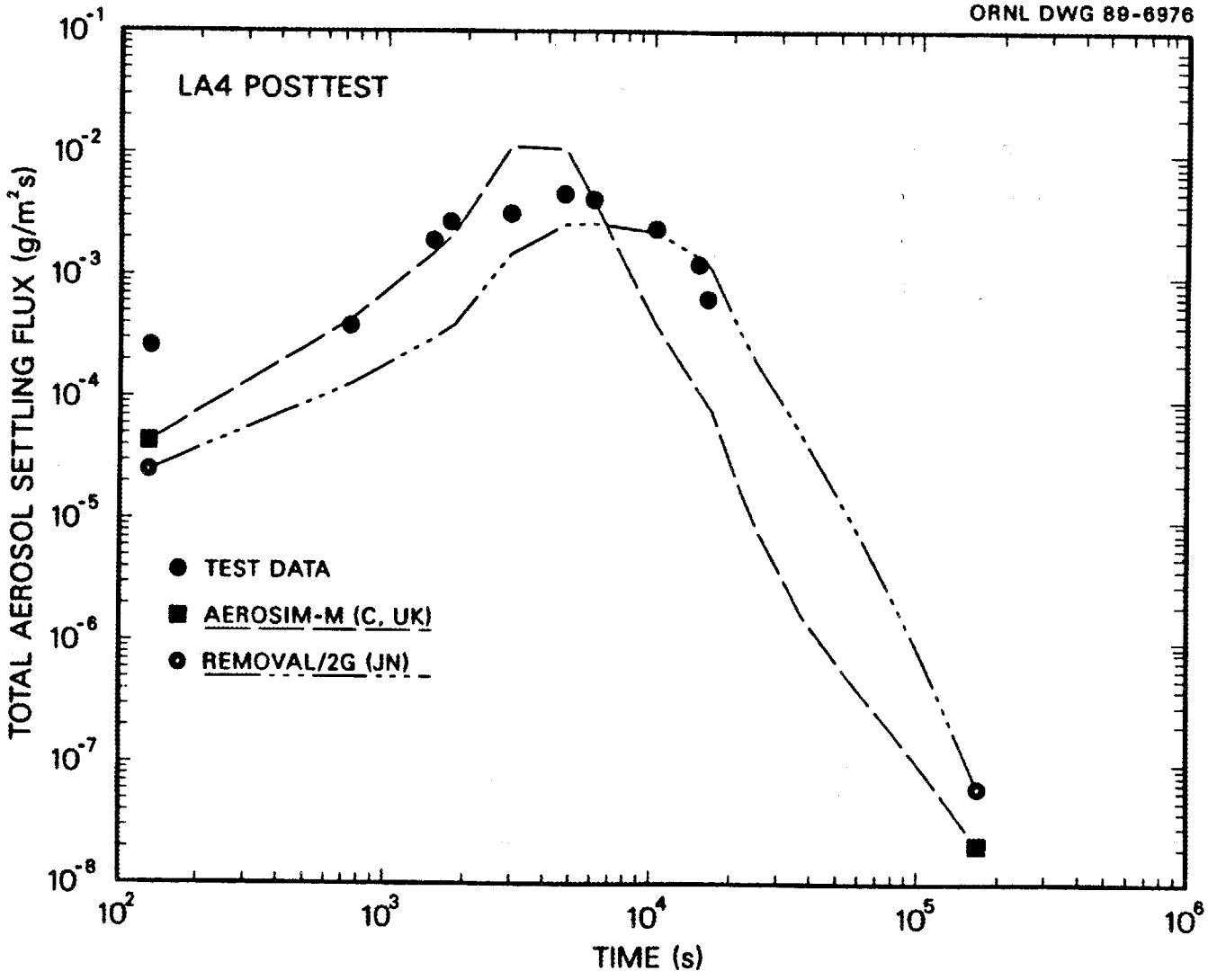

Fig. 29. LA4 posttest calculations - total aerosol settling flux vs time - for group 1 codes.

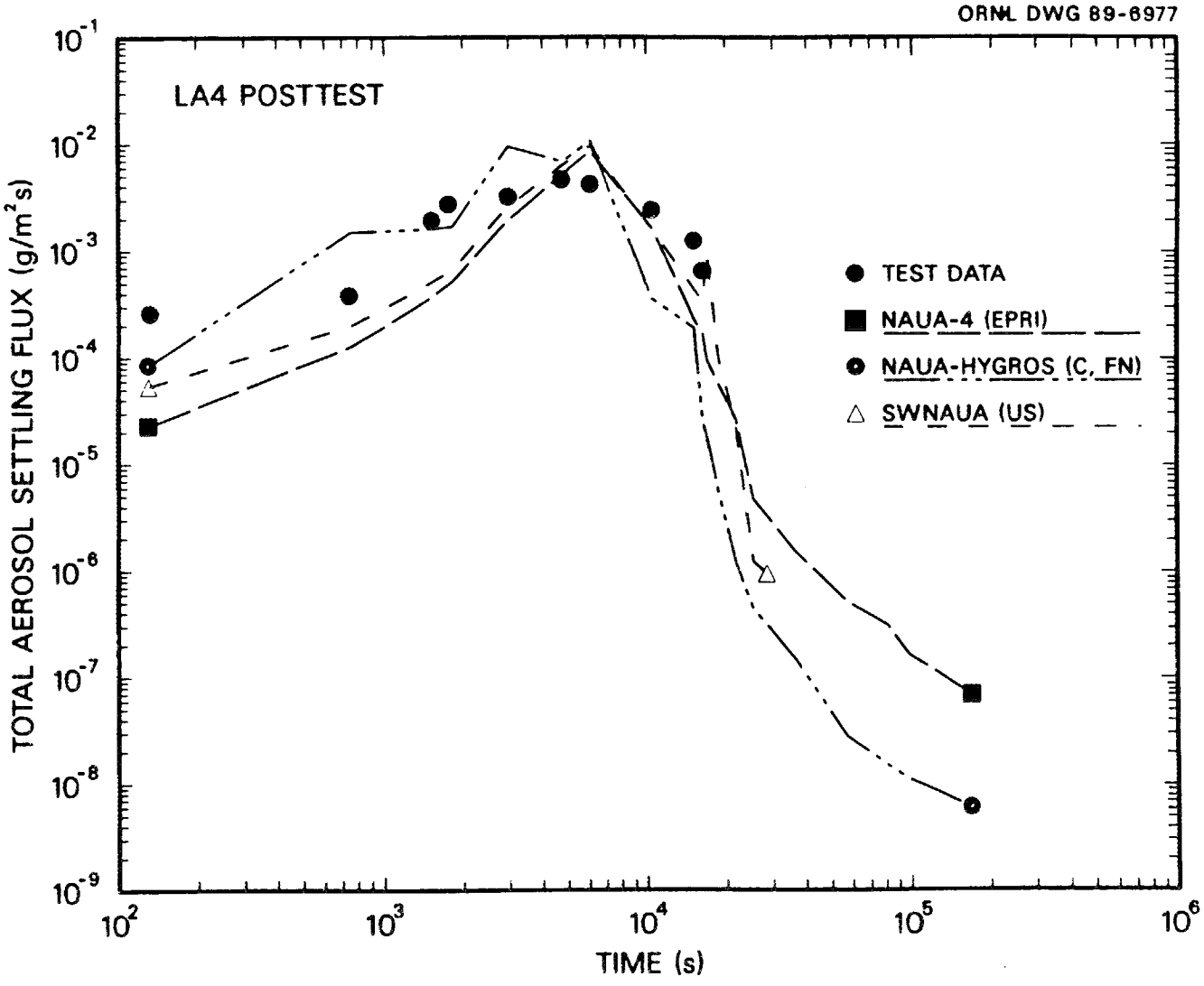

Fig. 30. LA4 posttest calculations - total aerosol settling flux vs time - for group 2 codes.

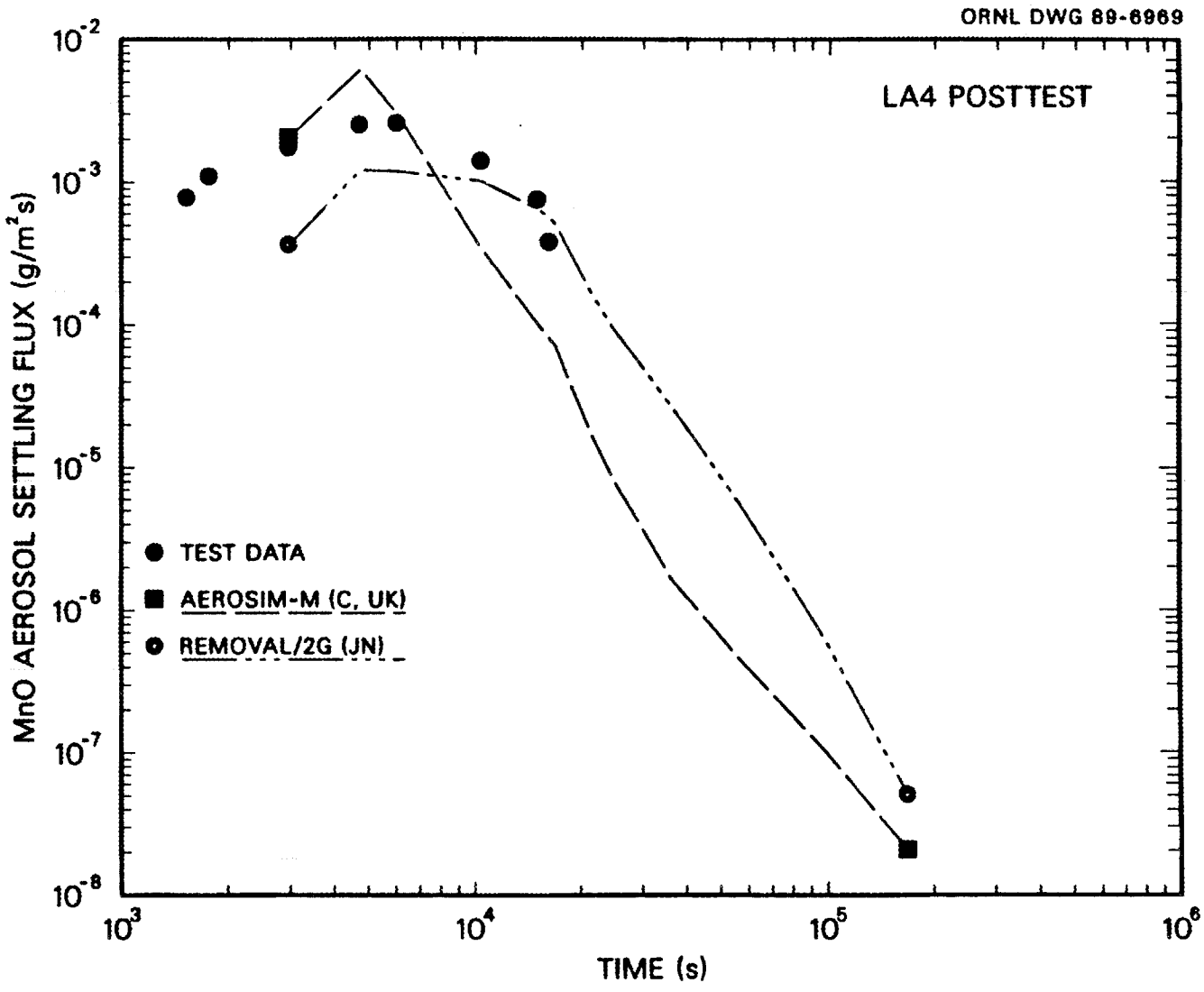

Fig. 31. LA4 posttest calculations - MnO aerosol settling flux vs time - for group 1 codes.

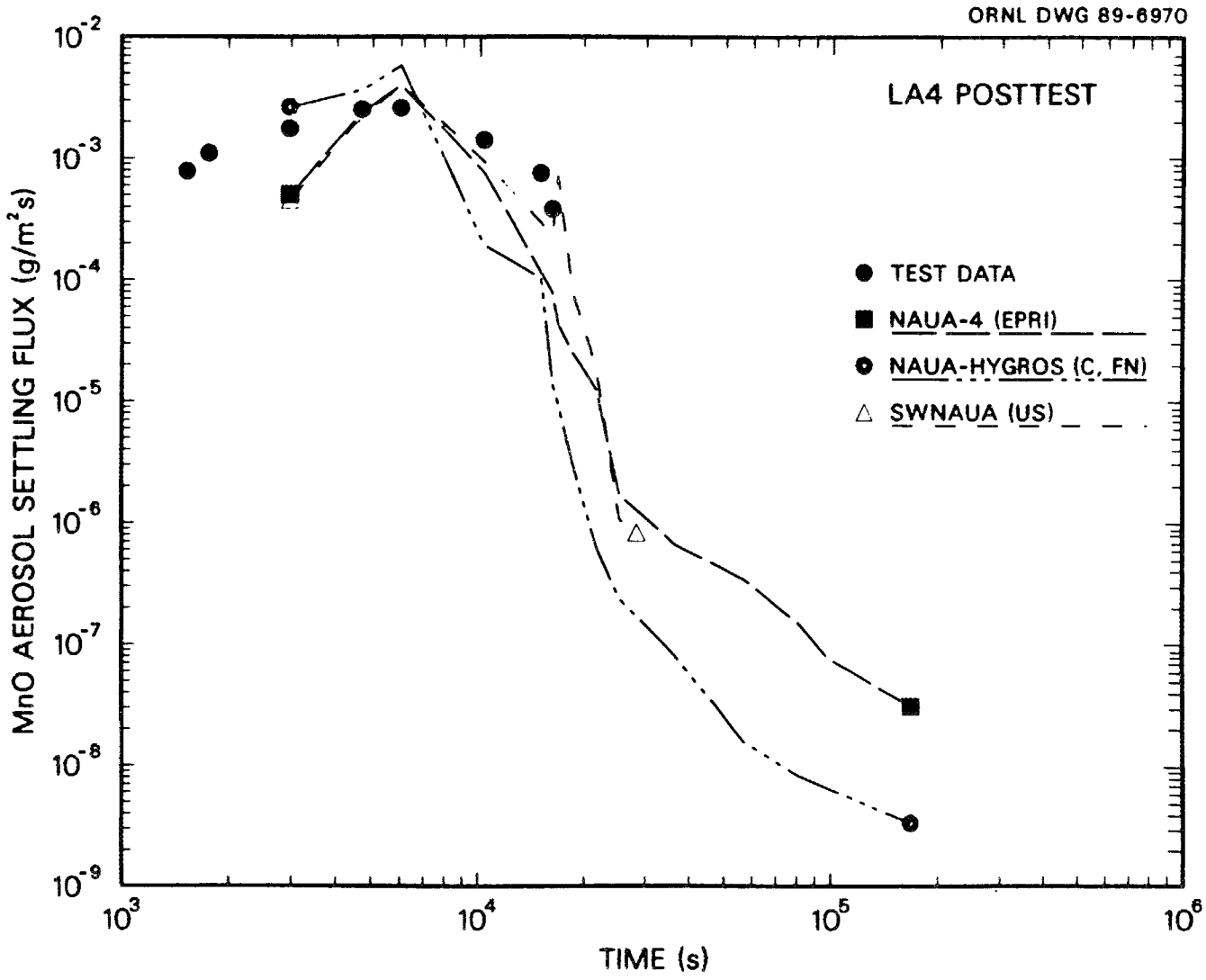

Fig. 32. LA4 posttest calculations - MnO aerosol settling flux vs time - for group 2 codes.

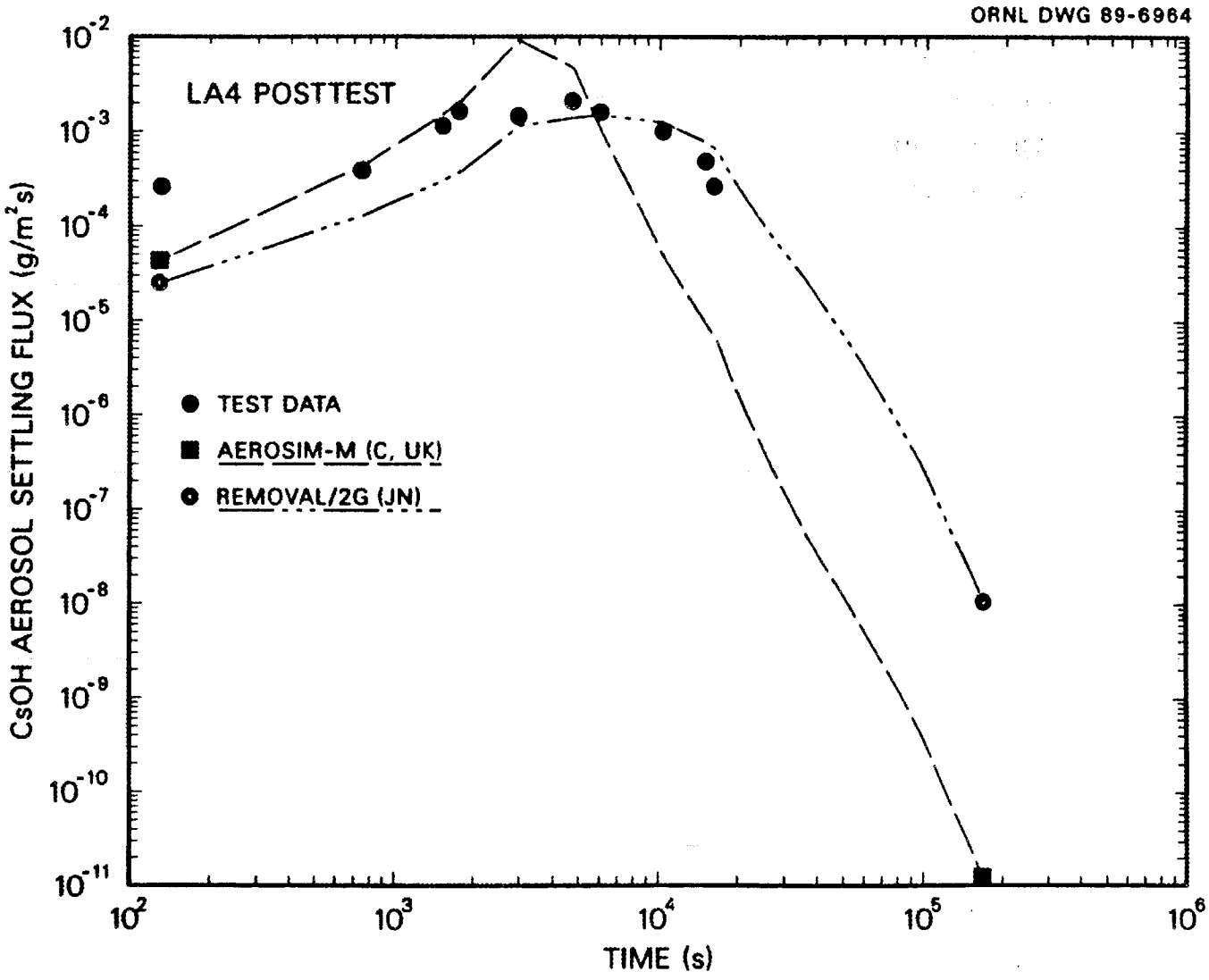

Fig. 33. LA4 posttest calculations - CsOH aerosol settling flux vs time - for group 1 codes.

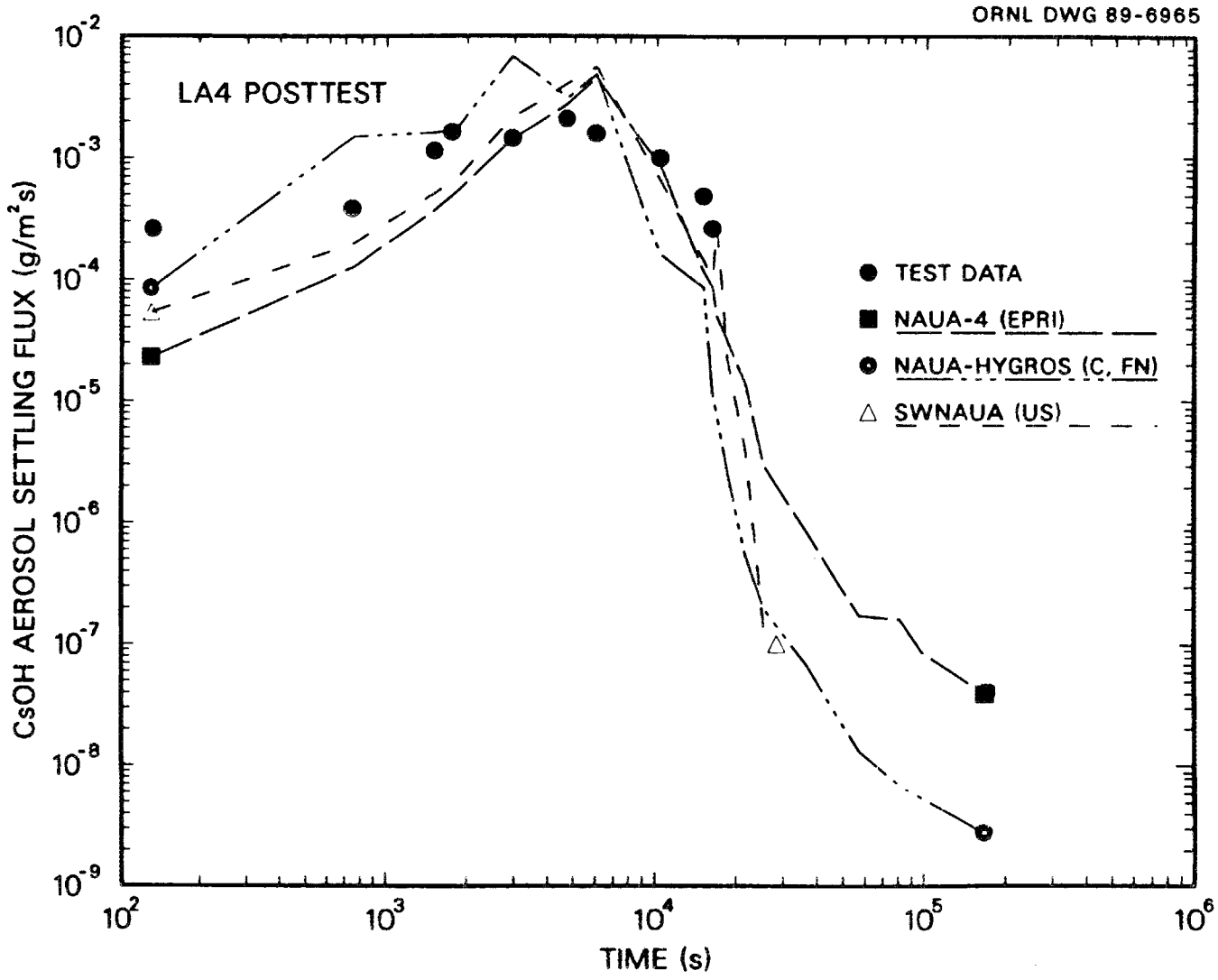

Fig. 34. LA4 posttest calculations - CsOH aerosol settling flux vs time - for group 2 codes.

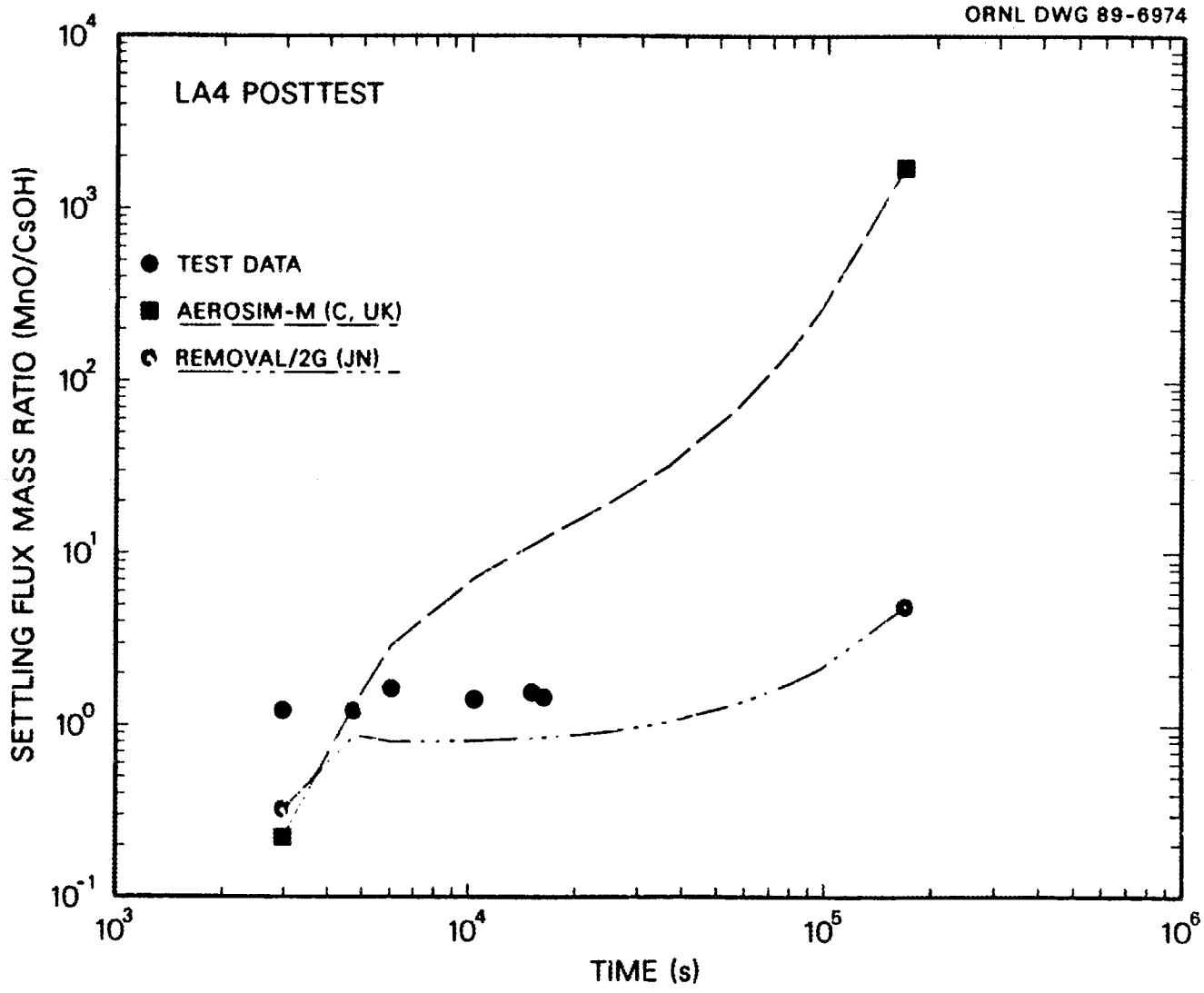

Fig. 35. LA4 posttest calculations - MnO/CsOH mass ratio of settling aerosol vs time - for group 1 codes.

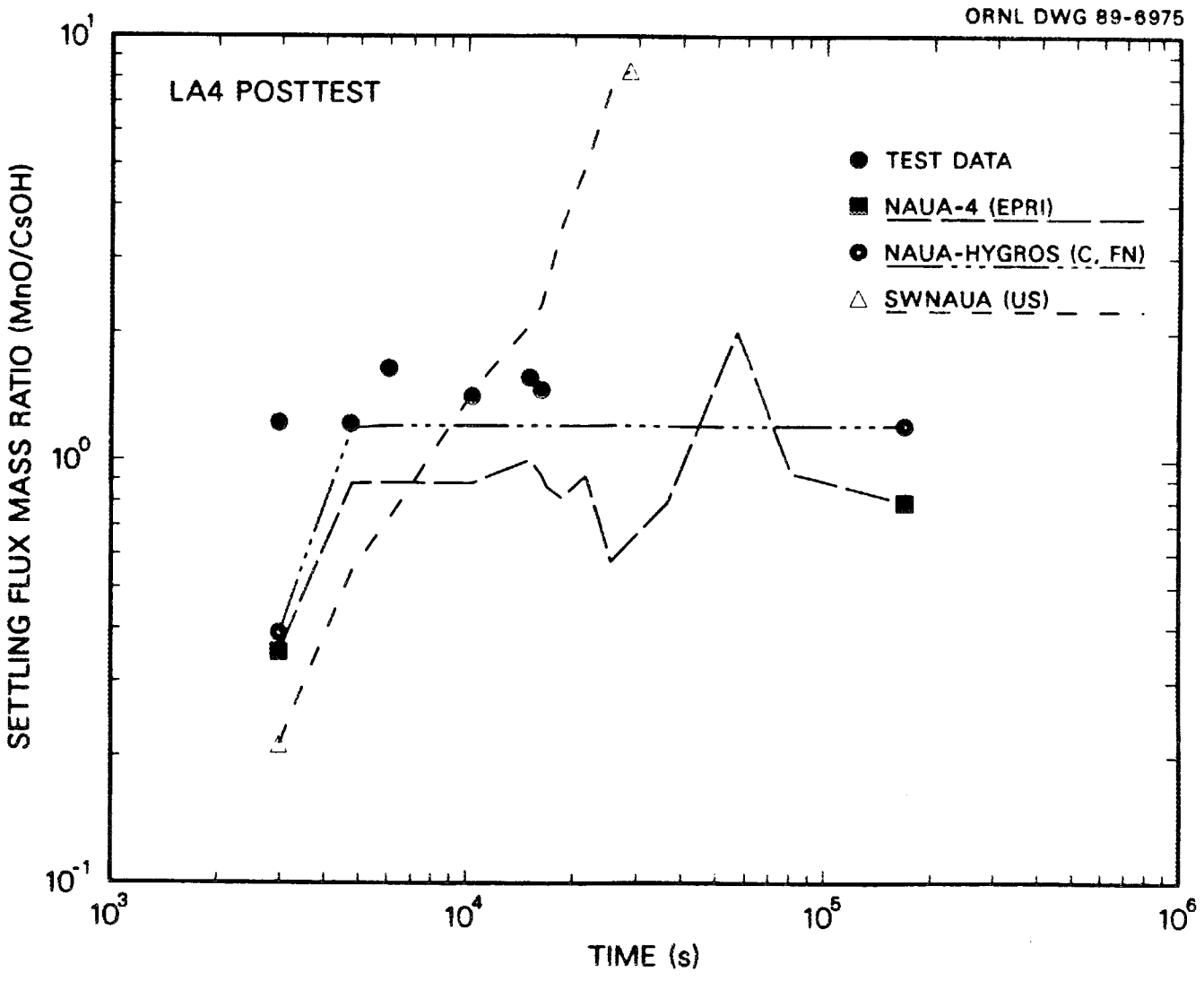

Fig. 36. LA4 posttest calculations - MnO/CsOH mass ratio of settling aerosol vs time - for group 2 codes.

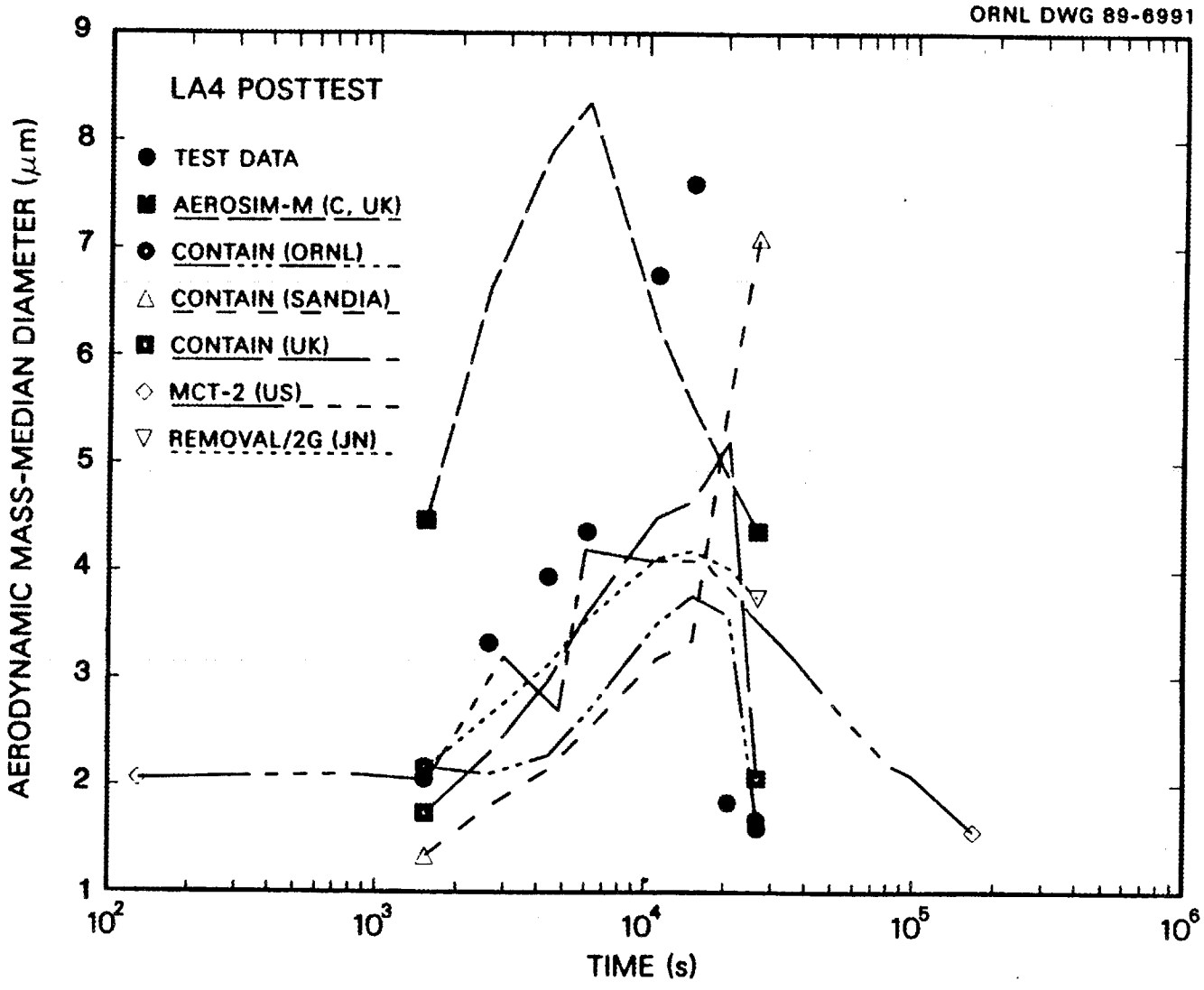

Fig. 37. LA4 posttest calculations - AMMD of total airborne aerosol vs time - as reported by group 1 codes.

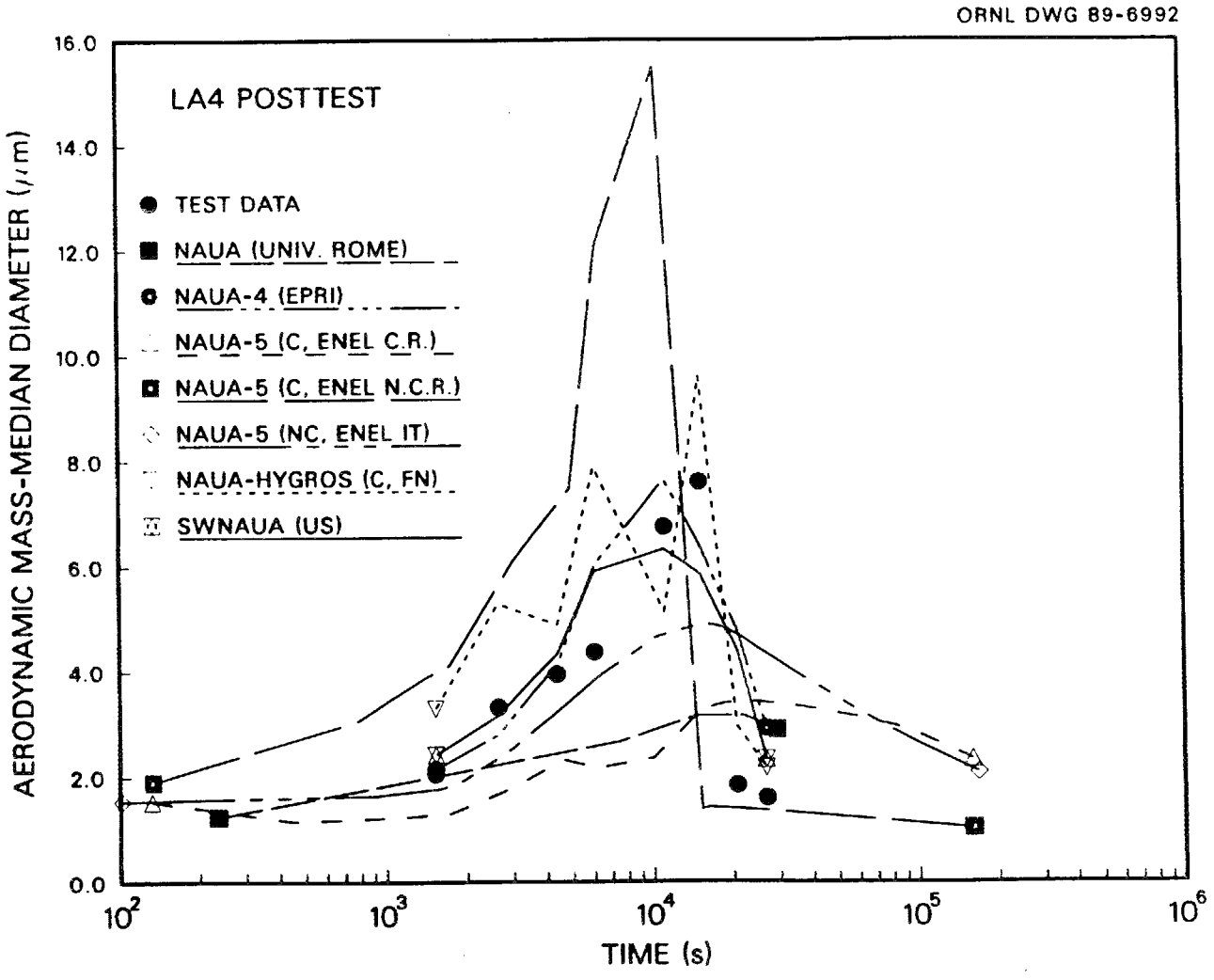

Fig. 38. LA4 posttest calculations - AMMD of total airborne aerosol vs time - as reported by group 2 codes.

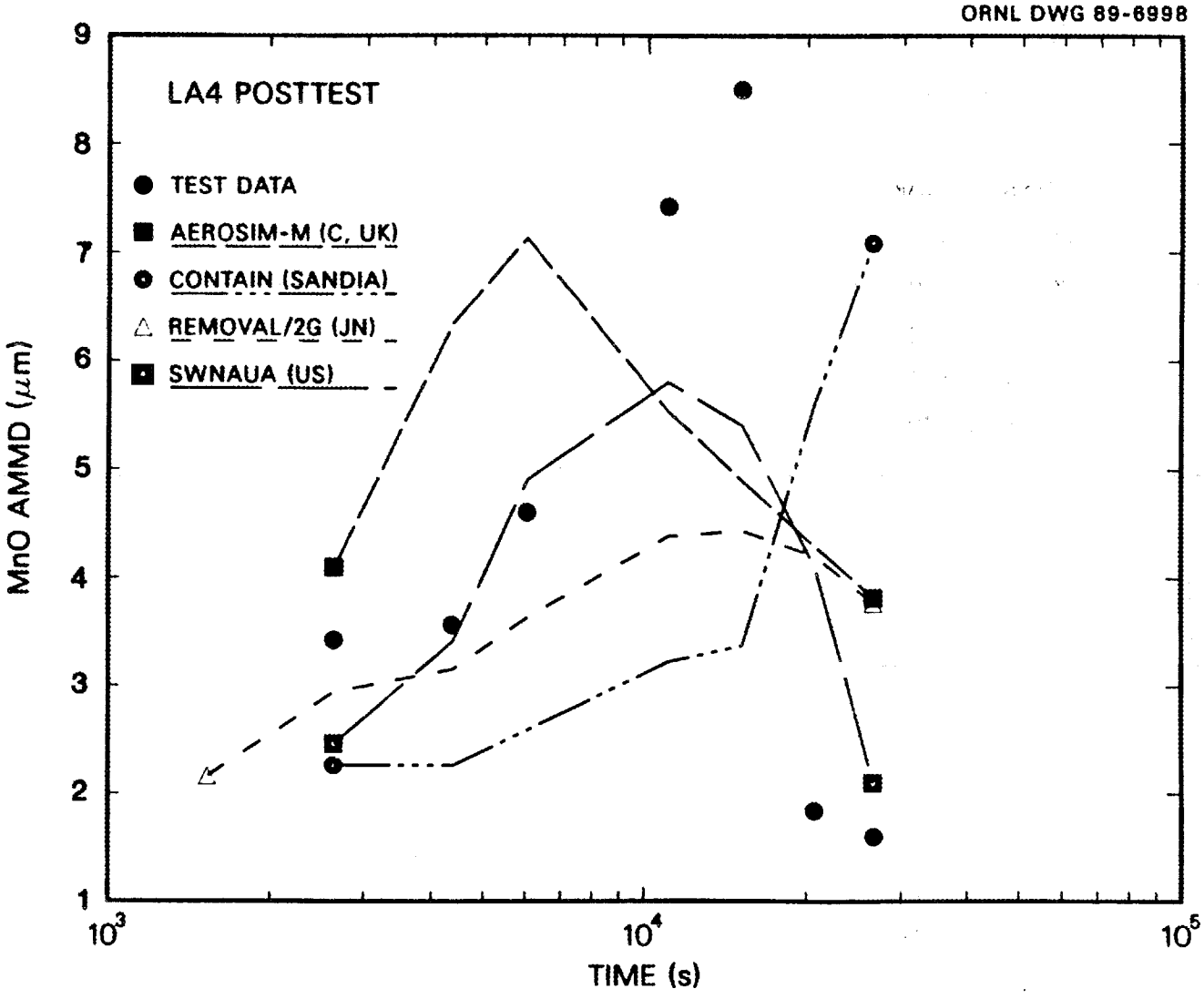

Fig. 39. LA4 posttest calculations - AMMD of MnO airborne aerosol vs time.

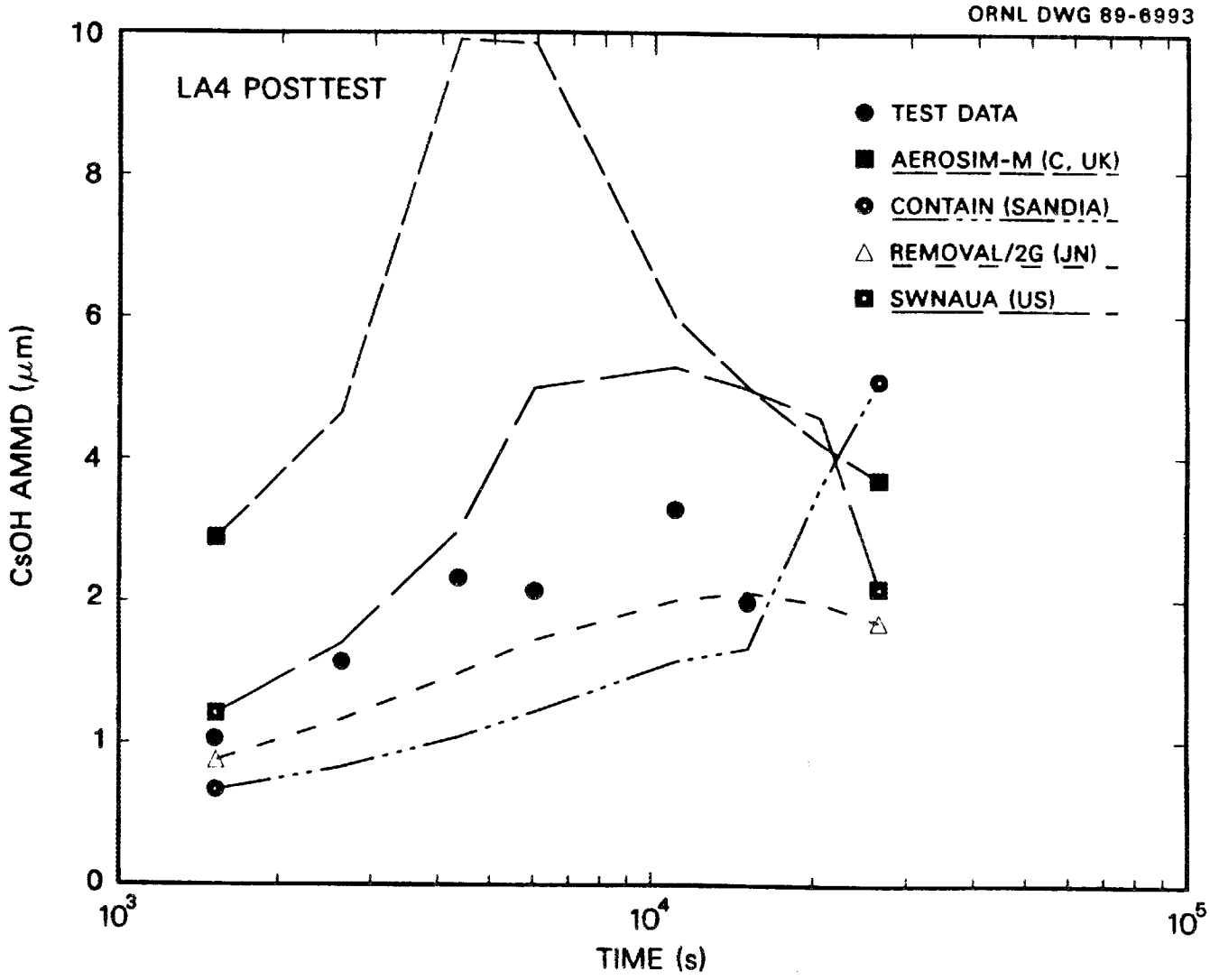

Fig. 40. LA4 posttest calculations - AMMD of CsOH airborne aerosol vs time.

deviation (GSD) of the mixed aerosol is plotted in Figs. 41 and 42 and the GSD of the individual species in Figs. 43 and 44. As in the case of the AMMD, we calculated the GSD according to Appendix B, utilizing the data reported by the code analysts (as requested in Table 5). The methods of Appendixes A and B for determining AMMD and GSD are recommended because they permit a direct comparison with the experimental cascade impactor data. Table 8 shows a comparison of the AMMD and the GSD values reported by the code users with the values which we calculated.

PSD plots are presented in Figs. 45 through 60 for the codes having a discrete distribution model. Each figure corresponds to a particular time in the experiment. In these figures, the normalized mass fraction of the aerosol in a size class, or size bin, is plotted as a function of the average AMMD of the size bin. The average AMMD is used rather than the actual diameter of the size bin, because in some cases different aerosol densities were assumed by different code analysts. Also, the calibration of the cascade impactors is based on AMMD. As discussed in Appendix A, the <u>mass fraction values</u> are for the <u>dry aerosol</u> and the <u>AMMD values</u> are for the <u>wet aerosol</u> (if conditions were such that steam has condensed on the aerosol). The normalized mass fraction was determined by dividing the actual mass fraction in each bin (as calculated from the distribution data provided by the codes) by a normalization factor. This factor is equal to the summation over all the bins of the product of the actual dry mass fraction in each bin and $[(\ln(d_2) - \ln(d_1)]$, where d_2 and d_1 are the upper and lower particle diameters, respectively, of the bin. Thus, a PSD curve, which is similar to a probability density function is generated. The normalization was performed to facilitate the comparison of the of PSD curves. If the curves were not normalized, they would be displaced vertically from one another, depending upon the bin size utilized by each code. The overall shapes of the curves, though, are unaffected by the normalization.

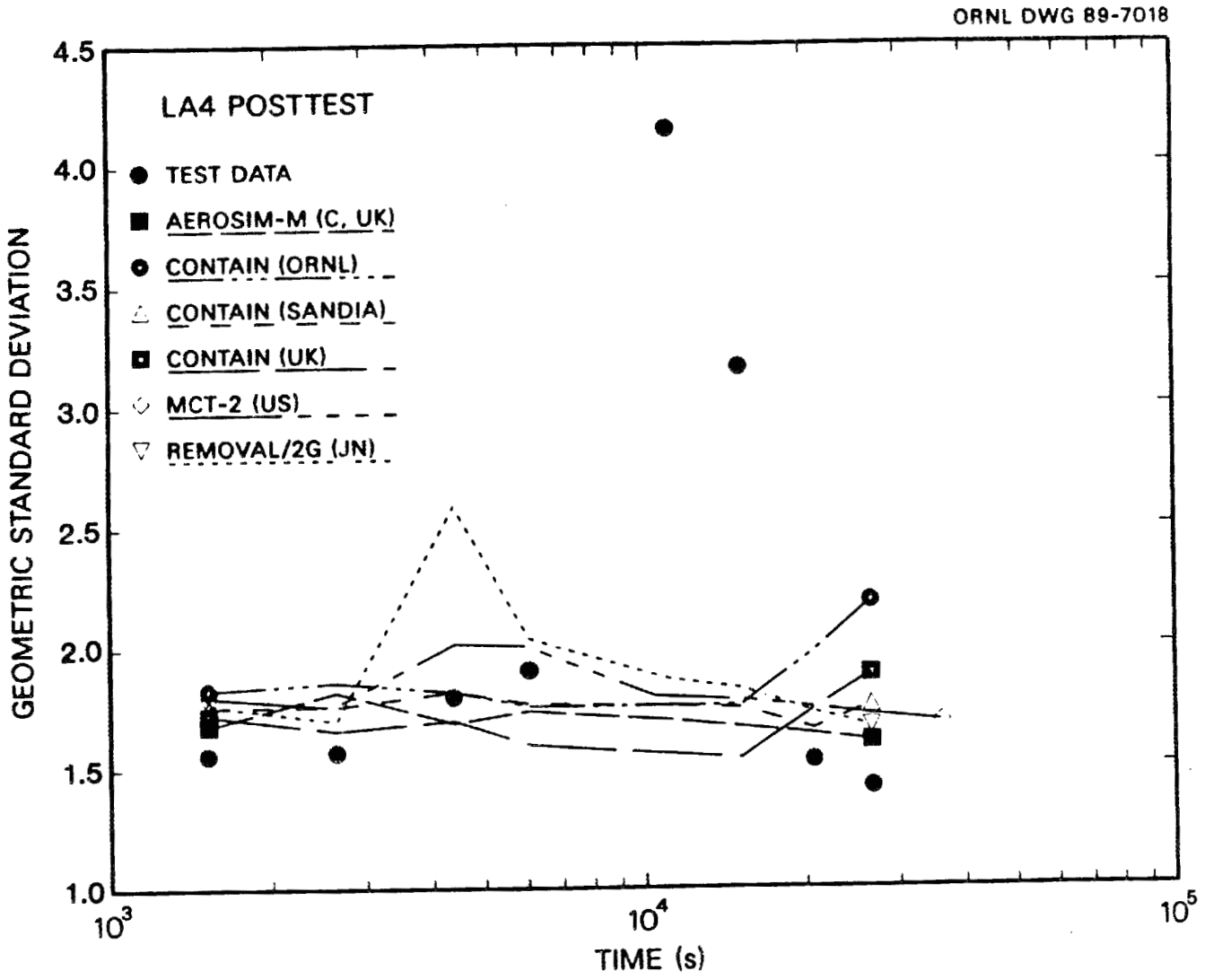

Fig. 41. LA4 posttest calculations - GSD of total airborne aerosol vs time - as reported by group 1 codes.

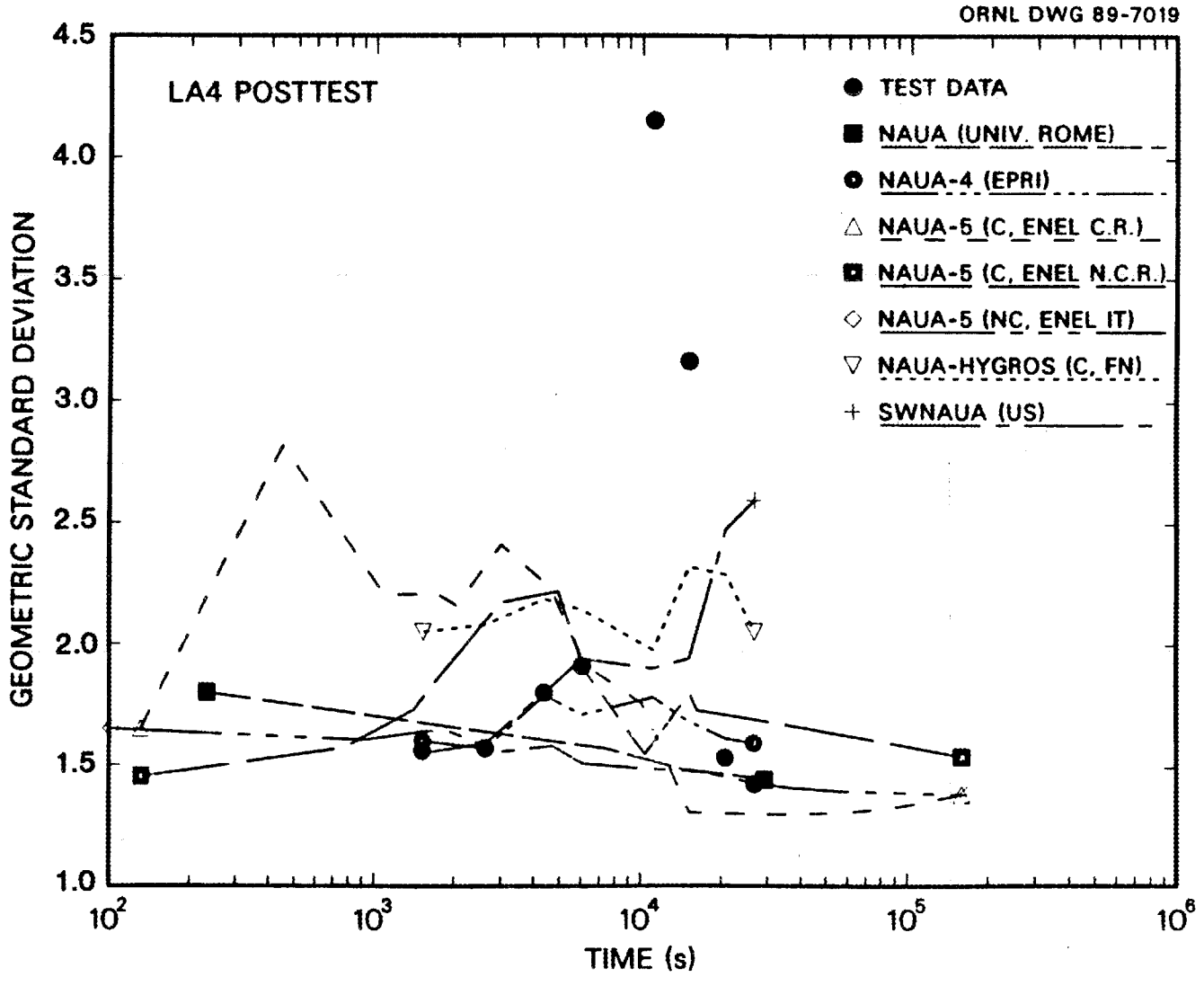

Fig. 42. LA4 posttest calculations - GSD of total airborne aerosol vs time - as reported by group 2 codes.

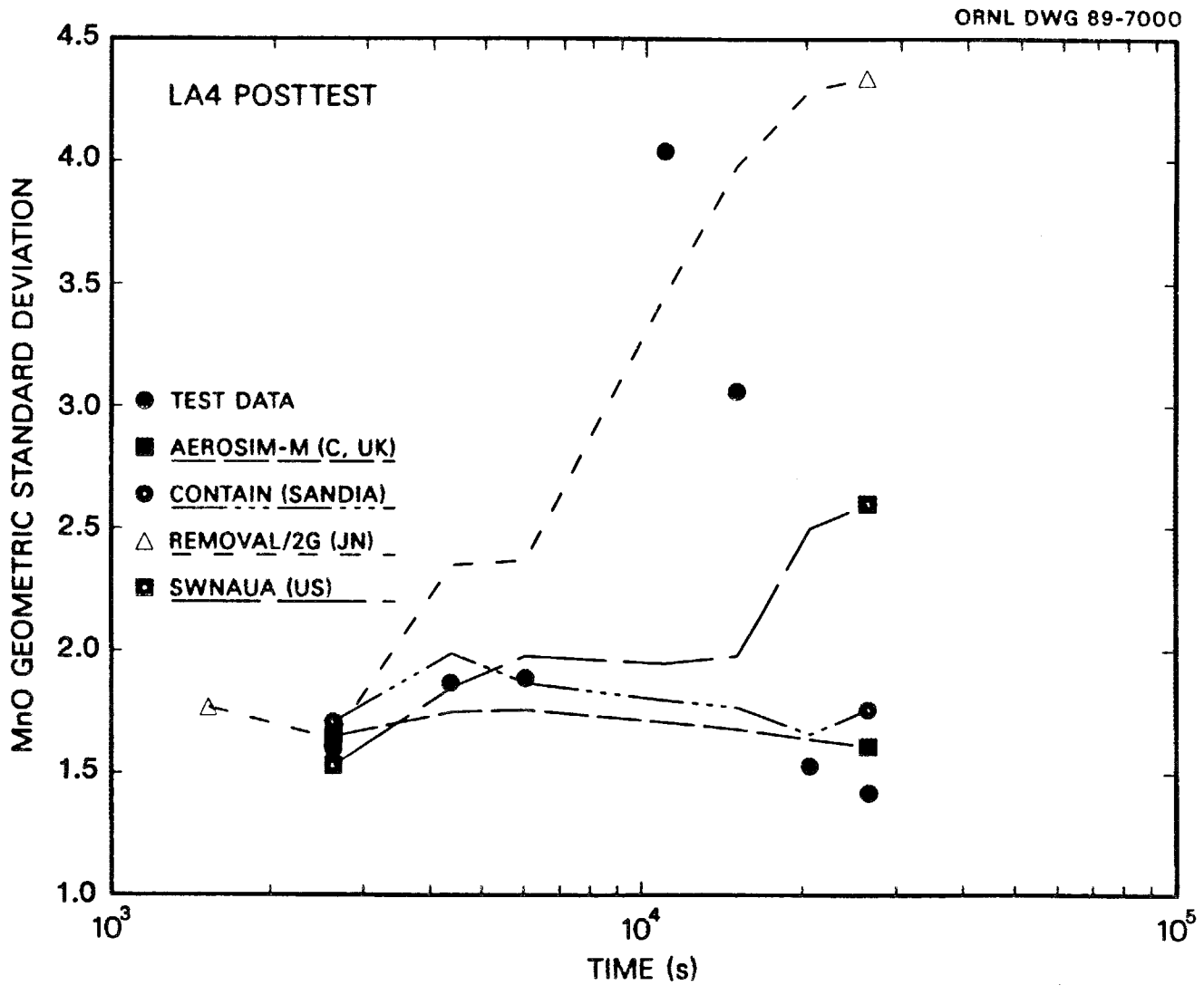

Fig. 43. LA4 posttest calculations - GSD of MnO airborne aerosol vs time.

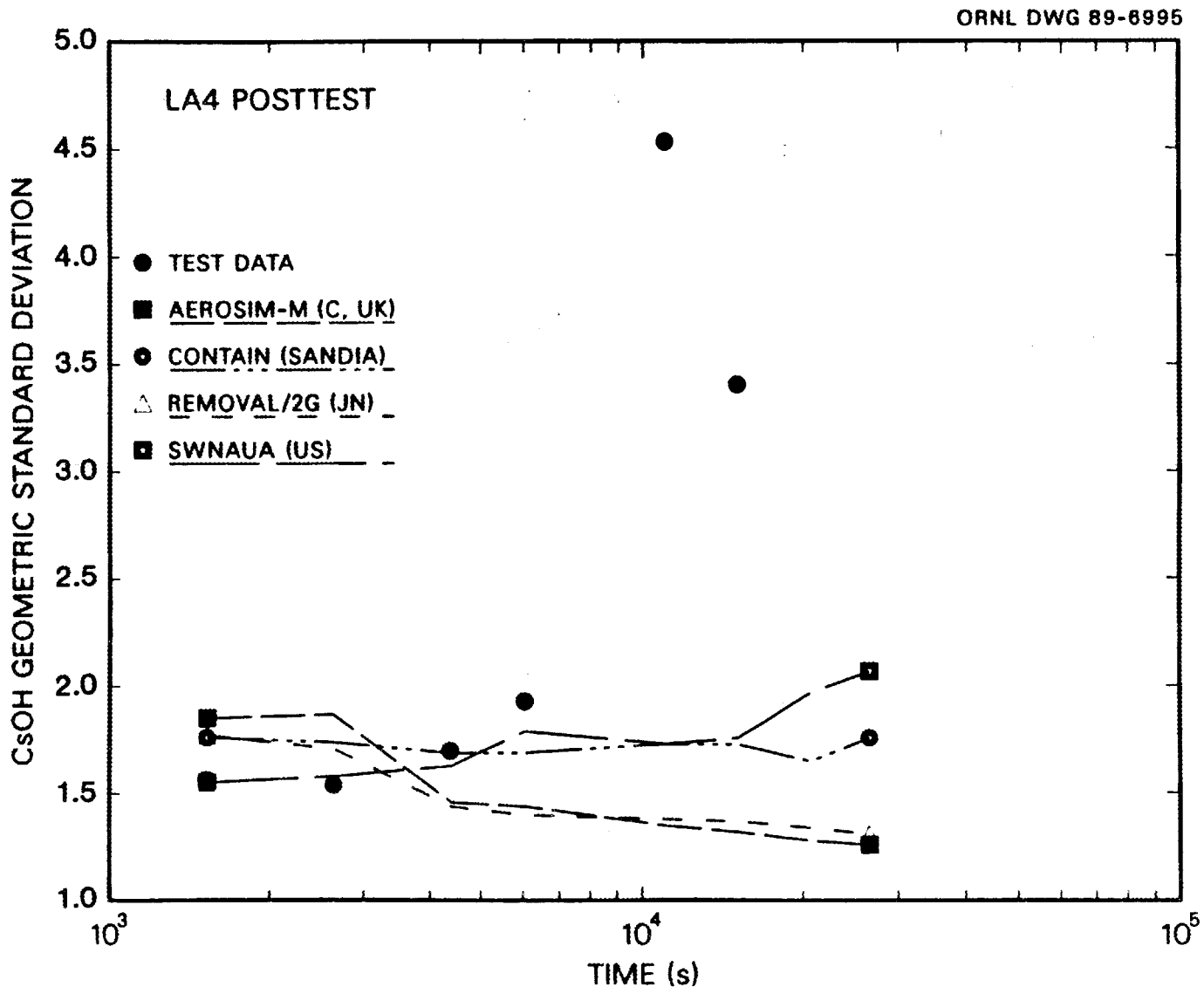

Fig. 44. LA4 posttest calculations - GSD of CsOH airborne aerosol vs time.

Table 8. Comparison of reported and calculated AMMD and GSD values calculated from PSDs

CONTAIN(ORNL)

Time (s)	AMMD reported (μm)	AMMD calculated from PSD (μm)	GSD reported	GSD calculated from PSD
1530	2.17	2.2	1.83	1.79
2640	2.11	2.1	1.86	1.84
4400	2.28	2.28	1.82	1.8
6060	2.67	2.67	1.76	1.74
11100	3.51	3.51	1.76	1.75
15150	3.77	3.77	1.76	1.74
20700	3.59	6.93	1.98	1.67
26600	1.68	1.68	2.19	2.18

NAUA-HYGROS(FN)

Time (s)	AMMD reported (μm)	AMMD calculated from PSD (μm)	GSD reported	GSD calculated from PSD
1530	3.3	3.16	2.05	1.99
2640	5.29	5.07	2.08	2.07
4400	4.89	4.91	2.19	2.07
6060	7.88	7.98	2.14	2.13
11100	5.13	5.37	1.98	1.98
15150	9.6	10.6	2.32	2.32
20700	2.96	3.35	2.29	2.4
26600	2.17	2.17	2.05	2.25

Table 8. Comparison of reported and calculated AMMD and GSD values calculated from PSDs (continued)

CONTAIN(SANDIA)

Time (s)	AMMD reported (μm)	AMMD calculated from PSD (μm)	GSD reported	GSD calculated from PSD
1530	1.34	1.43	1.76	1.76
2640	1.8	1.92	1.76	1.76
4400	2.15	2.32	1.82	1.82
6060	2.51	2.69	1.77	1.77
11100	3.19	3.43	1.76	1.76
15150	3.36	3.65	1.75	1.75
20700	5.61	6.02	1.66	1.66
26600	7.10	7.67	1.76	1.76

AEROSIM-M(UK)

Time (s)	AMMD reported (μm)	AMMD calculated from PSD (μm)	GSD reported	GSD calculated from PSD
1530	4.47	4.89	1.68	1.57
2640	6.63	5.95	1.82	1.9
4400	7.9	8.07	1.69	2.07
6060	8.35	7.84	1.74	2.02
11100	6.26	5.72	1.7	1.75
15150	5.53	5.01	1.67	1.66
20700	4.86	4.36	1.64	1.59
26600	4.37	3.86	1.61	1.55

Table 8. Comparison of reported and calculated AMMD and GSD values calculated from PSDs (continued)

NAUA(EPRI)

Time (s)	AMMD reported (μm)	AMMD calculated from PSD (μm)	GSD reported	GSD calculated from PSD
1530	2.04	2.15	1.6	1.6
2640	2.73	2.81	1.57	1.57
4400	3.97	4.14	1.79	1.79
6060	5.92	6.01	1.71	1.71
11100	7.31	7.64	1.78	1.78
15150	6.06	6.38	1.68	1.68
20700	4.58	4.8	1.61	1.61
26600	2.85	2.93	1.59	1.59

REMOVAL/2G(JN)

Time (s)	AMMD reported (μm)	AMMD calculated from PSD (μm)	GSD reported	GSD calculated from PSD
1530	2.15	1.28	1.77	1.68
2640	2.65	1.77	1.7	1.64
4400	3.13	2.2	2.59	1.72
6060	3.55	2.54	2.04	1.63
11100	4.12	3.0	1.87	1.57
15150	4.19	3.06	1.83	1.55
20700	4.03	2.93	1.73	1.51
26600	3.75	2.71	1.67	1.47

Table 8. Comparison of reported and calculated AMMD and GSD values calculated from PSDs (continued)

SWNAUA(US)

Time (s)	AMMD reported (μm)	AMMD calculated from PSD (μm)	GSD reported	GSD calculated from PSD
1530	2.42	2.42	1.55	1.55
2640	3.17	3.19	1.59	1.59
4400	4.34	4.34	1.8	1.8
6060	5.9	5.9	1.94	1.94
11100	6.32	6.34	1.9	1.9
15150	5.85	5.87	1.94	1.95
20700	4.43	4.43	2.47	2.47
26600	2.33	2.34	2.59	2.59

MCT-2(NYPA)

Time (s)	AMMD reported (μm)	AMMD calculated from PSD (μm)	GSD reported	GSD calculated from PSD
1560	2.05	2.15	1.8	1.76
2600	2.87	2.76	1.76	1.74
4420	2.95	3.32	2.02	1.88
6110	4.24	3.53	2.01	1.77
10800	4.32	3.61	1.81	1.63
15600	4.12	3.44	1.78	1.57
20400	3.84	3.24	1.76	1.53
26400	3.53	3.0	1.72	1.51

Table 8. Comparison of reported and calculated AMMD and GSD values calculated from PSDs (continued)

CONTAIN(UK)

Time (s)	AMMD reported (μm)	AMMD calculated from PSD (μm)	GSD reported	GSD calculated from PSD
1530	1.74	1.74	1.73	1.71
2640	2.29	2.29	1.66	1.63
4400	2.98	2.98	1.7	1.68
6060	3.6	3.6	1.6	1.58
11100	4.49	4.49	1.56	1.54
15150	4.65	4.65	1.54	1.52
20700	5.17	7.78	1.74	1.52
26600	2.07	2.07	1.89	1.87

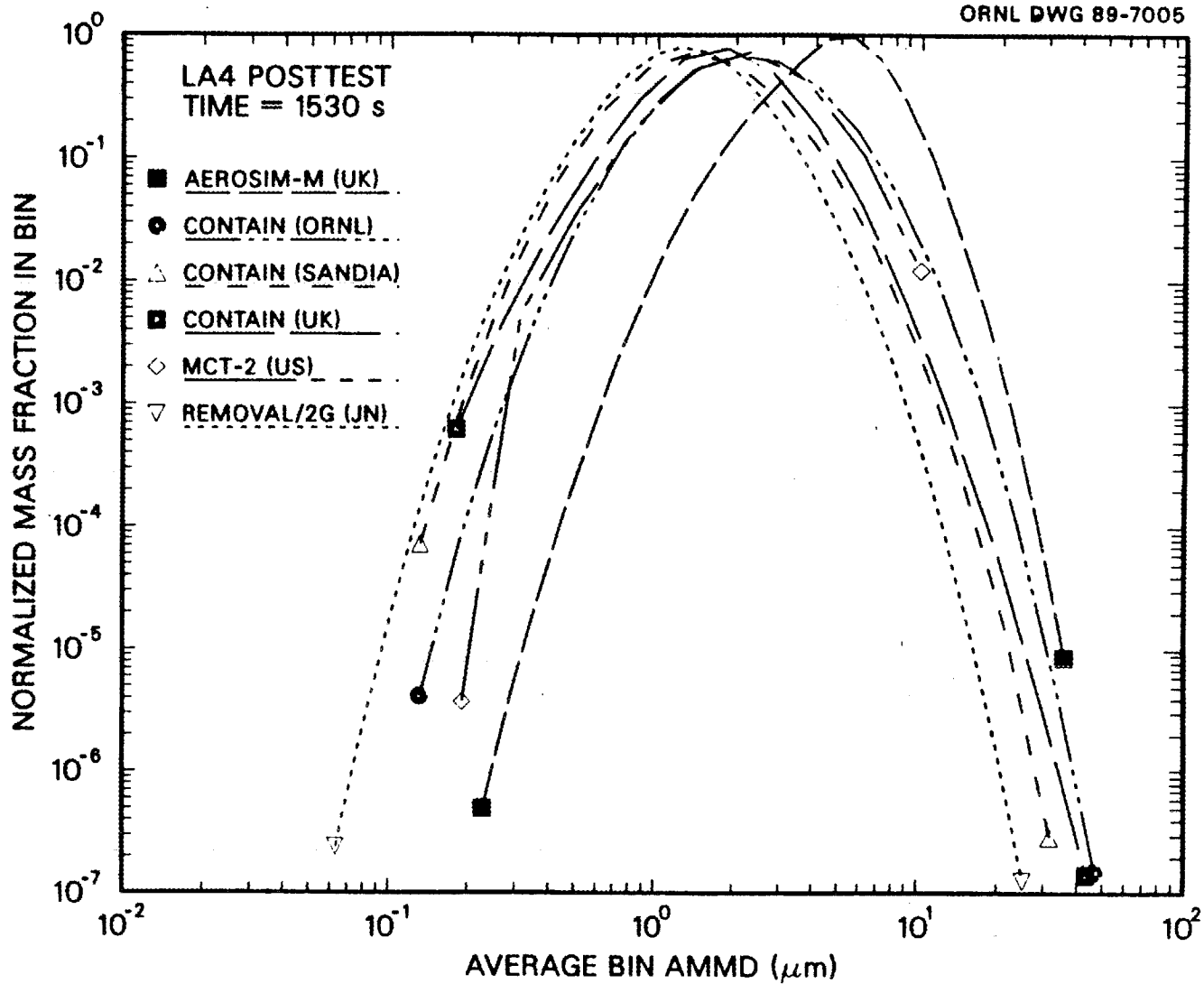

Fig. 45. LA4 posttest calculations - particle size distribution of airborne aerosol at 1,530 s - for group 1 codes.

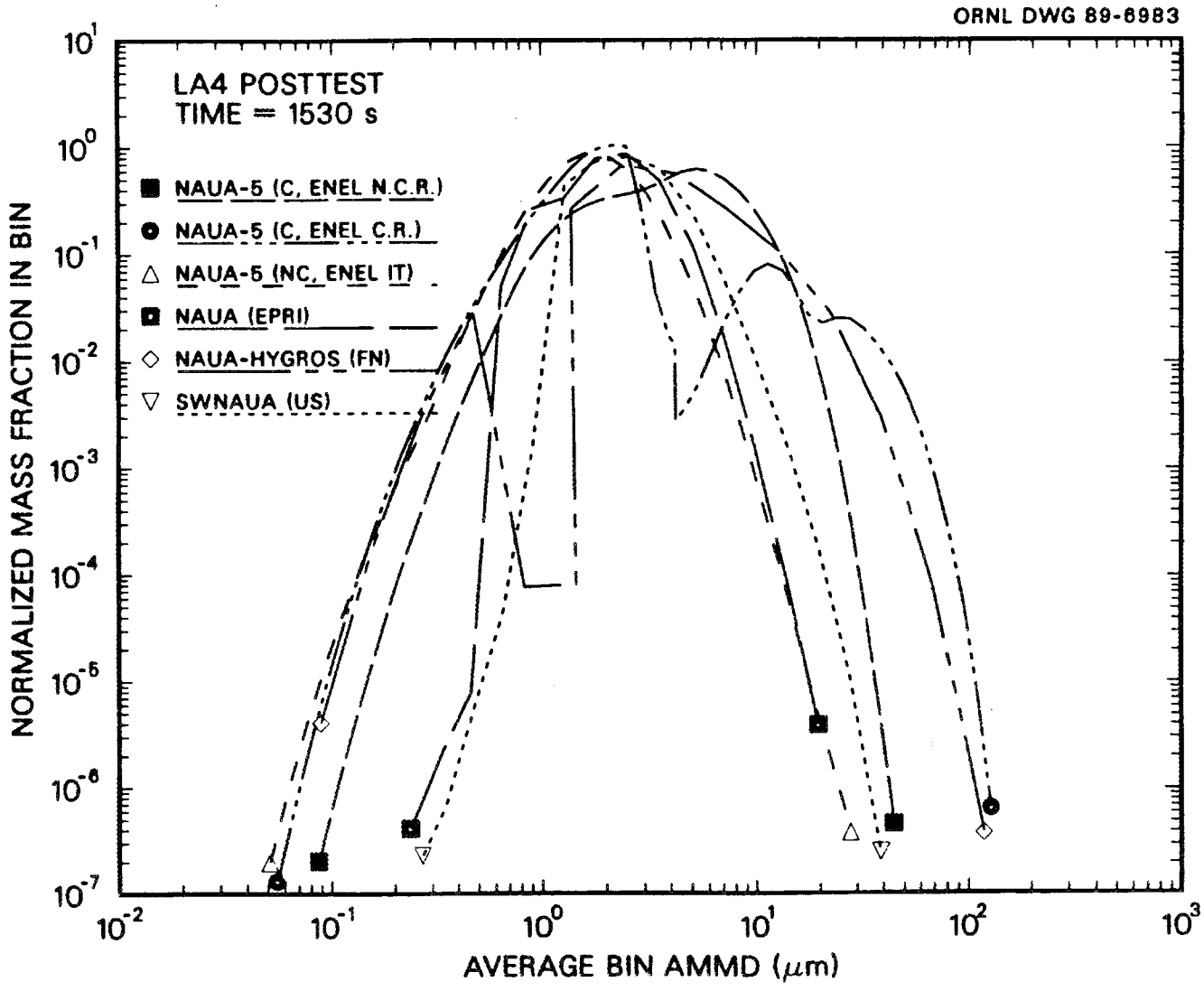

Fig. 46. LA4 posttest calculations - particle size distribution of airborne aerosol at 1,530 s - for group 2 codes.

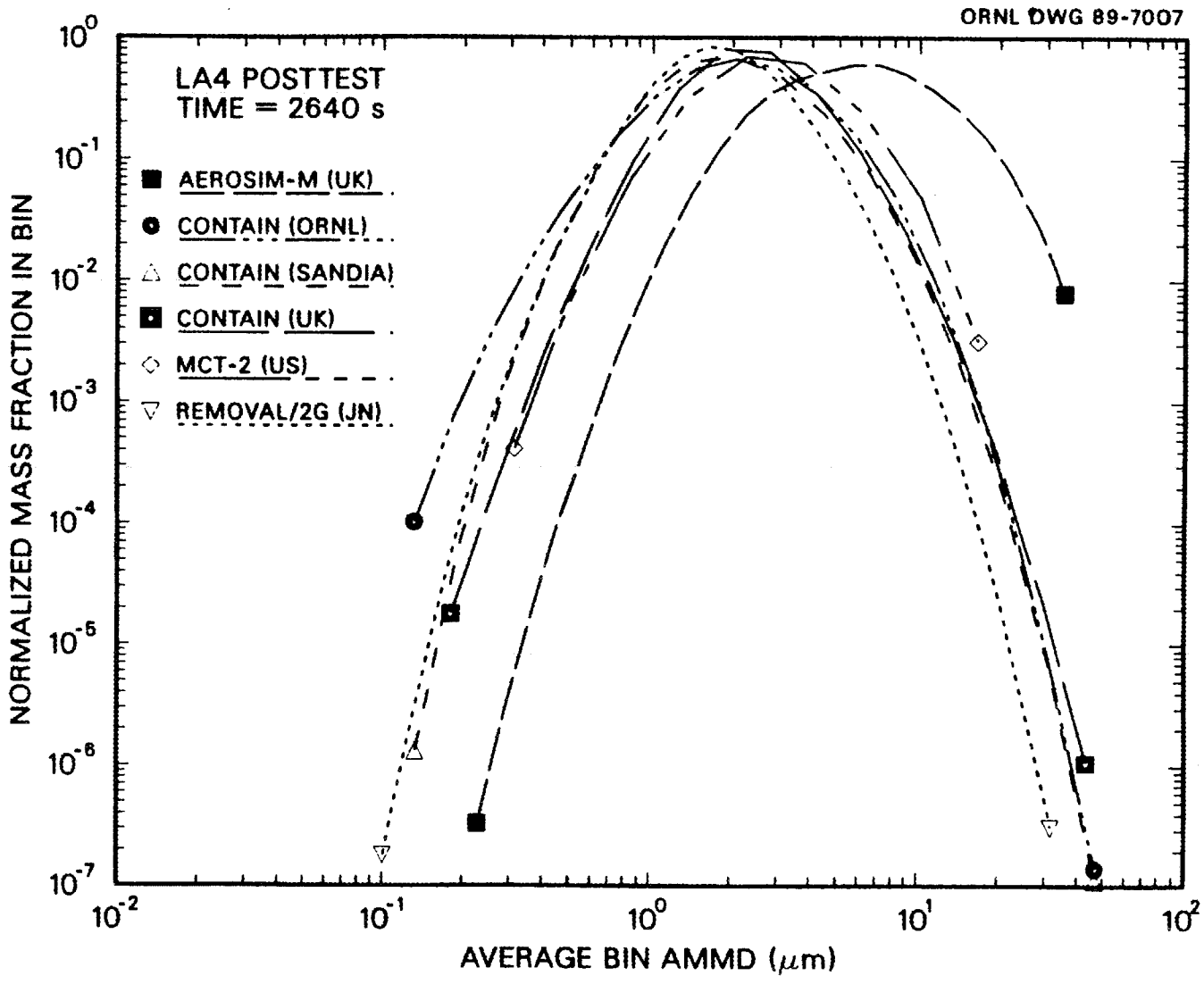

Fig. 47. LA4 posttest calculations - particle size distribution of airborne aerosol at 2,640 s - for group 1 codes.

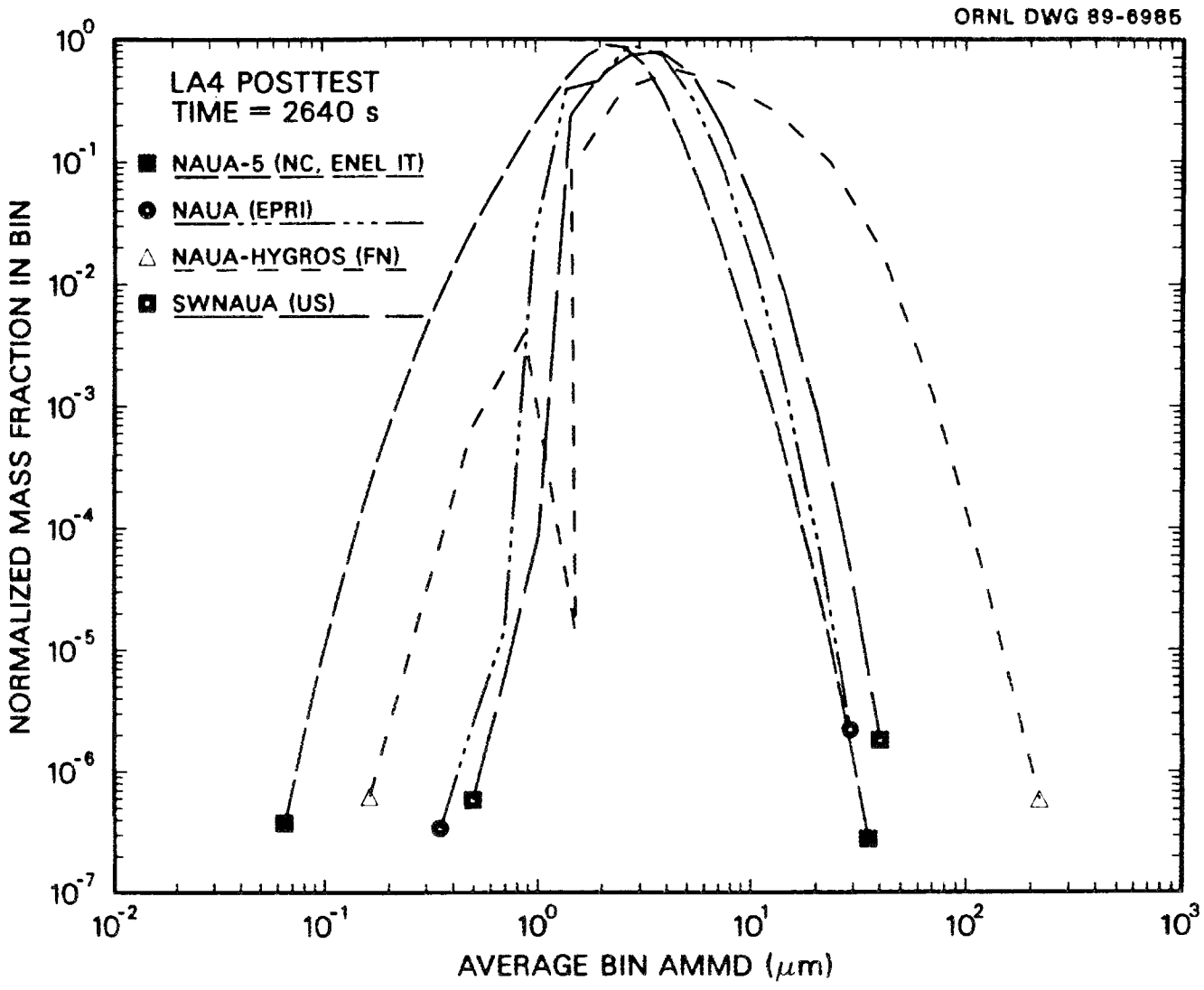

Fig. 48. LA4 posttest calculations - particle size distribution of airborne aerosol at 2,640 s - for group 2 codes.

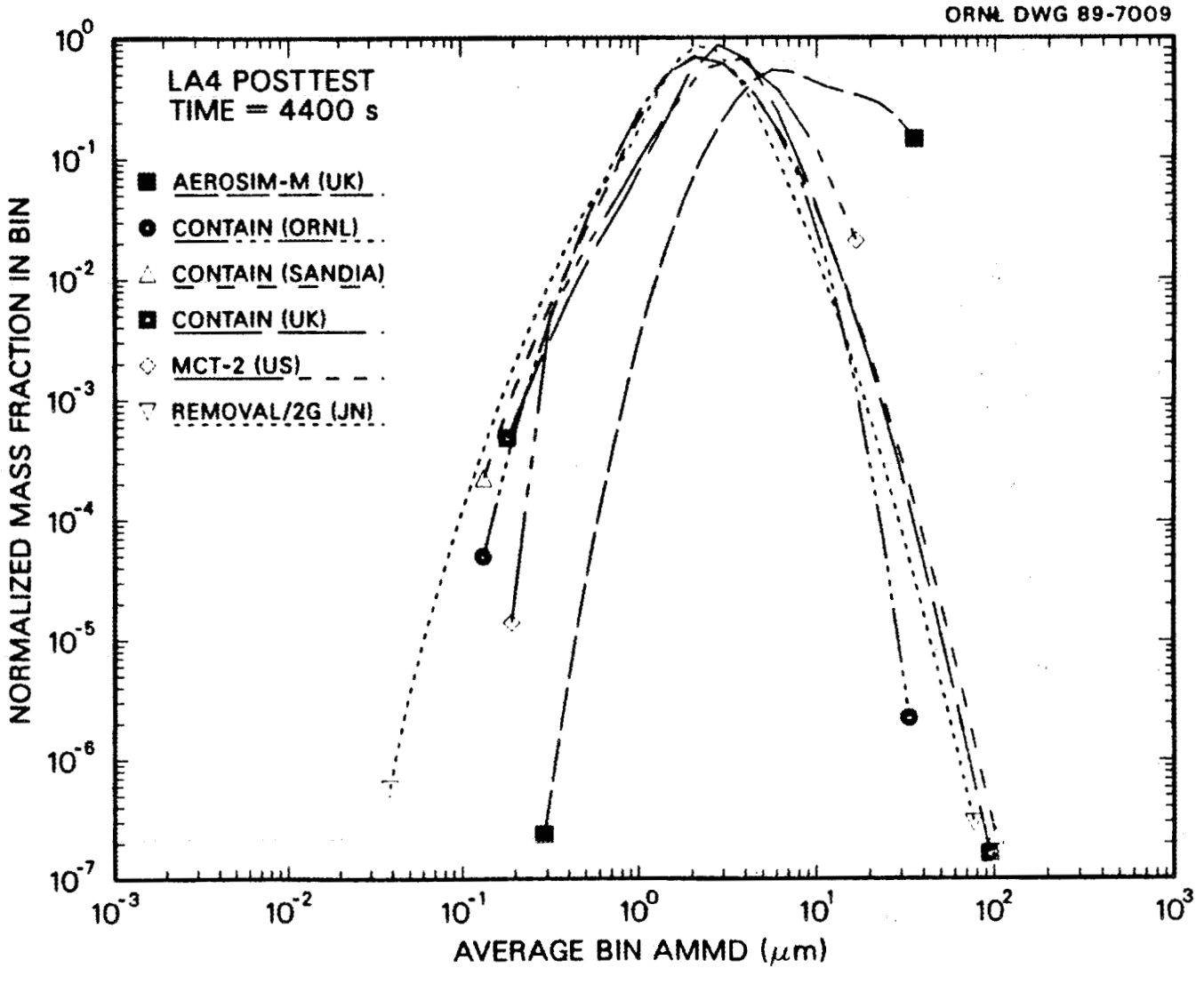

Fig. 49. LA4 posttest calculations - particle size distribution of airborne aerosol at 4.400 s - for group 1 codes.

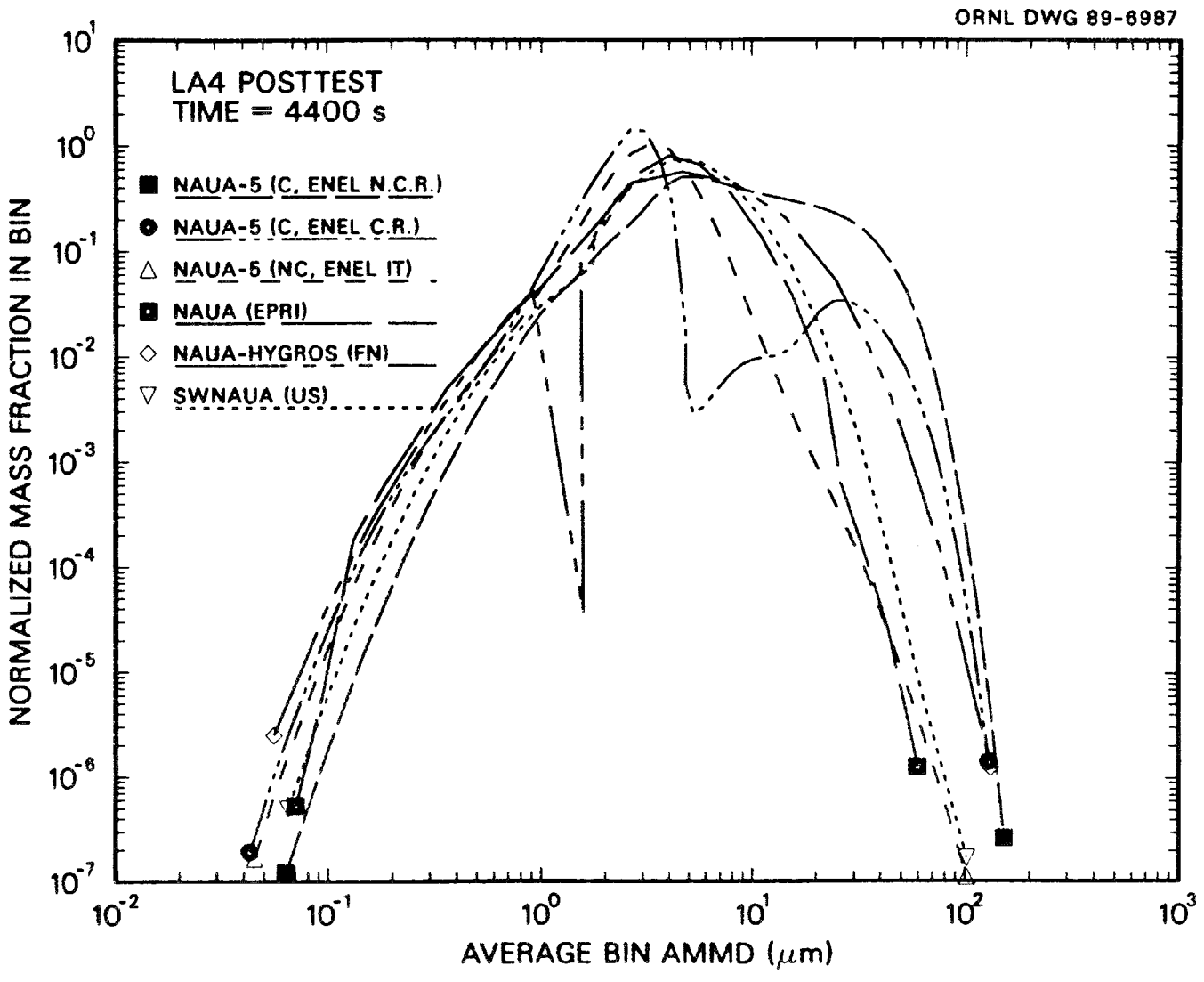

Fig. 50. LA4 posttest calculations - particle size distribution of airborne aerosol at 4.400 s - for group 2 codes.

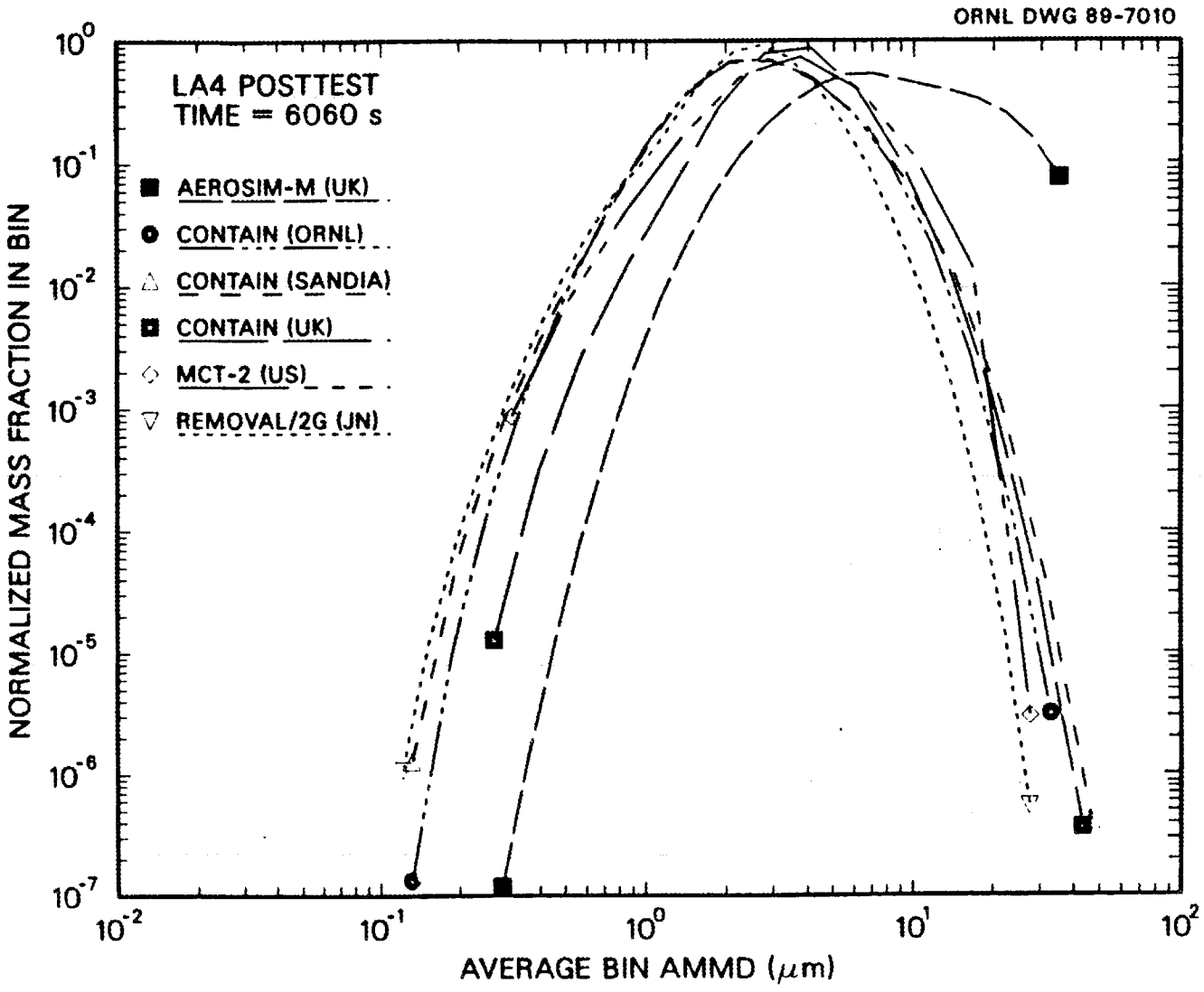

Fig. 51. LA4 posttest calculations - particle size distribution of airborne aerosol at 6,060 s - for group 1 codes.

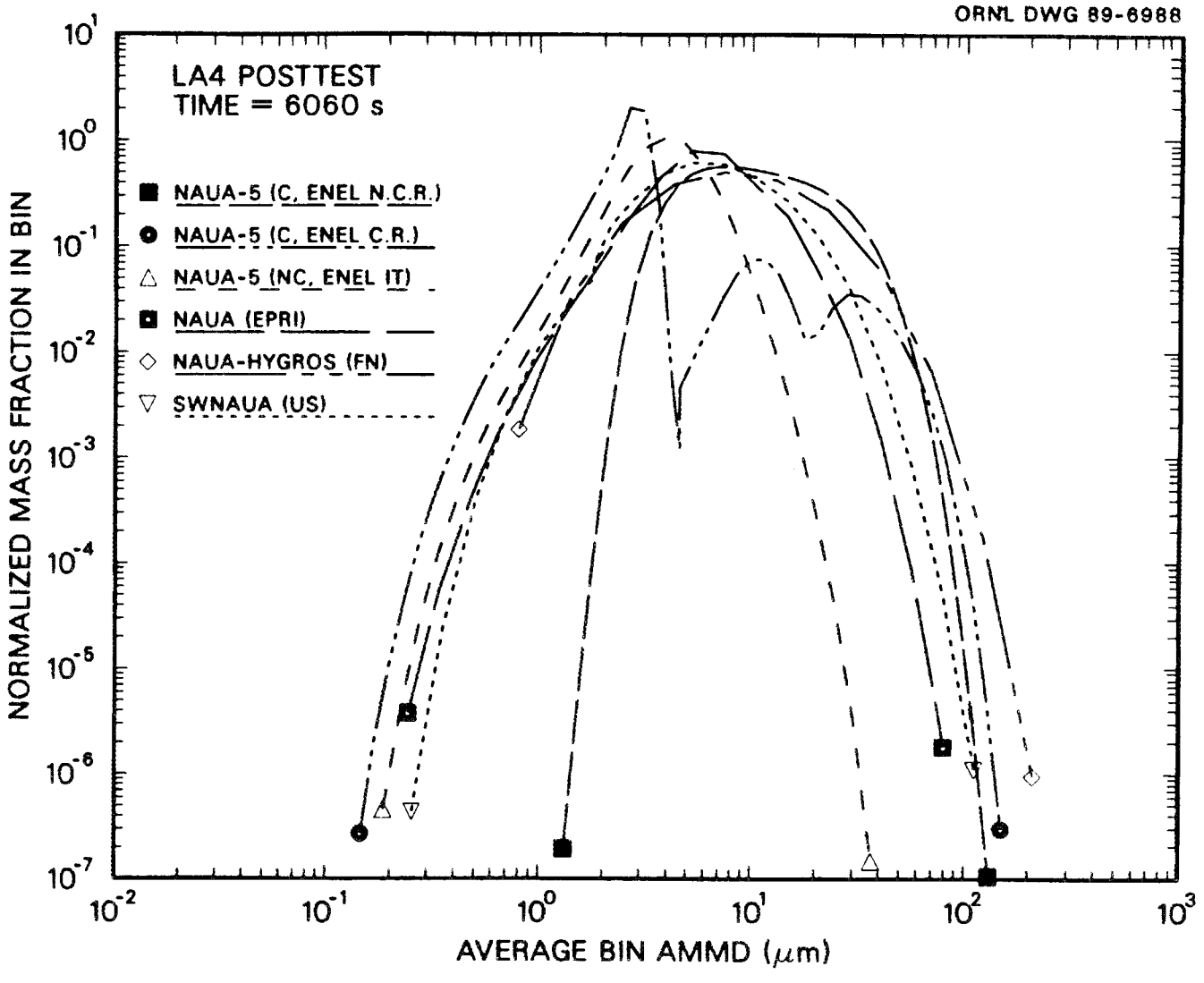

Fig. 52. LA4 posttest calculations - particle size distribution of airborne aerosol at 6,060 s - for group 2 codes.

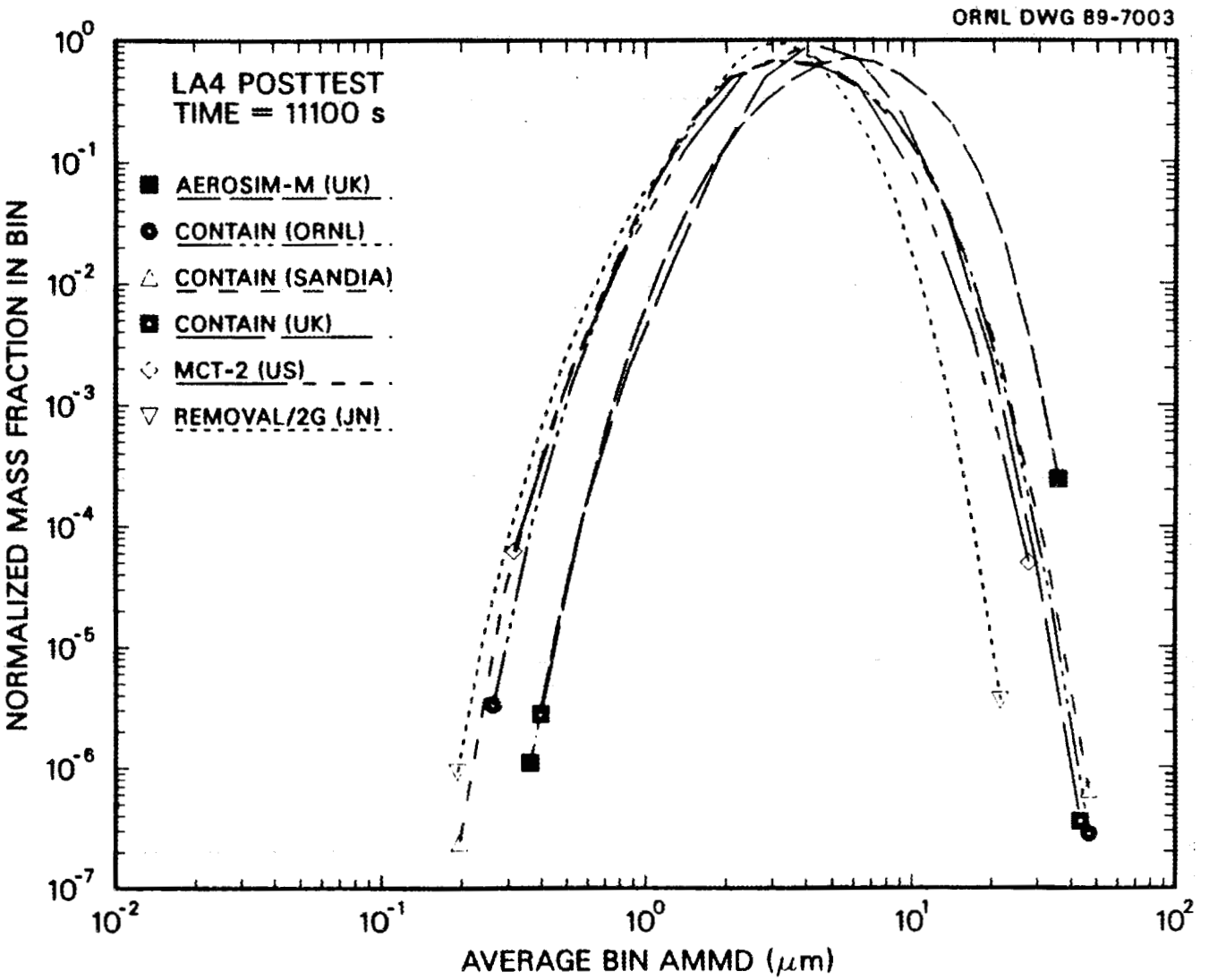

Fig. 53. LA4 posttest calculations - particle size distribution of airborne aerosol at 11,100 s - for group 1 codes.

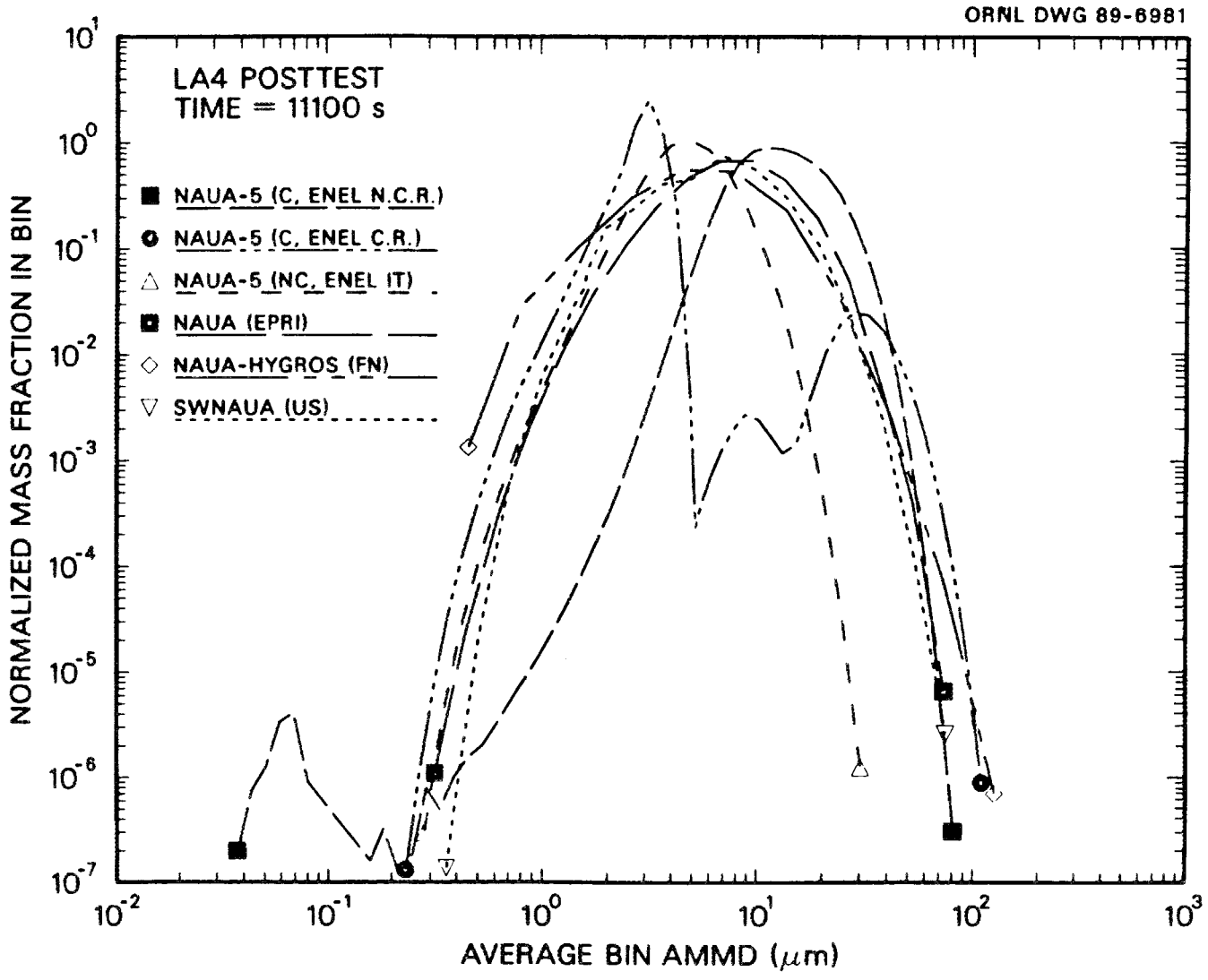

Fig. 54. LA4 posttest calculations - particle size distribution of airborne aerosol at 11,100 s - for group 2 codes.

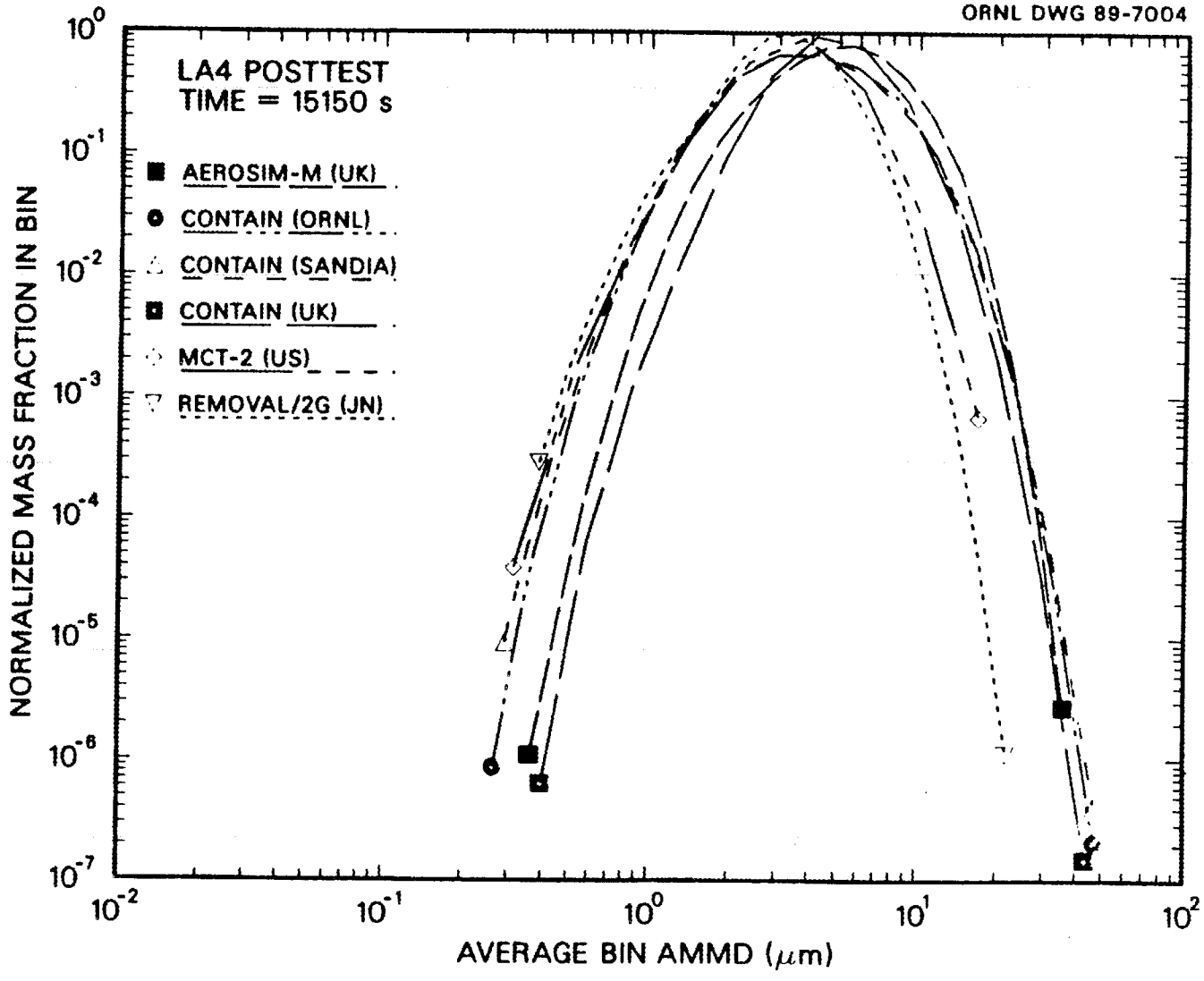

Fig. 55. LA4 posttest calculations - particle size distribution of airborne aerosol at 15,150 s - for group 1 codes.

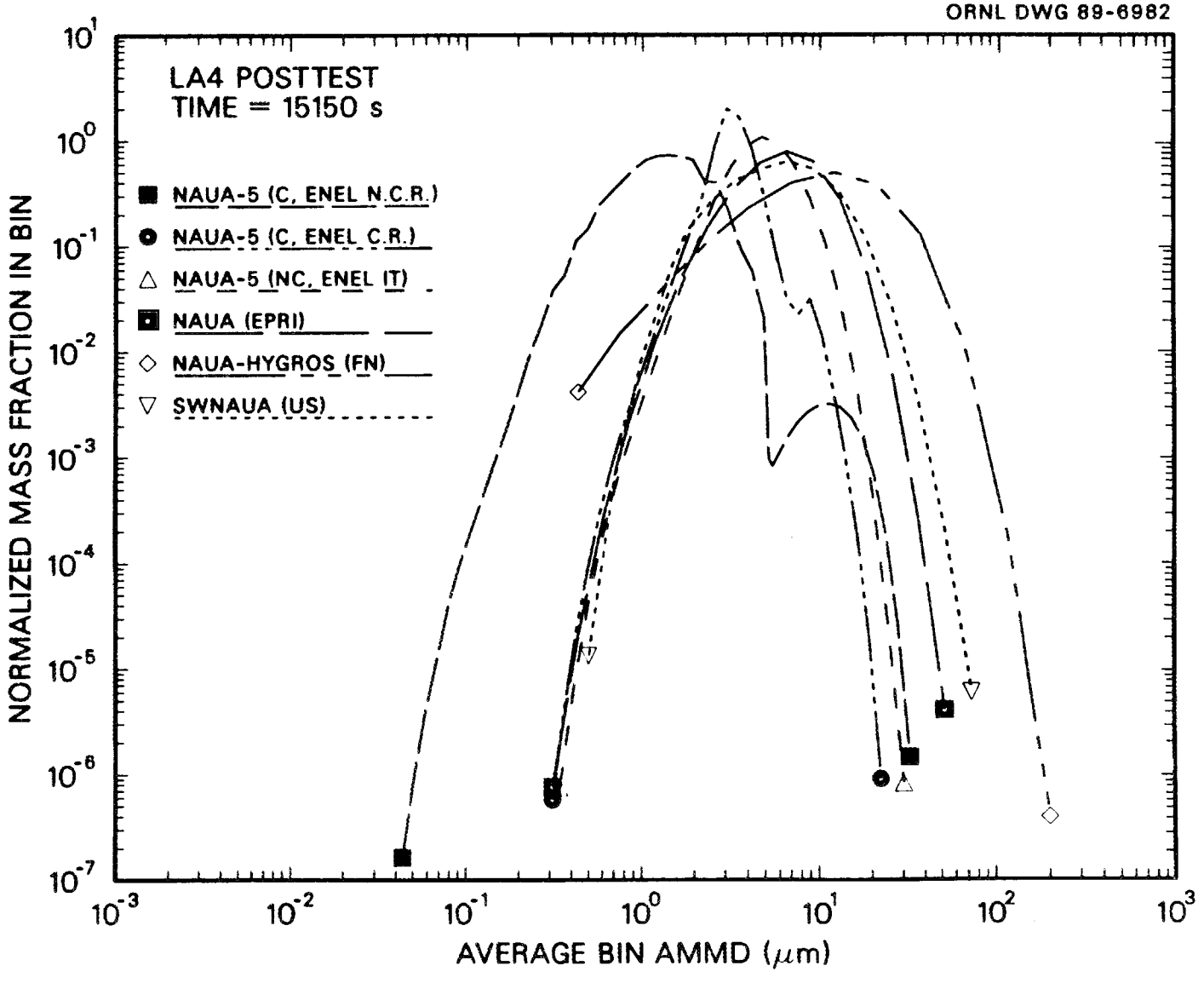

Fig. 56. LA4 posttest calculations - particle size distribution of airborne aerosol at 15,150 s - for group 2 codes.

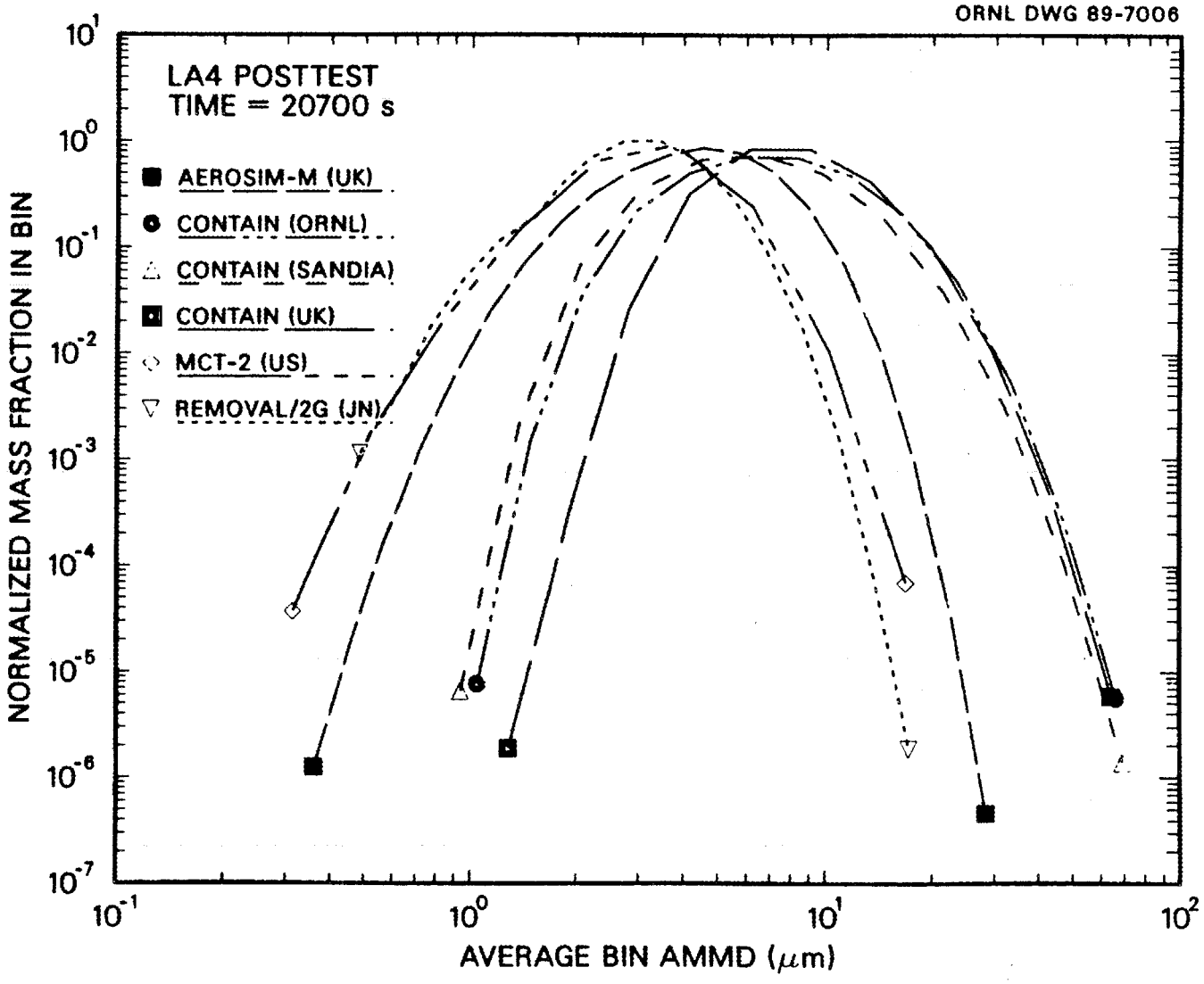

Fig. 57. LA4 posttest calculations - particle size distribution of airborne aerosol at 20,700 s - for group 1 codes.

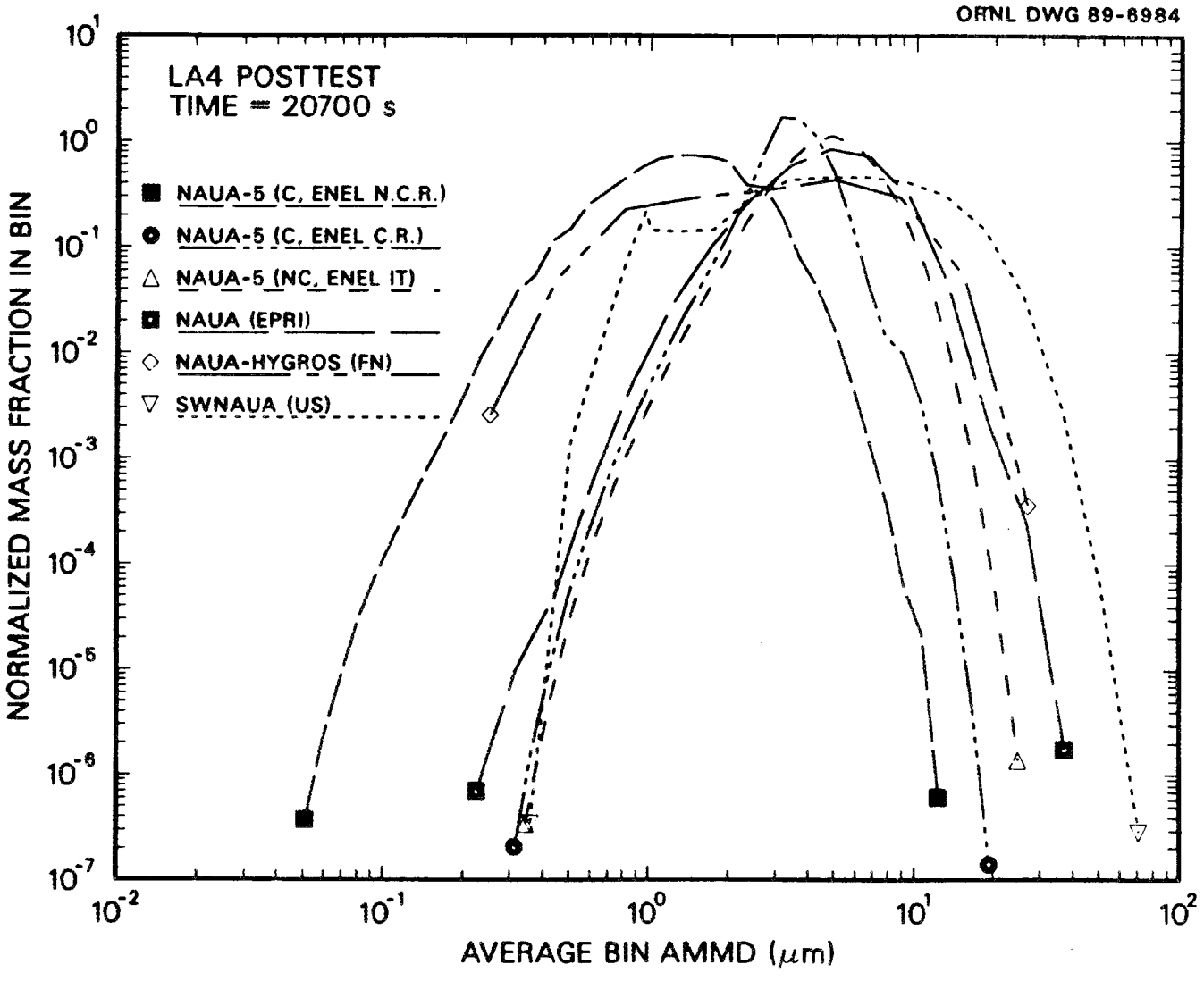

Fig. 58. LA4 posttest calculations - particle size distribution of airborne aerosol at 20,700 s - for group 2 codes.

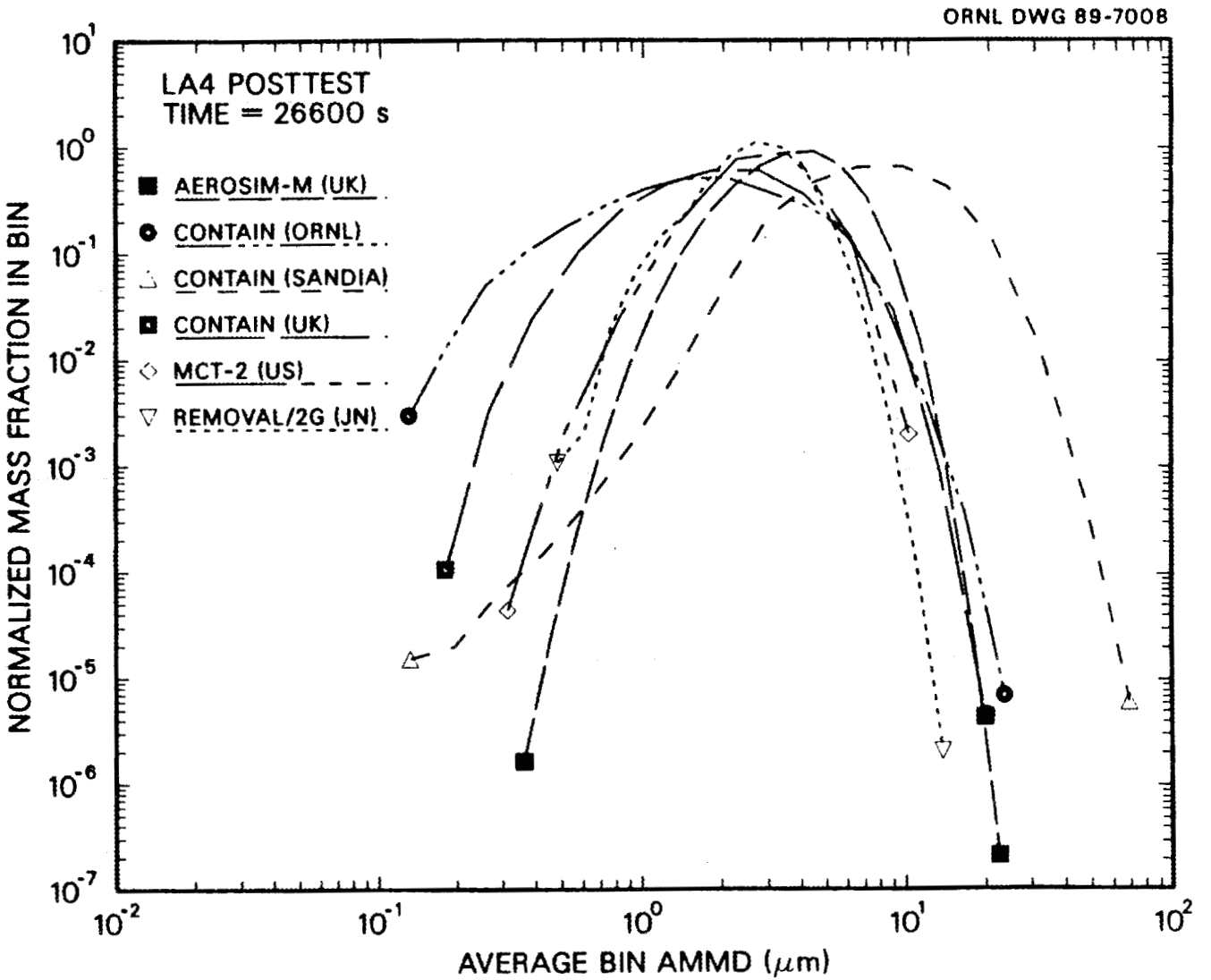

Fig. 59. LA4 posttest calculations - particle size distribution of airborne aerosol at 26,600 s - for group 1 codes.

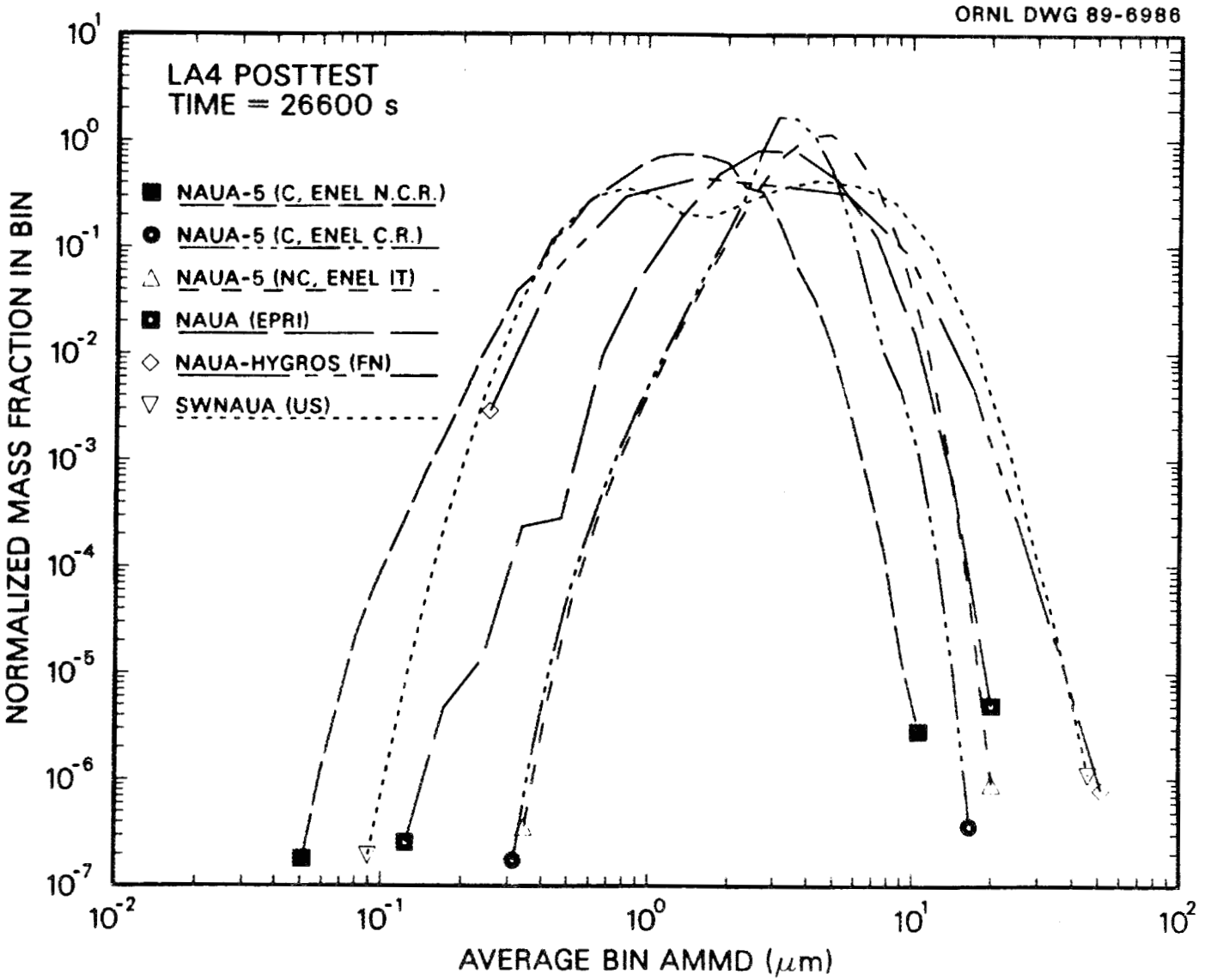

Fig. 60. LA4 posttest calculations - particle size distribution of airborne aerosol at 26,600 s - for group 2 codes.

5. LACE LA4 EXPERIMENTAL DATA

As mentioned in Sect. 2, the LA4 aerosol experimental data were provided in report LACE TR-025.[6] The aerosol data are summarized in this section.

Table 9 presents the CsOH, MnO, and total (CsOH + MnO) aerosol concentration vs time data as measured in test LA4. These measurements were made at several locations in the CSTF vessel using "cluster" and "through-the-wall" samplers. The mean and standard error (or standard deviation) of the mean were determined by standard expressions as

$$C_m = \Sigma(C_i)/N, \qquad (2)$$

$$E_{se} = [\Sigma(C_m - C_i)^2/(N(N - 1))]^{0.5}, \qquad (3)$$

where

C_m = mean aerosol concentration,

E_{se} = standard error of the mean,

C_i = measured aerosol concentration at sampling time, t_i

N = number of concentration measurements at each sampling tim

Note that the standard error that is calculated includes the error associated with each aerosol concentration measurement and the error associated with sampling at different locations in the vessel. If the vessel contents were perfectly mixed, the latter error would be zero.

Table 10 presents a summary of the measured aerosol removal by (1) gravitational settling, (2) wall plateout, and (3) transport by leakage from the CSTF vessel in test LA4. The values in Table 10, which were reported by HEDL in Table 6.45 of LACE TR-025,[6] were used for the calculation of relative errors, as described in the next section.

Table 11 presents the results of the cascade impactor measurements of AMMD and GSD for test LA4. The values in Table 11 were determined by HEDL by analysis of the cascade impactor data in Appendix D of report LACE TR-025.[6] Previously, we used the method described in Appendix C (which follows the guidelines given in Appendixes A and B) to analyze

Table 9. Experimental airborne aerosol concentrations for LACE LA4

Time (s)	Airborne MnO mass (g/m^3)	Standard deviation (%)	Airborne CsOH mass (g/m^3)	Standard deviation (%)	Total airborne dry mass (g/m^3)	Standard deviation (%)
132			9.370E-02		9.370E-02	
750			8.330E-01	93	8.330E-01	93
1530			2.460E+00		2.460E+00	1
1770			2.180E+00	42	2.180E+00	57
2976	1.200E+00	30	2.970E+00	15	4.170E+00	19
4740	2.320E+00	13	2.030E+00	36	4.350E+00	21
6060	2.130E+00	15	1.560E+00	17	3.690E+00	16
10440	3.740E-01	19	1.350E-01	31	5.090E-01	22
15120	7.710E-02	12	1.330E-02	5	9.040E-02	10
16320	5.190E-02	15	7.720E-03	10	5.962E-02	15
16920	4.040E-02	12	4.830E-03	17	4.523E-02	12
18600	1.260E-02	8	4.210E-04	59	1.302E-02	10
21720	3.610E-03	11	1.480E-05	45	3.625E-03	8
25380	1.360E-03	13	9.120E-06	72	1.369E-03	13
36600	1.930E-04	4	2.330E-06	129	1.953E-04	2
57120	2.320E-05	77	1.490E-06	126	2.469E-05	102
81000	1.170E-05	38	3.150E-07	59	1.201E-05	47
98400	9.420E-06	18	8.570E-07	166	1.028E-05	18
168000	3.660E-06	58	3.090E-07	74	3.969E-06	39

Table 10. Location of aerosol mass for LACE LA4

Location	MnO (g)	CsOH (g)	Total (g)
Settled	1927	2563	4490
Plated	228	304	532
Leaked	101	7	108
Total delivered to CSTF vessel	2256	2874	5130

Table 11. Experimental AMMD and GSD data for LACE LA4

Time (s)	AMMD (μm)	Geometric standard deviation
1524	2.06	1.56
2640	3.33	1.57
4380	3.95	1.8
6060	4.37	1.91
11100	6.75	4.15
15120	7.6	3.16
20700	1.84	1.53
26700	1.6	1.42

cascade impactor data. When the PSD is lognormal, which as HEDL[6] reported was generally the case, this method and the method used by HEDL[6] give comparable results for the AMMD and the GSD. If the distribution deviates significantly from lognormal behavior, the method in Appendix C would be recommended for analysis of the impactor data in order to compare with the PSD results reported by the code users (assuming the code users are employing the methods of Appendixes A and B).

6. CALCULATION AND ANALYSIS OF VARIANCE BETWEEN EXPERIMENTAL MEASUREMENTS AND CODE PREDICTIONS

Average errors were determined as a quantitative measure of the variance between the experimental data and the results of the code calculations. This average error is defined as

$$E_{av} = [(\Sigma E_{rms,i})/N_s]^{0.5}, \qquad (4)$$

where

E_{av} = average error,

$E_{rms,i}$ = The square of the relative error at ith sampling time,

N_s = number of sampling times.

The square of the relative, or fractional, error at a given sampling time is defined as

$$E_{rms,i} = [(C_{m,i} - C_{c,i})/C_{m,i}]^2 \qquad (5)$$

where

$C_{m,i}$ = measured variable value at the ith sampling time,

$C_{c,i}$ = calculated variable value at the ith sampling time.

For the cases where there is only one sampling time, such as for cumulative aerosol leaked, the average error is simply the absolute value of the fractional error with respect to the measured variable.

The use of the square of the relative error is preferred to the use of the square of the "absolute" error (i.e., $(C_{m,i} - C_{c,i})^2$ such as in the calculation of the standard deviation). For a variable whose

values vary over several orders of magnitude, the use of the "absolute" error generally shows the effects of errors only for the larger values of the variable. The reason is that, in most physical situations, the magnitude of the "absolute" error is found to be approximately proportional to the magnitude of the measured value of the variable - that is, the fractional, or relative, error is fairly constant. This is evidenced by Table 9.

The average errors for the suspended aerosol concentration are presented in Table 12. Here, average errors are given for the aerosol source period and for the period after termination of the aerosol source. The average errors for the total amounts of aerosol leaked, retained, plated, and settled are shown in Table 13. Tables 14 and 15 present similar information for each separate aerosol species. Finally, the average errors for AMMD and GSD are given in Table 16. The average errors in Tables 12 through 16 have been expressed as percentages by multiplying E_{av} by 100.

The average errors, along with the plots of the code predictions and the experimental data, may be used as an indication, but not as a quantitative measure, of how well a code simulates test LA4. While such a quantitative measure is indeed desirable, one cannot perform any statistically significant comparison without, at the least, estimates of the mean and standard deviation for the experimental measurements. For such estimates, a minimum of two, and preferably more, replicates of the test are required. One problem, in trying to compare with the results of a single experiment, is that the results themselves may differ significantly from the mean. Thus, a comparison of code predictions with the results of the single experiment may indicate an acceptable simulation; while in reality, a statistically significant difference existed between the simulation and the mean of the test results. Although standard deviations and error estimates were reported for test LA4, the run-to-run variance was not included. For example, the standard deviations reported in Table 9 for airborne aerosol concentrations included only the standard deviations associated with each concentration measurement and with sampling at different locations.

Table 12. LA4 - Average errors for airborne aerosol concentration

	Average error (%)					
	Total aerosol		MnO		CsOH	
Code	During source	After source	During source	After source	During source	After source
AEROSIM-M(UK)	36.0	32.6	29.0	34.4	41.0	18.0
CONTAIN(ORNL)	35.1	486.0	7.5	296.0	38.5	5838.0
CONTAIN(UK)	16.3	582.0	7.1	301.0	30.0	9064.0
CONTAIN(SANDIA)	29.1	221.0	9.4	97.9	33.4	7385.0
MAAP-3(SW)	17.1	866.0	20.6	489.0	16.1	11684.0
MCT-2(US)						
NAUA-HYGROS(FN)	30.7	11.1	23.8	6.3	30.8	112.0
NAUA(EPRI)	32.5	76.7	4.2	38.0	34.3	1069.0
NAUA-5(C,ENEL,NCR)	33.2	5.3	40.0	3.0	34.0	55.0
NAUA-5(C,ENEL,CR)	25.2	411.0	15.3	220.0	24.8	7890.0
NAUA-5(NC,ENEL)	18.0	338.0	3.9	162.0	22.3	8950.0
NAUA(UNIV. ROME)	50.0	2380.0				
REMOVAL/2G(JN)	29.7	406.0	12.9	294.0	31.0	7627.0
SWNAUA(US)	27.8	1.0	4.8	0.7	28.7	19.0

Table 13. LA4 - Average errors for cumulative total aerosol leaked, retained, plated, and settled mass

Code	Leaked Total mass (g)	Leaked Error (%)	Retained Total mass (g)	Retained Error (%)	Plated Total mass (g)	Plated Error (%)	Settled Total mass (g)	Settled Error (%)
AEROSIM-M(UK)	35.6	-67	5093	1.4	236	-56	4857	8
CONTAIN(ORNL)	1010	835	4126	-17.8	813	53	3313	-26
CONTAIN(SANDIA)	874	709	4171	-16.9	685	29	3486	-22
CONTAIN(UK)	766	609	4466	-11.1	641	20	3825	-15
MAAP-3(SW)	476	341	4655	-7.3	1395	162	3260	-27
MCT-2(US)	140	30	5016	-0.1	1614	203	3414	-24
NAUA-HYGROS(FN)	2.9	-97	5126	2.1	527	-1	4599	2
NAUA -5(EPRI)	34.8	-68	5109	1.7	703	32	4406	-2
NAUA-5(C,ENEL,NCR)	0.9	-99	5129	2.1	206	-61	4923	10
NAUA-5(C,ENEL,CR)	442	309	4683	-6.8	610	15	4073	-9
NAUA-5 (NC,ENEL)	757	601	4367	-13.0	579	9	3788	-16
NAUA(UNIV. ROME)	1170	983	3930	-21.7	1630	206	2300	-49
REMOVAL/2G(JN)	672	522	4383	-12.7	1203	126	3180	-29
SWNAUA(US)	22.9	-79	5054	0.6	574	8	4480	-0
EXPERIMENTAL	108		5022		532		4490	

Table 14. LA4 - Average errors for cumulative MnO aerosol leaked, retained, plated, and settled mass

Code	Leaked		Retained		Plated		Settled	
	Total mass (%)	Error	Total mass (g)	Error (%)	Total mass (g)	Error (%)	Total mass (g)	Error (%)
AEROSIM-M(UK)	34.6	-66	2220	3	117	-49	2103	
CONTAIN(ORNL)	535	430	1715	-20	361	58	1354	-33
CONTAIN(SANDIA)	372	268	1786	-17	260	14	1526	-24
CONTAIN(UK)	368	264	1952	-9	264	16	1688	-16
MAAP-3(SW)	252	150	2010	-7				
MCT-2(US)	74	-27	2196	2				
NAUA-HYGROS(FN)	1.6	-98	2254	5	199	-13	2055	2
NAUA(EPRI)	16.3	-84	2235	4	243	7	1992	-1
NAUA-5(C,ENEL,NCR)	0.5	-100	2224	3	69	-70	2155	7
NAUA-5(C,ENEL,CR)	225	123	1997	-7	272	19	1725	-14
NAUA-5(NC,ENEL)	346	243	1876	-13	199	-13	1677	-16
NAUA(UNIV. ROME)								
REMOVAL/2G(JN)	350	247	1882	-13	482	111	1400	-30
SWNAUA(US)	18.7	-81	2215	3	245	7	1970	-2
EXPERIMENTAL	101		2155		228		1927	

Table 15. LA4 - Average errors for cumulative CsOH aerosol leaked, retained, plated, and settled mass

Code	Leaked		Retained		Plated		Settled	
	Total mass (g)	Error (%)	Total mass (g)	Error (%)	Total mass (g)	Error (%)	Total mass (g)	Error (%)
AEROSIM-M(UK)	1.3	-81	2873	0.2	119	-61	2754	7
CONTAIN(ORNL)	475	6686	2411	-15.9	452	49	1959	-24
CONTAIN(SANDIA)	502	7071	2385	-16.8	425	40	1960	-24
CONTAIN(UK)	398	5586	2514	-12.3	377	24	2137	-17
MAAP-3(SW)	224	3100	2645	-7.7				
MCT-2(US)	66	843	2819	-1.7				
NAUAHYGROS (FN)	1.3	-81	2872	0.2				
NAUA(EPRI)	18.5	164	2873	0.2	459	51	2414	-6
NAUA(C,ENEL,NCR)	0.4	-94	2905	1.3	137	-55	2768	8
NAUA(C,ENEL,CR)	217	3000	2686	-6.3	338	11	2348	-8
NAUA(NC,ENEL)	412	5786	2491	-13.1	380	25	2111	-18
NAUA(UNIV. ROME)								
REMOVAL/2G(JN)	322	4500	2501	-12.8	721	137	1780	-31
S##AUA(US)	4.2	-40	2838	-1.0	328	8	2510	-2
EXPERIMENTAL	7		2867		304		2563	

Table 16. LA4 - average errors for AMMD and GSD

Code	Average error (%) AMMD	GSD
AEROSIM-M(UK)	112	28
CONTAIN(ORNL)	48	35
CONTAIN(SANDIA)	147	28
CONTAIN(UK)	69	32
MAAP-3(SW)		
MCT-2(US)	62	28
NAUA-HYGROS(FN)	50	36
NAUA(EPRI)	62	27
NAUA-5(NC, ENEL)		
NAUA-5(C, ENEL C.R.)		
NAUA-5(C, ENEL N.C.R.)		
NAUA(UNIV. ROME)		
REMOVAL/2G(JN)	68	31
SWNAUA(US)	55	43

Also, the estimates of errors in the values for aerosol location (such as given in Table 6.45 of report LACE TR-025[6] And Table H.13 of File LA4APA33.DAT[7]) were estimates of measurement errors for the single test. If several replicates of test LA4 had been performed, the total standard deviations for aerosol concentration and aerosol location would be even greater because the run-to-run variation would then be included. Thus, the confidence limits for the means of the test results would be greater and there would be a greater probability that the code predictions would not differ significantly from the test results.

Finally, because of the uncertainties in the input data, such as aerosol feed rates and source aerosol PSD parameters, there are confidence limits associated with the code predictions. Any statistical comparison between the predictions and test results should take these uncertainties into account. Unfortunately, estimates of confidence limits for the code predictions are not available.

Since a quantitative measure cannot be made, the average errors that have been calculated and the plots that have been prepared are simply used to judge qualitatively how well a code simulates test LA4. For this purpose, the experimental airborne aerosol concentrations and the measurements of aerosol location are assumed to be good approximations to mean values that would be obtained from several replicates of test LA4. Uncertainties about the experimental AMMD and GSD values are discussed in the next section.

7. COMPARISON OF EXPERIMENTAL RESULTS AND CODE PREDICTIONS

Airborne Aerosol and Water Concentrations

Figures 2 through 7 and Table 12 show that, in general, all codes predicted the airborne aerosol concentration fairly well during the aerosol source periods. The AEROSIM-M(UK) and NAUA-5(C,ENEL N.C.R.) codes predicted that the onset of the decrease in aerosol concentration occurred noticeably earlier than was actually observed. As seen from Figs. 9 and 10, these two codes calculated considerably greater airborne

water concentrations than were measured. This was likely the cause of the relatively early decline in aerosol concentration.

Figures 2 through 7 show that, except in the case of the MCT-2(US) code, the airborne aerosol concentrations calculated by the "dry" codes deviated from the experimental concentrations very soon after the end of the aerosol source period. After that time, the calculated concentrations were significantly greater than the experimental values until the end of the test, as seen from Figs. 2 through 7 and Table 12. Although it was a "dry" code, the MCT-2(US) code predictions of the aerosol concentration behavior were more like those of the "wet" codes. While the concentrations calculated by the MCT-2(US) code did not track the experimental data as well as the concentrations calculated by some of the "wet" codes, the aerosol concentrations predicted by the MCT-2(US) code at the end of the test were the lowest of all. The reason for this appears to be related to the MCT-2(US) plating calculations, which is discussed later.

The "wet" codes CONTAIN(ORNL), CONTAIN(SANDIA), CONTAIN(UK), and NAUA-5(C,ENEL C.R.) predicted aerosol behaviors after the end of the aerosol source period that corresponded to those for the "dry" codes. The similarity of the results of the CONTAIN codes to those of the "dry" codes appears to be that the CONTAIN codes calculated the presence of airborne water over a much shorter period of time than the other "wet" codes. This is seen in Figs. 9 and 10. However, Fig. 10 shows that NAUA-5(C,ENEL C.R.) calculated amounts of airborne water comparable to those for the other NAUA-based codes and the AEROSIM-M(UK) code. The NAUA-5(C,ENEL C.R.) code predicted that the airborne water concentration dropped to zero just after 10,000 s. Although it was tracking the experimental data up until that time, the aerosol concentration calculated by the NAUA-5(C,ENEL C.R.) code approached that of the NAUA-5(NC,ENEL) code at approximately 20,000 s, as seen in Fig. 3. Figure 38 shows that around the time of 10,000 s, the aerosol AMMD was significantly lower for the NAUA-5(C,ENEL C.R.) code than for the NAUA-5(NC, ENEL) code. At later times, the AMMDs were approximately equal. This behavior of the AMMDs explains the behavior of the aerosol concentrations for these two codes.

Of the "wet" codes, the NAUA(EPRI), NAUA-HYGROS(FN), and SWNAUA(US) codes provided the best simulations of the suspended aerosol behavior from the end of the source period until approximately 30,000 s, as indicated by Figs. 2 through 7. The NAUA(EPRI) concentrations began to deviate from the experimental data at about 20,000 s, followed by the NAUA-HYGROS(FN)concentrations at about 30,000 s. Afterwards, the concentrations predicted by these two codes remained significantly greater than the experimental data. The SWNAUA(US) code predictions for these later times were not available because the calculations were carried out only to 28,465 s. Table 10 indicates that the "wet" codes AEROSIM-M(UK) and NAUA-5(C,ENEL N.C.R.) also provided good simulations of the suspended aerosol behavior after the end of the source period. Figs. 2 through 7 show that although the shape of the aerosol concentration curve for the NAUA-5(C,ENEL N.C.R.) code was very similar to that for the experimental data, the predicted curve was displaced to earlier times. The shape of the aerosol concentration curve for the AEROSIM-M(UK) calculation was significantly different from that for the experimental data.

Figure 8 shows that the experimental MnO/CsOH mass ratio of the airborne aerosol increased with time. As would be expected, the mass ratio increased during the aerosol source period because of the use of both separate and overlapping aerosol generation periods. However, after the end of the aerosol source period until the start of the vent period, the MnO/CsOH mass ratio continued to increase rather significantly. At the start of the vent period, the mass ratio increased very sharply. After this sharp increase, the behavior of the mass ratio is indeterminate. As seen in Table 9, the standard deviations of the aerosol concentration measurements are, in general, larger after the start of the vent period, especially when the concentrations are very low. Thus, there should be more uncertainty in the experimental mass ratios after the start of the vent period. As seen in Fig. 8, this appears to be the case. If the behavior of the experimental mass ratio after the start of the vent period were to be characterized, the tendency would be to conclude that it became fairly constant.

The increase in the MnO/CsOH mass ratio that was observed experimentally after the end of the aerosol source period indicates that the CsOH was settling faster than MnO over the entire particle size range. Since pure CsOH aerosol was injected in the first period and pure MnO aerosol in the third period, some increase in the MnO/CsOH ratio after the source period might be anticipated. The reason is that the CsOH particles have been in the CSTF vessel longer and have had more time to grow into larger particles, which settle faster. However, the significant increase in the mass ratio up to the start of the vent period and the very sharp increase after the start of the vent period would not be expected if the two aerosol species were being affected in a similar manner by the conditions in the CSTF vessel atmosphere. On the contrary, the settling of the CsOH aerosol appears to have been enhanced. A feasible explanation for this phenomenon is that steam was condensing preferentially on the CsOH aerosol. This could indeed be the case due to the hygroscopic nature of CsOH and if agglomeration has not occurred to a significant extent. In support of this preferential condensation, the sharp increase in the mass ratio after the start of the vent period coincided with an increase, as measured by HEDL[6] in the airborne water concentration.

Since the single component codes assume that all particles have the same composition, they would not predict any variation in the MnO/CsOH mass ratio after the end of the source period. The multicomponent codes account for differences in aerosol composition from size bin to size bin and consequently can predict, to some extent, variations in the mass ratio. This is demonstrated by the CONTAIN codes in Fig. 8. However, the multicomponent codes typically do not have the ability to predict independent aerosol behavior, such as postulated above for CsOH. The reason for this is that by averaging the composition in each size bin, they assume that agglomeration has occurred in each size bin. In Fig. 8, though, three multicomponent codes appear to predict independent aerosol behavior. The AEROSIM-M(UK) and SWNAUA(US) codes predicted a continual increase in the MnO/CsOH mass ratio. The REMOVAL\2G(JN) code initially calculated a gradual increase in the mass ratio, and then a significant increase after approximately 30,000 s.

This may or may not be similar to the effect which was discussed in the LA2[7] posttest report. In the LA2 calculations,[8] the REMOVAL/2G(JN) code did not update the particle density for a size bin after the number of particles in that bin became very small. Furthermore, this only applied to the MnO aerosol. It is uncertain if this is the case for the LA4 test because PSD calculations were made only up to 26,600 s. The mass ratio calculated by the AEROSIM-M(UK) code continued to increase up until the end of the test. This could be related to the airborne water concentration. As seen in Fig. 9, the AEROSIM-M(UK) code predicted the presence of water throughout the test. Thus, if AEROSIM-M(UK) did address independent aerosol behavior as well as the hygroscopic property of CsOH, then the calculated increase in mass ratio would be expected. The MnO/CsOH mass ratio results for the SWNAUA(US) code simulated the experimental mass ratio data reasonably well up to about 30,000 s. Unfortunately, calculations were not performed for later times. Figure 10 shows that the SWNAUA(US) code did not predict the presence of condensed water after about 25,000 s. It would be interesting to see whether or not the SWNAUA(US) code would have predicted that the mass ratio approached a constant value at later times.

Figures 9 and 10 illustrate that the NAUA(EPRI), NAUA-HYGROS(FN), and the SWNAUA(US) codes, which included the hygroscopic behavior of CsOH, provided the best simulations to the experimental airborne water concentrations for the relatively short period of time the measurements were made. The water concentration behavior with time predicted by the NAUA-5(C, ENEL C.R.) code was similar to that for these three codes. However, the concentration approached zero significantly earlier than did the concentrations either calculated by these three codes or experimentally measured. The AEROSIM-M(UK) and NAUA-5(C, ENEL N.C.R.) codes calculated the greatest airborne water concentrations from about 1,000 to 10,000 s. For the ENEL code, the elimination of the Kelvin effect from the condensation model evidently resulted in the high concentrations. The details of the AEROSIM-M(UK) condensation model are not known. The airborne water concentration behaviors predicted by the three CONTAIN codes differed considerably from those of the other codes. For the CONTAIN codes, condensation began at the start of the vent

period. For the CONTAIN(ORNL) and CONTAIN(UK) codes, condensation ended before 30,000 s. CONTAIN(SANDIA) predicted condensation up to their last calculation at 81,000 s. From Figs. 2 and 9, in the case of the CONTAIN codes, the magnitude of the final aerosol concentration appears to be inversely related to the length of time for which airborne water was present.

In summary, the codes that include the hygroscopic property of the CsOH aerosol appear to provide the best simulations of the experimental data for the airborne aerosol and condensed water concentrations. Since the airborne aerosol behavior is directly related to the mechanisms for aerosol removal from the atmosphere, i.e., plating, settling, and leakage, these codes would be expected to provide the best predictions for the final locations of the aerosol. Furthermore, we may propose that the best measure of a code's performance is how well the calculated airborne aerosol concentrations match the experimental data. For example, there was very little aerosol leakage in test LA4. It is conceivable that for test LA4 a particular code could predict very closely the amounts of aerosol leakage, plating, and settling, while predicting the airborne aerosol behavior very poorly. However, if such a code were then used to simulate test LA2, in which there was significant aerosol leakage,[8] the code's performance in predicting both airborne aerosol behavior and final aerosol location most likely would not be acceptable.

Aerosol Deposition and Leakage

Figures 11 and 12 and Table 13 show that the aerosol leakage calculated by the AEROSIM-M(UK), MCT-2(US), NAUA(EPRI), NAUA-5(C, ENEL N.C.R.), NAUA-HYGROS(FN), and SWNAUA(US) codes most closely matched the measured leakage. As discussed above, this was expected for the codes that provided the best simulations to the airborne aerosol behavior. Since the amount of leakage was a function of the airborne aerosol concentration at the start of the vent period, the AEROSIM-M(UK), MCT-2(US), and NAUA-5(C, ENEL N.C.R.) codes also did well. Even though their predicted airborne aerosol behaviors were significantly different

from that observed experimentally, the calculated airborne aerosol concentrations at the start of the vent period were near the measured value. The other codes calculated substantially greater amounts of aerosol leakage, since their airborne aerosol concentrations at the start of the vent period were much greater than the experimental concentration. In Figures 13 and 14 and Table 13, the amounts of retained aerosol predicted by the six codes that provided the best predictions to aerosol leakage were necessarily the closest to the measured value of retained aerosol. The other codes calculated lesser amounts of retained aerosol. In Table 13, the sum of leaked and retained aerosol mass for some codes does not equal the experimental value. This is the result of the method used by a particular code for inputting the aerosol feed rates as a function of time.

Similar to the effect on the amount of aerosol leakage, the MnO/CsOH mass ratio in the leaked aerosol was a function of the mass ratio of airborne aerosol at the start of the vent period. From Fig. 8, the only two codes that would be expected to reasonably approximate the experimental mass ratio value would be AEROSIM-M(UK) and SWNAUA(US). An inspection of Tables 12 and 13 reveals this to be the case.

As an indication of how closely the amount of settled aerosol calculated by a code may be expected to agree with the experimental value, the settling velocities in Figs. 15 through 18 may be examined. Although somewhat difficult to evaluate, the NAUA(EPRI) and SWNAUA(US) codes appear to provide the best estimates to the experimental settling velocities. These two codes, then, should provide good estimates for the amount of settled aerosol. At times less than 10,000 s when the airborne aerosol concentrations are the largest, the AEROSIM-M(UK), NAUA-HYGROS(FN), and NAUA-5(C, ENEL N.C.R.) codes calculate greater settling velocities than measured. Consequently, these codes would be expected to predict larger amounts of settled aerosol than measured. The NAUA-5(C, ENEL N.C.R.) code calculated greater settling velocities at times less than about 6,000 s and lower velocities at later times. How well this code might predict the amount of settled aerosol is rather uncertain. The remaining codes calculated lower settling velocities

than measured. Thus, the amounts of settled aerosol calculated by these codes should be lowest of all.

A comparison of the experimental settling velocities for the individual components, as provided by the velocity ratio plot in Fig. 19, shows that the MnO aerosol had the larger settling velocity at early times and the CsOH aerosol settled faster at later times. Thus, the effect upon the MnO/CsOH mass ratio of the settled aerosol is uncertain. Figure 19 also shows that the AEROSIM-M(UK), REMOVAL/2G(JN), and SWNAUA(US) codes predicted greater settling velocities for CsOH. This is the reason for the continual increase in the airborne MnO/CsOH mass ratio for these codes, as seen in Fig. 8. Calculations by the SWNAUA(US) code for later times would have been worthwhile to see whether or not the settling velocity ratio remained at about the same level. Because of the behavior of the settling velocity ratio, the settled aerosol for these three codes would be expected to be somewhat enriched in CsOH.

In Fig. 19, the greater settling rates for MnO during the first part of the test are not consistent with the idea that steam condensation is occurring preferentially on CsOH because of its hygroscopic character. HEDL[6] stated that some cooling of the preheated deposition coupons occurred before they were inserted into the CSTF vessel. It is possible that condensing steam could have washed some of the aerosol from the coupon. Since CsOH is soluble, greater losses of this aerosol could have resulted. Consequently, the experimental settling flux, and the calculated settling velocity, would have been reduced more for CsOH than for MnO. The small size of the deposition coupons (17.2 cm^2) would probably enhance this effect. For deposition samples taken at the same time, differences in the measured settling flux by as much as a factor of 4 were observed. Thus, the experimental error in the calculated settling velocity ratios is rather large.

The results for settled aerosol in Figs. 20 and 21 and Table 13 are more or less as envisioned from the above evaluation of the settling velocities. The total amount of settled aerosol for the NAUA(EPRI), SWNAUA(US), and NAUA-HYGROS(FN) codes agreed very well with the measured value. The NAUA-HYGROS(FN) code appears to have provided somewhat

better agreement than expected from the above discussion. Considering also the rather unusual behavior of the NAUA-HYGROS(FN) curve in Fig. 16, it may be possible that the settling flux results reported in the code output were not consistent with the values actually calculated internally by the code. The amounts of settled aerosol were largest for the AEROSIM-M(UK) and NAUA-5(C, ENEL N.C.R.) codes but were within the 95% confidence limits of the experimental value. The remaining codes calculated lower settled aerosol amounts. The settled aerosol value for the NAUA(UNIV. ROME) code seems to be abnormally low. The reason for this is seen from the examination of the plating results which follows below. In Figs. 22 and 23, a meaningful comparison of calculated and experimental values cannot be made for the MnO/CsOH mass ratio of the settled aerosol. This is due to the large uncertainty in the experimental value and the fact that the mass ratio of the total aerosol feed was different for essentially all of the codes. The latter effect was a result of the differences in the input of aerosol feed rates into the codes.

Figures 24 and 25 and Table 13 show that several of the codes provided good estimates to the measured amount of plated aerosol. As seen in Figs. 24, 25, and 28, most of the plating occurred by diffusiophoresis. The larger amounts of plated aerosol calculated by the MAAP-3(SW), REMOVAL/2G(JN), MCT-2(US), and NAUA(UNIV. ROME) codes indicate that either the diffusiosphoresis models or the steam condensation rates used in the calculations were significantly different from those of the other codes. The lower amounts of plated aerosol calculated by the AEROSIM-M(UK) and NAUA-5(C, ENEL N.C.R.) codes were a result of the high amounts of settled aerosol predicted by these codes, as discussed previously. For the same reasons as for the settled aerosol, a comparison of calculated and experimental values for the Mno/CsOH mass ratio of the plated aerosol does not seem useful. In Figs. 26 and 27, the AEROSIM-M(UK) and SWNAUA(US) codes calculated greater mass ratios because their larger CsOH settling velocities caused the airborne aerosol to be richer in MnO. The NAUA-5(C, ENEL C.R.) code also calculated a greater mass ratio for the plated aerosol. However, this resulted from the prediction that the majority of the plating did

not occur until after the end of the aerosol source period, as seen in Fig. 25. The aerosol settling during the source period enriched the airborne aerosol in MnO somewhat for the NAUA-5(C,ENEL C.R.) code. This was not observed for the NAUA-5(C, ENEL N.C.R.) code because, as shown by Fig. 25, the plating was essentially completed for this code by the end of the aerosol source period.

Figures 29 through 34 present the settling flux data, from which the settling velocities discussed previously were determined. The results for the AEROSIM-M(UK) and NAUA-HYGROS(FN) codes dropped below the experimental values at about 6,000 to 8,000 s. As seen in Figs. 2 and 3, this occurred because the airborne aerosol concentrations for these codes earlier began to diverge from the measured concentrations to lower values. Over the time period for which the experimental data were available, the codes simulated the measured settling flux reasonably well. In Figs. 35 and 36, the AEROSIM-M(UK) and SWNAUA(US) codes predict a continual increase in the MnO/CsOH mass ratio of the settling flux. This is a result of the increasing MnO/CsOH mass ratio of the airborne aerosol predicted by these codes. Considering the hygroscopic nature of CsOH, a similar behavior would be expected for the settling flux mass ratios that were determined experimentally. This is not observed in Figs. 35 and 36. However, as discussed previously for the settling velocities, the standard deviations of the settling flux measurements were quite large. Consequently, there is considerable error in the settling flux ratios.

Aerosol Particle Size Distribution Parameters

In Figs. 37 and 38, essentially all of the codes predicted that the AMMD attained a maximum value at some time around 10,000 s. Although Table 14 shows that the average errors for the AMMD were more or less the same for the codes, inspection of Figs. 37 and 38 reveals that the NAUA(EPRI), NAUA-HYGROS(FN), and SWNAUA(US) codes appear to provide the best approximations to the experimental behavior of the AMMD with time. Again as pointed out previously, these codes accounted for the hygroscopic property of the CsOH aerosol. The AEROSIM-M(UK) and

NAUA-5(C, ENEL N.C.R.) codes calculated peaks in the AMMD curve at earlier times than observed experimentally, and the CONTAIN codes calculated peaks at later times. The AMMD behaviors for these five codes appear to be related to their results for the airborne water concentration as shown in Figs. 9 and 10. For the CONTAIN(ORNL) and CONTAIN(UK) codes, the peaks are more pronounced using the calculated rather than the reported AMMD values in Table 8. At 20,700 s, when both codes predicted that water was condensed on the aerosol, the reported AMMD values in Table 8 were for the wet aerosol.

In Figs. 39 and 40, the experimental AMMD attained greater values for the MnO aerosol than for the CsOH aerosol. The AEROSIM-M(UK) and SWNAUA(US) codes predicted the opposite behavior. The AEROSIM-M(UK) code demonstrated the greatest difference in AMMD between the two species, the AMMD of CsOH being about twice that of MnO at one time. Larger AMMD values for CsOH are consistent with the greater settling velocity of CsOH as compared to MnO. In the LA2 posttest report,[8] the possibility that fragmentation of the aerosol occurs during collection in the cascade impactor was discussed. If this was actually the case, then the CsOH aerosol may have been affected more than the MnO aerosol. The results from the AEROSIM-M(UK) and SWNAUA(US) codes indicate that these codes are simulating independent behaviors of the aerosol species, as pointed out previously.

In Figs. 41 and 42, none of the codes predicted as large a GSD value as measured experimentally. From Table 8, the GSDs for REMOVAL/2G(JN) that were calculated from the PSDs were smaller than the reported values plotted in Fig. 41. Because of the differences in the AMMDs for CsOH and MnO as calculated by AEROSIM-M(UK), a significant increase in the GSD shown for this code in Fig. 41 might have been expected. As seen in Fig. 8 for the AEROSIM-M(UK) code, the considerably greater concentration of MnO as compared to CsOH negated any effect of the AMMD difference on the GSD of the combined aerosol. In Fig. 42, the SWNAUA(US) code predicted a significant increase in GSD. As seen in Fig. 8, the MnO/CsOH concentration ratio was also fairly large at the time of the GSD increase. Thus, an increase in the GSD of MnO is indicated. The NAUA-5(C, ENEL C.R.) code calculated a peak in

the GSD curve at a relatively early time. This was caused by the condensation model used, which does not allow condensation below a certain aerosol particle diameter. The effect of the condensation model is seen more clearly in the PSD plots which are discussed below.

In Figs. 43 and 44, the experimental GSDs for the separate aerosol species were about the same. As expected from Figs. 41 and 42, none of the codes provided good simulations of the experimental behaviors of the GSD with time. In Fig. 43, the REMOVAL/2G(JN) code predicted a significant increase in the GSD for MnO. This is unexpected from the GSD for the combined aerosol in Fig. 41. The SWNAUA(US) code also predicted a noticeable increase in the GSD for MnO. As discussed above, this was the reason for the increase in the GSD of the combined aerosol.

To examine the PSD curves calculated by the codes, the "group 1" set of codes is considered first. The results for these codes are presented in Figs. 45, 47, 49, 51, 53, 55, 57, and 59. For the times through 6060 s, the PSD for the AEROSIM-M(UK) code was shifted to the right, to greater particle diameters, as compared to the PSDs for the other codes. During this time period, the AEROSIM-M(UK) code predicted significant amounts of airborne water and the other codes predicted none, as seen in Fig. 9. At 11,100 and 5,150 s, the AEROSIM-M(UK) PSD curve shifted to the left towards the PSDs of the other codes as the water concentration for the AEROSIM-M(UK) code decreased. At 20,700 s, the PSD curves of the three CONTAIN codes have shifted to the right as a result of the water condensation indicated in Fig. 9. The AEROSIM-M(UK) water concentration is relatively low and its PSD curve is similar to those of the MCT-2(US) and REMOVAL/2G(JN) codes. At 26,600 s, after the CONTAIN(ORNL) and CONTAIN(UK) codes show no airborne water in Fig. 9, the PSD curve for the CONTAIN(SANDIA) code was the only one shifted towards larger particle sizes. However, as seen in Fig. 9, the CONTAIN(SANDIA) water concentration was about the same as that of the AEROSIM-M UK) code at this time. The difference in PSDs may be the result of a difference in the distribution of the condensed water on the aerosol particles.

At 26,600 s for the "group 1" set of codes, the PSD curves differed considerably at the smaller particle sizes. After evaporation

of water from the aerosol for the CONTAIN(ORNL) and CONTAIN(UK) codes as shown by Fig. 9, these two codes showed the greatest fractions of very small aerosol particles at 26,600 s. Before condensation at 15,150 s, the aerosol concentrations were 2.37 and 1.99 g/m^3 for CONTAIN(ORNL) and CONTAIN(UK), respectively. After evaporation at 26,600 s, the aerosol concentrations were 0.056 and 0.094 g/m^3 for CONTAIN(ORNL) and CONTAIN(UK), respectively. Considering that from 15,150 s to 26,600 s for these two codes the mass fractions of the smaller particle sizes increased by about three orders of magnitude, the actual concentration of aerosol particles with the very small diameters somehow increased. That this was indeed the case may be seen in the output provided by the code users, in which the mass concentration of the aerosol was given as a function of particle size. This increase in small diameter particles may be attributed to the aerosol "deagglomeration" phenomenon discussed in the LA2 posttest report.[8] Further evidence of this phenomenon is seen in the examination of the PSD curves for the "group 2" set of codes.

The PSD results for the "group 2" set of codes are presented in Figs. 46, 48, 50, 52, 54, 56, 58, and 60. For the NAUA-5(C, ENEL C.R.) code, the inclusion of the Kelvin effect in the condensation model caused the PSD curves to have a multi-modal appearance. The condensation model for the NAUA-HYGROS(FN) code must also have included the Kelvin effect since multi-model PSD curves were also calculated by this code. The PSD curve for theNAUA-5(NC, ENEL) code showed the least amount of variation with time. This was the only code of this group that did not predict the condensation of water on the aerosol. The changes in the PSD curves for the other codes may be attributed primarily to the changes in airborne water concentration for each code.

The PSD curves for the ENEL codes may be compared as another indication of the aerosol "deagglomeration" phenomenon. At 26,600 s, the aerosol concentration for the NAUA-5(C, ENEL N.C.R.) code is about three orders of magnitude less than that of the other two ENEL codes. However, as seen in Fig. 60, the mass fraction of aerosol with an AMMD of about 0.35 μm is about five orders of magnitude higher for the NAUA-5(C, ENEL N.C.R.) code. The NAUA-5(C, ENEL C.R.) code had no

condensation of water on particles with an AMMD of less than about 2 μm. The NAUA-5(NC, ENEL) code had no condensation on the aerosol. Considering that the only difference between these three codes is the water condensation model, it appears that, for the NAUA-5(C, ENEL N.C.R.) code, the condensation of water followed by evaporation created aerosol mass at the smaller particle sizes. As in the case of the CONTAIN codes, this may be attributed to the aerosol "deagglomeration" phenomenon.

The aerosol "deagglomeration" phenomenon may be responsible for the fact that the codes that include condensation of water on the aerosol do not predict the very low aerosol concentrations that are experimentally measured towards the end of the test. At 160,000 s, the NAUA-5(C, ENEL N.C.R.) code predicted an AMMD of ~1 and the other two ENEL codes predicted AMMDs of about 2. Since the settling velocity depends on the square of the particle size, the settling velocities for these aerosols differed by a factor of 4. If the calculations had been carried out to later times, the aerosol concentration curve for the NAUA-5(C, ENEL N.C.R.) code, as seen in Fig. 3, apparently would have been crossed by the curves for the other two ENEL codes.

8. CONCLUSIONS

The main conclusions from this code comparison exercise for LACE test LA4 are as follows:

1. The codes that included the hygroscopic property of the CsOH aerosol provided the best simulations of the experimental data for the airborne aerosol and condensed water concentrations. Consequently, these codes also provided the best predictions of the final locations of the aerosol.
2. The codes that included the hygroscopic property ofthe CsOH aerosol also provided the best predictions of the AMMD behavior. However, none of the codes simulated the behavior of the GSD of the aerosol satisfactorily.

3. As stated in the LA2 posttest report,[8] the stimulation of condensation of steam on the aerosol is very likely the key to the prediction of aerosol behavior. Important factors in the simulation of this condensation phenomenon are the steam saturation conditions, the condensation model itself, and the numerical technique utilized in the condensation calculation.
4. The AEROSIM-M(UK) and SWNAUA(US) codes appear to have the capability to account for the independent behavior of the aerosols. That is, the behavior of unagglomerated as well as agglomerated aerosol species may be simulated. Such indedependent behavior was indicated experimentally by the behavior of the MnO/CsOH mass ratio of the airborne aerosol.
5. The particle size distribution curves calculated by codes that included condensation of steam on the aerosol demonstrated the aerosol "deagglomeration" phenomenon discussed in the LA2 posttest report.[8] The effect of this phenomenon is to artificially increase the concentration of aerosol particles in the small particle size range.

9. RECOMMENDATIONS

The recommendations that result from this code comparison activity for LACE test LA4 are as follows:

1. For simulating aerosol under conditions such as existed for LACE test LA4, codes should be modified to account for the hygroscopic property of certain aerosols.

2. If the outcome of certain accident scenarios could be significantly influenced by the independent behavior of the aerosols, the computer codes should be modified to account for such behavior.
3. The aerosol deagglomeration phenomenon should be investigated to see if it has any effect on the simulation of accident scenarios. If so, computer codes should be modified to minimize the effects of this phenomenon.

REFERENCES

1. L. D. Muhlestein, Hanford Engineering Development Laboratory, "Transmittal of LA4 Final Test Plan (LACE-TP4)," letter to LACE Program participants, July 3, 1986.

2. J. H. Wilson, "Initial Instructions for LA4 Blind Posttest Aerosol Calculations," letter to LACE program participants, February 12, 1987.

3. J. H. Wilson, "Corrected Aerosol Feed Rate Values for LA4 Blind Posttest Calculations," letter to LACE program participants, March 12, 1987.

4. J. H. Wilson,"LA4 Posttest Aerosol Calculations Using Corrected Steam Flow Rates," letter to LACE program participants, August 6, 1987.

5. R. K. Hilliard, et al., Late Containment Failure with Overlapping Aerosol Injection Periods, Test LA4 - Input Conditions for Blind Posttests Aerosol Behavior Code Calculations, report on IBM-PC floppy disks to LACE participants, Hanford Engineering Development Laboratory, December 19, 1986.

6. R. K. Hilliard, et al., "Appendix A of LACE TR-007, Failure to Isolate Containment, Test LA2 - Summary of Thermal Hydraulic and Aerosol Experimental Data," report on IBM-PC floppy disks to LACE participants, Hanford Engineering Development Laboratory, December 19, 1986.

7. J. D. McCormack, et al., Final Report of Experimental Results of LACE Test LA4 - Late Containment Failure with Overlapping Aerosol Injection Periods, LACE TR-025, Westinghouse Hanford Company, October 1987.

8. J. H. Wilson and P. C. Arwood, Summary of Posttest Aerosol Code-Comparison Results for LWR Aerosol Containment Experiment (LACE) Test LA2, LACE TR-009, September 1988.

APPENDIX A

RECOMMENDED PROCEDURE FOR DETERMINATION OF AMMD

The calculation of the aerodynamic mass-median diameter (AMMD) by a code should be done in a manner that will allow direct comparison with the cascade impactor data. To accomplish this, the AMMD calculation should (1) be consistent with the definition of a median diameter, (2) be based on the distribution of weight of dry aerosol vs the size of the wet aerosol (if steam has condensed on the aerosol), and (3) take into account the variation of aerosol density with diameter (unless the code assumes that the density is constant for all particle sizes). This appendix discusses how the AMMD calculation should be performed to conform to these criteria.

By definition, the mass median diameter is "that diameter below which 50% of the mass of the particle size distribution lies." Thus, when analyzing the cascade impactor data, the cumulative mass which has a smaller size than the diameter of a particular stage (i.e., all mass that has passed through that stage to the remaining stages and the filter) is plotted vs the diameter of that stage. The mass median diameter (which is also the AMMD, since the impactor was calibrated with particles having a density of 1 g/cm^3) is, then, that diameter corresponding to 50% of the cumulative mass. In order to compare with the experimental impactor data, the codes should calculate the AMMD in a similar manner. In particular, the results from the "discrete" codes should be plotted as cumulative mass vs the upper diameter of the size bin. The upper diameter, rather than the average diameter, of the size bin is used for the plot since the diameter of all mass in a size bin is smaller than or equal to the upper bin diameter.

In the experimental measurements with the cascade impactors, the aerosol particles are collected on the stages of the impactors according to the aerodynamic size of the particles. If steam has condensed on the aerosol, the aerodynamic size is that of the wet particles. However, the analysis of the amount of aerosol on each impactor stage is made after the water that was present has been evaporated. Therefore, the

AMMD and the GSD values that are reported are based on the amount of dry aerosol on each impactor stage and on the aerodynamic size of the wet aerosol collected on each stage. In order to make a meaningful comparison between the experimental measurements, the code results should be plotted as the cumulative mass of dry aerosol vs the upper diameter of the size bin.

Some "discrete" codes include the variation of aerosol density from size bin to size bin. The density may vary due to differences in composition of MnO and CsOH and/or to differences in the amount of condensed water on the aerosol. If the code includes the variation of density with size bin, the average diameter of each size bin should be converted to the corresponding average aerodynamic diameter by multiplying by the square root of the density for the particular size bin. The AMMD then can be determined by plotting the cumulative mass of dry aerosol vs the upper aerodynamic diameter of the size bin. As above, the upper aerodynamic diameter of a size bin may be calculated as the geometric mean of the average aerodynamic diameter of that size bin and the average aerodynamic diameter of the next larger size bin.

APPENDIX B

RECOMMENDED PROCEDURE FOR DETERMINATION OF GSD

One method of calculating the geometric standard deviation (GSD) involves taking the ratio of the aerodynamic diameter at 84.13% cumulative mass (when plotting the particle size data as in Appendix A) to the aerodynamic mass median diameter. However, this method applies only if the distribution is lognormal. Some codes calculate GSD by a formula, such as

$$\ln(GSD) = (\Sigma(n_i(\ln d_i - \ln d_g)^2)/N)^{0.5}, \qquad (B.1)$$

where n_i is the number of particles with diameter d_i, d_g is the geometric mean diameter, and N is the total number of particles. Those methods for determining GSD do not apply strictly to the cascade impactor data, since the experimental particle size distributions typically are not lognormal, and also since the number of particles collected on each impactor stage is unknown.

In order to compare with the cascade impactor data, a recommended approach would be to modify the above formula by replacing n_i with the weight of aerosol having an aerodynamic diameter d_i, replacing N with the total weight of aerosol, and replacing $\ln d_g$ with a logarithmic aerodynamic mass mean diameter. This logarithmic aerodynamic mass mean diameter may be written as

$$\Sigma w_i \ln d_i, \qquad (B.2)$$

where w_i is the weight fraction of aerosol with aerodynamic diameter d_i. Furthermore, w_i is the weight fraction of <u>dry</u> aerosol in size bin i (as in the calculation of the AMMD in Appendix A) and d_i is the <u>average</u> aerodynamic diameter of size bin i (not the upper aerodynamic diameter of size bin i as in the calculation of the AMMD). As in Appendix A, the density used to calculate the average aerodynamic diameter of size bin i should be the density of the wet aerosol in that size bin if steam has condensed on the aerosol.

APPENDIX C

METHOD UTILIZED FOR ANALYSIS OF CASCADE IMPACTOR DATA

The experimental AMMD values were determined from the cascade impactor data as described in Appendix A. That is, the cumulative mass which has a smaller size than the diameter of a particular stage (i.e., all mass that has passed through that stage to the remaining stages and the filter) was plotted vs the diameter of that stage (log probability paper was used for the plot). A smooth curve was drawn through the data points and the aerodynamic mass median diameter was determined as that diameter corresponding to 50% of the cumulative mass. A smooth curve was drawn rather than fitting a straight line through the data points because the experimental particle size distributions typically were not lognormal.

For determination of the GSD, the experimental particle size range (corresponding to the smallest and largest stages of the cascade impactor) was divided into a number (typically 20) of size bins (the widths of the size bins being equal on a log scale). From the smooth curve drawn through the cascade impactor data points on log probability paper, the weight fraction of aerosol in each size bin was calculated. This weight fraction was equal to the cumulative weight fraction at the upper diameter of the size bin minus the cumulative weight fraction at the lower diameter of the size bin. The GSD was then calculated using the recommended formula in Appendix B.

LACE TR-084
ORNL/M-991

INTERIM DISTRIBUTION

1-3. P. C. Arwood
4. J. T. Bell
5. R. K. Genung
6. E. K. Johnson
7. C. E. Pugh
8. F. M. Scheitlin
9. M. G. Stewart
10-11. J. H. Wilson
12. A. L. Wright
13. A. Zucker
14-15. Office of Scientific and Information Center, Department of Energy, P. O. Box 62, Oak Ridge, TN 37831
16. Office of Assistant Manager, Energy Research and Development, Oak Ridge Operations, Oak Ridge, TN 37831
17. Laboratory Records
18. Laboratory Records - RC
19. ORNL Patent Section
20. Central Research Library
21. Document Reference Section